

JOURILL OF University of Tehran SCIENCES

Abu Reyhan al-Biruni (973-1048) Iranian Scientist ISLAMIC REPUBLIC OF IRAN

ISSN 1016-1104

Vol. 35, No. 4, Autumn 2024

CONTENTS INSTRUCTIONS TO AUTHORS 303 **BIOLOGY:** Identification of TYR Whole Gene Deletion in a Patient with Oculocutaneous Albinism by 305 Next Generation Sequencing M. R. Pourreza, Gh. Dargahi, M. Hoseinzadeh, N. Tabibi, M. A. Tabatabaiefar Comparison Between HLA-B Allele Groups Among Peripheral Blood Stem Cell Donation 311 Volunteers from Various Iranian Ethnicities F. Yari, F. Sabaghi, N. Bagheri, A. Teimurpour, M. Zaman-Vaziri, F. Mortezapour Barfil, M. Sobhani MATHEMATICS, STATISTICS, AND COMPUTER SCIENCES: On Projection Invariant Rickart Modules 321 Y. Maleki, A. Moussavi, Y. Kara A New Bivariate Shock Model Covering All Degrees of Dependencies 329 H. A. Mohtashami-Borzadaran, H. Jabbari, M. Amini Modeling Mortality in Heart Failure Patients: Considering Time-Varying Effects – 341 A Bayesian Survival Analysis Utilizing Bayesian AFT Model with the INLA Method S. Vijayan, S Kavitha, V. Saranaya **PHYSICS:** Preparation of Polymer Nanocomposites Containing Multiwall Carbon Nanotubes 351 Functionalized by Chloroform Plasma F. Pourfayaz, A. Gholami 359 PERSIAN TRANSLATION OF ABSTRACTS 367 **AUTHOR INDEX** 375 KEYWORD INDEX



In the Name of Allah, the Beneficent, the Merciful

JOURNAL OF SCIENCES

ISLAMIC REPUBLIC OF IRAN

CHAIRMAN AND EDITOR

Mohammad Reza Noori-Daloii, Ph.D.

EDITORIAL BOARD

Alireza Abbsai, Ph.D.

University of Tehran, Tehran, Iran
Abdolhossein Amini, Ph.D.

University of Tehran, Tehran, Iran
Aziz N. Behkami, Ph.D.
Shiraz University, Shiraz, Iran
Farshad Ebrahimi, Ph.D.
Shahid Beheshti University, Tehran, Iran
Hassan Ebrahimzadeh, Ph.D.
University of Tehran, Tehran, Iran
Mehdi Ghandi, Ph.D.
University of Tehran, Tehran, Iran
Mehdi Khoobi, Ph.D.
Tehran University of Medical Sciences, Tehran, Iran

Hassan Mehdian, Ph.D.

Kharazmi University, Tehran, Iran

Mohsen Mohammadzadeh, Ph.D.

Tarbiat Modares University, Tehran, Iran

Mohammad Reza Noori-Daloii, Ph.D.

Tehran University of Medical Sciences, Tehran, Iran

Abdolhamid Riazi, Ph.D.

Amir Kabir University, Tehran, Iran

Jafar Zafarani, Ph.D.

Isfahan University, Isfahan, Iran

Hossein Zakeri, Ph.D.

Kharazmi University, Tehran, Iran

EDITORIAL ASSISTANT

Zahra Roshani

MANAGERIAL ASSISTANTS

Hasan Noori-Daloii Elaheh Poorakbar

TYPESETTING AND LAYOUT

Ali Azimi

Journal of Sciences, Islamic Republic of Iran is published quarterly by The University of Tehran,
16th St., North Kargar Ave, Tehran, Islamic Republic of Iran
Tel.: (0098-21)88334188, 88012080-212
Fax: (0098-21) 88334188
P.O. Box 13145-478
http://jsciences.ut.ac.ir
E-mail: jsciences@ut.ac.ir
E-mail: nooridaloii@sina.tums.ac.ir

ISSN 1016-1104

Instructions to Authors

1. General Policy

The Journal of Sciences, Islamic Republic of Iran (J. Sci. I. R. Iran) is published quarterly by the University of Tehran. Contributions from all fields of basic sciences may be submitted by scientists from all over the world.

The papers submitted to this journal should not have been published previously, except in the form of a brief preliminary communication, nor submitted to another journal. The decision to accept a contribution rests with the Editorial Committee of the *J. Sci. I. R. Iran.* Manuscripts will be considered for publication in the form of articles, preliminary communications, notes and review articles. The work should be original or a through review by an authoritative person in a pertinent field.

2. Copyright

Submission of a manuscript implies that the author(s) agree to transfer copyright to the *J. Sci. I. R. Iran* when the contribution is accepted for publication. Reproduction of the text, figures, or tables of this journal is allowed only by permission of the Editorial Committee.

3. Preparation of Manuscripts

3.1. General considerations. Manuscripts must be submitted in English according to Journal Instructions (It is necessary to submit at least 2 files including "Title page" and "Main file"). They must be typewritten in Microsoft Word (all versions). Authors are requested to reserve margins of at least 3 cm at the top and bottom of each page and at least 4 cm on the left-hand side.

Tables and illustrations (both numbered in Arabic numerals) should be prepared on separate pages. Tables require a heading and figures a legend, also prepared on a separate page. In Electronic submission, figures should be with the following caveats: all figures should be submitted at a minimum of 300 dpi and saved as TIFF files (avoid submitting JPEG files) after your text file.

Manuscripts should be kept to a minimum length and should be subdivided into labeled sections (Introduction, Materials and Methods, Results, Discussion, Acknowledgement, References). A current issue of *J. Sci. I. R. Iran* should be consulted.

3.2. **Title page.** The title of a manuscript should reflect concisely the purpose and findings of the work in order to provide maximal information for a computerized title search. Abbreviations, symbols, chemical formulae, references, and footnotes should be avoided.

The authors' full first names, middle initials and last names should be given, followed by the address(es) of the contributing department(s). (e.g. Department, Faculty, University, City, Country).

Telephone, Fax and Email of corresponding author should be footnoted on the bottom of the first page of each manuscript. Footnotes may be added to indicate the present mailing address(es) of the author(s). (e.g. *Corresponding author, Tel: 00982188012080, Fax: 00982188012081, E-mail: jsciences@ut.ac.ir).

Special types of print should be indicated as follows:

Type	Mark	Symbol	Example	Example (Printed)
Boldfacea	Single underline		Introduction	Introduction
Italic ^b	Wave-like underline	$\sim\sim$	In vivo	In vivo
Small capital ^c	Double underline		0.2 <u>m</u>	0.2 M
Boldface italic ^d	Underline with wavy line	$\overline{\sim}$	 <u>R</u>	R

- a) Headings, designated numbers of chemical compounds, subheadings.
- b) Configurational prefixes ((R)-, (S)-, cis-, trans-, tert-, etc); Latin words or abbreviations, words in languages other than English; trade names of compounds (first letter should be capitalized); names of authors if mentioned in the text.

Vol. 35 No. 4 Autumn 2024 J. Sci. I. R. Iran

c) Symbols of molar and normal concentrations (M and N), D- and L-, the names or initials of the nomenclature of species.

d) Italicized terms and prefixes in headings.

The total number of pages (including references, tables, copies of formula collections (if any), schemes and figures should be marked in the upper left-hand corner of the first page of each copy. The complete address, including phone number, and E-mail address of the correspondence author should also be given.

3.3. *Main File:*

- a) The title of the article (The first letter of each word must be capital).
- b) Abstract should be self-explanatory and intelligible without references to the text and titles, it must not exceed 250 words.
- c) At least between three to five keywords should be chosen by the author(s).
- d) Introduction
- e) Materials and Methods
- f) Results and Discussion (they can be separate section too)
- g) Figures and Tables (if There are any)

Theoretical articles must have atleast two main title: Introduction and Results.

3.4. References. References may be numbered alphabetically or sequentially in the order they are cited in the text. References typed with double spacing are to be listed in numerical order at the end of the main text. They should be addressed according to the following examples:

Journals:

Noori-Daloii M.R., Swift R.A., Kung H.J., Crittenden L.B., and Witter R.L. Specific integration of REV proviruses in avian bursal lymphomas. *Nature*, **294** (5841): 574-576 (1981).

Noori Daloii M.R., Saffari M., Raoofian R., Yekaninejad M., Saydi Dinehkabodi O., and Noori-Daloii A.R. The multidrug resistance pumps are inhibited by silibinin and apoptosis induced in K562 and KCL22 leukemia cell lines. *Leukemia Research*, **38** (5): 575-580 (2014).

Books:

Rang G.M. and Petrocelli S.R. *Fundamentals of Aquatic Toxicology*. Hemisphere Publishing Corporation, New York, 1129 p. (1991).

Chapters in Books:

Walsh J.H. Gastrointestinal hormones. In: Johnson L., Christensen J., Jackson M., Jacobson E., and Walsh J.H. (Eds.), *Physiology of the Gastrointestinal Tract*, 2nd Ed., Raven, New York, pp. 181-254 (1987).

Thesis:

Kossir A. Extraction liquid-liquid du Zinc (II) en milieu cyanure. Application ala valorization des minerais de zinc oxides, Ph.D. *Thesis*, University of Paris (VI), 116 p. (1991).

Please note that papers with incorrect formatted references will be returned.

4. Forwarding Address

Manuscripts should be submitted to the journal site (http://jscinces.ut.ac.ir).

M.R. Noori-Daloii, Ph.D.
J. Sci. I. R. Iran
University of Tehran
P.O. Box 13145-478 Tehran, I. R. Iran
http://jsciences.ut.ac.ir
E-mail: jsciences@ut.ac.ir

Identification of *TYR* Whole Gene Deletion in a Patient with Oculocutaneous Albinism by Next Generation Sequencing

M. R. Pourreza^{1,5}, Gh. Dargahi^{2,5}, M. Hoseinzadeh^{1,5}, N. Tabibi^{3,5}, M. A. Tabatabaiefar^{1,4,5*}

Received: 16 March 2025 / Revised: 24 May 2025 / Accepted: 27 July 2025

Abstract

Oculocutaneous albinism (OCA) comprises a group of genetically heterogeneous, autosomal recessive disorders characterized by a partial or complete absence of melanin pigmentation in the skin, hair, and eyes, associated with visual impairment. In this study, we analyzed several genes in an Iranian male infant affected by OCA. Clinical investigations and laboratory evaluations were performed for the proband. A pedigree chart was also drawn. Genomic DNA was extracted from the proband and both parents. A targeted gene panel was sequenced by next-generation sequencing to identify pathogenetic variants. A deletion of exons 1–5 in the *TYR* gene was confirmed in the proband. Logically, the parents should be heterozygous for this mutation. The results of this research demonstrate the efficiency of targeted high-throughput sequencing in diagnosing heterogeneous disorders like OCA and detecting large genomic rearrangements. This deletion mutation may have resulted from an unequal crossing-over event in an ancestral lineage.

Keywords: Oculocutaneous albinism (OCA); TYR gene deletion; Next-generation sequencing (NGS).

Introduction

Oculocutaneous albinism (OCA) comprises a group of rare genetically heterogeneous disorders caused by defects in the melanin biosynthesis pathway, resulting in complete or partial loss of pigmentation in the skin, hair, and eyes (1). Optic system abnormalities, such as nystagmus, photophobia, iris translucency, foveal hypoplasia, strabismus, retinal hypopigmentation, and decreased visual acuity are also observed in affected individuals (2, 3). The incidence of OCA ranges from 1 in 10,000 to 20,000 in newborns across different ethnic

¹ Department of Genetics and Molecular Biology, Isfahan University of Medical Sciences, Isfahan, Islamic Republic of Iran.

² Department of Genetics and Molecular Biology, Najafabad Branch, Islamic Azad University, Najafabad, Islamic Republic of Iran.

³ Department of Medical Genetics, Faculty of Medical Sciences, Tarbiat Modares University, Tehran, Islamic Republic of Iran

⁴ Pediatric Inherited Diseases Research Center, Research Institute for Primordial Prevention of Noncommunicable Disease, Isfahan University of Medical Sciences, Isfahan, Islamic Republic of Iran.
⁵ Department of Research and Development, Harmonic Medical Genetics Lab, Isfahan, Islamic Republic of Iran

^{*} Corresponding Author: Tel: +989122886157; Email: tabatabaiefar@med.mui.ac.ir, tabatabaiefar@gmail.com

populations. This indicates that approximately 1 in 70 people carries an OCA-related gene mutation (3, 4) (Table 1).

OCA is an autosomal recessive genetic disorder classified into a non-syndromic form, caused by mutations in several genes such as *TYR*, *TYRP1*, *OCA2*, *SLC45A2*, *SLC24A5*, *SLC24A4* genes, and a syndromic form, which results from defects in various genes including *AP3B1*, *HPS1*, *HPS3*, *HPS4*, *HPS5*, *HPS6*, *DTNBP1*, *BLOC1S3*, *PLDN*, *LYST*, *MYO5A*, *RAB27A*, and *MLPH* genes (5, 6). Additionally, mutations in GPR143 are the only known and major cause of X-linked ocular albinism (6–8).

Defects in the *TYR* gene cause OCA1, the most prevalent subtype of the disorder among Caucasian populations, representing approximately 50% of reported cases (9–11). The *TYR* gene spans more than 50 kb of genomic DNA on chromosome 11q14.3, consisting of five exons and encoding a 529 amino-acid protein (12, 13). A tyrosinase-related gene (tyrosinase-like gene) exists on chromosome 11q, containing only exons 4 and 5, and shares 98.5% homology with the *TYR* gene (14, 15). Tyrosinase catalyzes essential steps in the melanin biosynthesis pathway, including the conversion of tyrosine to dopaquinone (16, 17).

OCA1 is clinically classified into two forms: OCA1A, the most affected subtype, results from a total lack of *TYR* activity, whereas OCA1B is characterized by residual enzyme activity (18). It is impossible to accurately distinguish OCA subtypes based solely on clinical features. Therefore, molecular analysis is important for precise diagnosis and effective genetic counseling. Here, we report a patient affected by OCA. Targeted enrichment and next-generation sequencing (NGS) of 14 genes were performed to discover the causative mutation in this family.

Material and Methods

Subject and Clinical evaluations:

A two-month-old boy was referred to Emam Hossein Children's Hopital. The patient was the only child of a consanguineous Iranian parents, related as first cousins. He was delivered following an uneventful gestation and normal hospital birth. At birth, a weight of 4.2 kg was recorded, with a head circumference of 39 cm and a length of 51 cm. Gray-blue irises, nystagmus and generalized hypopigmentation of the hair, eyelashes, eyebrows, and skin were observed. Additionally, facial abnormalities were noted. However, ophthalmologic

Table 1. A List of genes involved in OCA.

	Symbol	Description	Category	Reference
1	TYR	Tyrosinase	Protein Coding	(30,31)
2	SLC24A5	Solute Carrier Family 24 Member 5	Protein Coding	(30,31)
3	SLC45A2	Solute Carrier Family 45 Member 2	Protein Coding	(30,31)
4	TYRP1	Tyrosinase Related Protein 1	Protein Coding	(30,31)
5	LRMDA	Leucine Rich Melanocyte Differentiation Associated	Protein Coding	(30,31)
6	DCT	Dopachrome Tautomerase	Protein Coding	(30,31)
7	HPS6	HPS6 Biogenesis Of Lysosomal Organelles Complex 2 Subunit 3	Protein Coding	(30,31)
8	HPS4	HPS4 Biogenesis Of Lysosomal Organelles Complex 3 Subunit 2	Protein Coding	(30,31)
9	HPS3	HPS3 Biogenesis Of Lysosomal Organelles Complex 2 Subunit 1	Protein Coding	(30,31)
10	MC1R	Melanocortin 1 Receptor	Protein Coding	(30,31)
11	HPS1	HPS1 Biogenesis of Lysosomal Organelles Complex 3 Subunit 1	Protein Coding	(30,31)
12	HPS5	HPS5 Biogenesis Of Lysosomal Organelles	Protein Coding	(30,31)
13	<i>GPR143</i>	G Protein-Coupled Receptor 143	Protein Coding	(30,31)
14	BLOC1S6	Biogenesis Of Lysosomal Organelles Complex 1 Subunit 6	Protein Coding	(30,31)
15	DTNBP1	Dystrobrevin Binding Protein 1	Protein Coding	(30,31)
16	LRMDA	Leucine-Rich Melanocyte Differentiation-associated protein; LRMDA	Protein Coding	(30,31)
17	AP3B1	Adaptor-Related Protein complex 3, Beta-1 Subunit; AP3B1	Protein Coding	(30,31)
18	MLPH	Synaptotagmin-Like Protein lacking C2 Domains A; SLAC2A.	Protein Coding	(30,31)

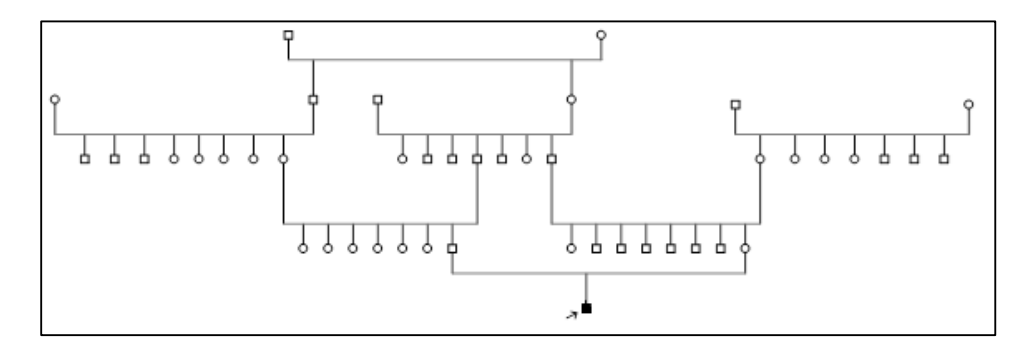


Figure 1. Family pedigree. An infant boy affected by OCA1A resulted from a consanguineous marriage. There is no family history of the disease.

evaluation and examination of internal organs revealed no abnormalities. His mental development was normal. A family history assessment showed no similar phenotype among any first-degree or second-degree relatives (Figure 1). High-performance liquid chromatography (HPLC) amino acid analysis was performed, and all results were within the normal range.

Ethical approval

This study was approved by the ethics community of Isfahan University of Medical Science (2400173). Informed consent was obtained from the parents in accordance with ethics guidelines.

Next generation sequencing experiments

Informed consent was obtained from the parents in accordance with the ethics committee guidelines of (Isfahan University of Medical Sciences). Genomic DNA was extracted from peripheral blood using the standard salting-out method (19,20). Genetic sequencing was carried out using a custom-designed NimbleGen capture chip targeting the genes of TYR, OCA2, TYRP1, SLC45A2, AP3B1, HPS1, HPS3, HPS4, HPS5, HPS6, DTNBP1 and BLOCIS3 (20). Targeted next-generation sequencing was subsequently performed on an Illumina platform (San Diego, CA) at BGI Clinical Laboratories. The sequencing platform covered more than 95% of the target regions with a sensitivity of exceeding 99%. Deletions, duplications, point mutations and microinsertions (<20 bp) were simultaneously detected using tools provided by Thermo Fisher Scientific Inc. (USA).

Results

NGS data analysis revealed sixteen DNA variants in seven genes, one of which was identified as pathogenic (TYR). Three homozygous and two heterozygous variants were found in the OCA2 gene. Four homozygous variants were found within HPS4. Both AP3B1 and HPS5 had two

homozygous variants each. Heterozygous variants were observed in the *HPS1* and *HPS3* genes. Seven synonymous variants, six nonsynonymous variants, and two intronic variants were found (17). The observation of the BAM files through the IGV software showed that the proband was homozygous for the exon 1–5 deletion mutation of the *TYR* gene. According to HGVS nomenclature (21), this variant is designated as NM_000372.5(TYR):c.(1-5)del at the cDNA level. This deletion is expected to disrupt the entire coding sequence of *TYR*, leading to an entire loss of tyrosinase function and fulfills the criteria American college of medical genetics guideline for being categorized as pathogenic.

Discussion

Oculocutaneous albinism (OCA) exists in two forms: syndromic and non-syndromic, and it is a genetically heterogeneous disorder (Table 1). In this study, we presented a case of albinism with facial anomalies and identified the mutation using targeted-enrichment high-throughput sequencing. The results demonstrate the high efficiency of this technique in the molecular analysis of heterogeneous disorders and large genomic aberrations (17). In contrast to African and African-American populations, where *OCA2* is the most common cause of albinism (1, 15, 22), about 60% of Iranian patients have a homozygous or compound heterozygous mutation within *TYR*, in agreement with the Caucasian population (23, 24).

Surprisingly, despite being a rare inherited disease and the elevated prevalence of consanguineous marriages in Iran (25), it most often occurs in such families without previous history, as stated by Khordadpoor-Deilamani et al (24), and mentioned in this report.

Approximately 500 causative mutations have been documented in the Human Gene Mutation Database (HGMD(26)). These mutations are all associated with the single *TYR* gene located on chromosome11q14.3 (13).

While most mutations found within *TYR* are missense mutations, a few small insertions and deletions have been reported (27) (Figure 2). Gross deletions are a rare cause of disease. Therefore, we aimed to gather data on some pathogenic or likely pathogenic deletions in *TYR* and

their associated Phenotype (28) (Table 2).

Whole gene deletions have been previously reported in compound heterozygous states, and the patients had the OCA1B phenotype (10,29). Due to the large deletion, verifying the mutation via Sanger sequencing was not a

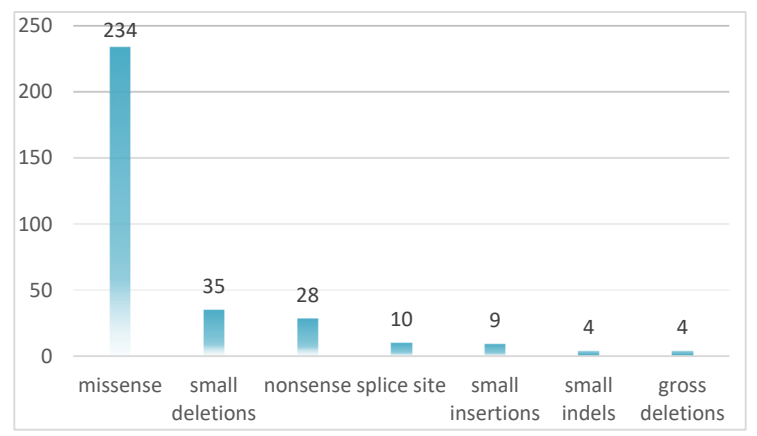


Figure 2. Prevalence of different types of *TYR* mutations. According to human gene mutation database (HGMD) missense mutations are the most common types of mutations found within *TYR*. Small deletion mutations stand at the second place and after that nonsense, splice site and small insertions have the major role respectively. Small indels and gross deletions are not very common in the pathogenesis of the disease.

Table 2. Overview of TYR Gene deletions (28).

Variation	Condition	Classification
NM_000372.5(TYR): c.25del)	Skin/Hair/Eye pigmentation 3, Light/Dark Skin	Pathogenic
NM_000372.5(TYR):c.69del	Skin/Hair/Eye pigmentation 3, Light/Dark Skin	Pathogenic
NM_000372.5(TYR):c.178_179del	Skin/Hair/Eye pigmentation 3, Light/Dark Skin	Pathogenic/Likely pathogenic
NM_000372.5(TYR):c.216del	Tyrosinase-negative oculocutaneous albinism	Pathogenic
NM_000372.5(TYR):c.221_222del	not provided	Pathogenic
NM_000372.5(TYR):c.404_621del	not provided	Pathogenic
NM_000372.5(TYR):c.422del	Skin/Hair/Eye pigmentation 3, Light/Dark Skin	Likely pathogenic
NM 000372.5(TYR):c.466 447del	Skin/Hair/Eye pigmentation 3, Light/Dark Skin	Pathogenic
NM 000372.5(TYR):c.549del	Skin/Hair/Eye pigmentation 3, Light/Dark Skin	Likely pathogenic
NM 000372.5(TYR):c.572del	Skin/Hair/Eye pigmentation 3, Light/Dark Skin	Pathogenic
NM 000372.5(TYR):c.573del	Skin/Hair/Eye pigmentation 3, Light/Dark Skin	Pathogenic
NM 000372.5(TYR):c.580del	not provided	Pathogenic
NM 000372.5(TYR):c.649del	Skin/Hair/Eye pigmentation 3, Light/Dark Skin	Pathogenic
NM_000372.5(TYR):c.692_696del	Skin/Hair/Eye pigmentation 3, Light/Dark Skin	Likely pathogenic
NM_000372.5(TYR):c.696del	not provided	Pathogenic/Likely pathogenic
NM_000372.5(TYR):c.781_784del	not provided	Pathogenic
NM 000372.5(TYR):c.787 790del	not provided	Pathogenic
NM_000372.5(TYR):c.820_3del	Tyrosinase-negative oculocutaneous albinism	Likely pathogenic
NM_000372.5(TYR):c.825_828del	not provided	Pathogenic
NM_000372.5(TYR):c.841del	Skin/Hair/Eye pigmentation 3, Light/Dark Skin	Pathogenic
NM_000372.5(TYR):c.911_914del	not provided	Pathogenic
NM_000372.5(TYR):c.943_948del	nonsyndromic Oculocutaneous Albinism	Likely pathogenic
NM_000372.5(TYR):c.1037-10 1041del	not provided	Pathogenic
NM_000372.5(TYR):c.1059del	Skin/Hair/Eye pigmentation 3, Light/Dark Skin	Likely pathogenic
NM_000372.5(TYR):c.1141_1160del	not provided	Pathogenic
NM_000372.5(TYR):c.1164del	Skin/Hair/Eye pigmentation 3, Light/Dark Skin	Pathogenic
NM_000372.5(TYR):c.1177del	Skin/Hair/Eye pigmentation 3, Light/Dark Skin	Pathogenic
NM_000372.5(TYR):c.1214del	Skin/Hair/Eye pigmentation 3, Light/Dark Skin	Likely pathogenic
NM_000372.5(TYR):c.1237del	not provided	Pathogenic
NM_000372.5(TYR):c.1267del	Tyrosinase-negative oculocutaneous albinism	Pathogenic
NM 000372.5(TYR):c.1322del	Tyrosinase-negative oculocutaneous albinism	Pathogenic

simple task (15). however, employing a quantitative method such as MLPA, array CGH, or quantitative real-time PCR could be considered to assess gene dosage (20).

To our current understanding, this is the first report of a truly homozygous state of This deletion mutation and the first report of whole gene deletion in Iran. As a hypothesis, the mutation may have resulted from unequal crossing over between the gene and its pseudogene on chromosome 11q, which leads to gene deletion. Due to consanguineous marriages, it seems that the mutation has been inherited from a common ancestor.

Conclusion

The results support clinical diagnosis. The phenotypes of the infant and the molecular findings suggest OCA1A. We expect that identifying the mutant gene will significantly improve genetic counseling for the pedigree and assist in future pregnancies. Therefore, the parents and other family members should consider genetic counseling and testing.

Funding

This work was financially supported by Isfahan University of Medical Sciences (Grant No. 197060, 2400173).

Data availability

The datasets used and/or analyzed during the current study are available from the corresponding author on reasonable request.

Conflict of Interest

The authors declare no conflict of interest.

Informed consent

Written informed consent was obtained from all participants in the study and written consent to participate was obtained from the parents of the patient (younger than the age of 16). Written informed consent for publication of clinical details and images was also obtained from all participants and from the parents of participants under the age of 18.

References

- Luo L, Ma M, Yang Y, Zhao H. Case Report: Genetic analysis of oculocutaneous albinism type 2 caused by a new mutation in the OCA2. Front Pediatr [Internet]. 2025 Apr 17 [cited 2025 July 7];13. Available from: https://www.frontiersin.org/journals/pediatrics/articles/10. 3389/fped.2025.1508198/full
- 2. Gargiulo A, Testa F, Rossi S, Di Iorio V, Fecarotta S, de Berardinis T, et al. Molecular and clinical characterization

- of albinism in a large cohort of Italian patients. Invest Ophthalmol Vis Sci. 2011 Mar;52(3):1281–9.
- Grønskov K, Ek J, Brondum-Nielsen K. Oculocutaneous albinism. Orphanet Journal of Rare Diseases. 2007 Nov 2;2(1):43.
- Mártinez-García M, Montoliu L. Albinism in Europe. J Dermatol. 2013 May;40(5):319–24.
- Kamaraj B, Purohit R. Mutational analysis of oculocutaneous albinism: a compact review. Biomed Res Int. 2014;2014:905472.
- Shakil M, Akbar A, Aisha NM, Hussain I, Ullah MI, Atif M, et al. Delineating Novel and Known Pathogenic Variants in TYR, OCA2 and HPS-1 Genes in Eight Oculocutaneous Albinism (OCA) Pakistani Families. Genes. 2022 Mar;13(3):503.
- Bassi MT, Schiaffino MV, Renieri A, De Nigris F, Galli L, Bruttini M, et al. Cloning of the gene for ocular albinism type 1 from the distal short arm of the X chromosome. Nat Genet. 1995 May;10(1):13–9.
- Schnur RE, Gao M, Wick PA, Keller M, Benke PJ, Edwards MJ, et al. OA1 mutations and deletions in X-linked ocular albinism. Am J Hum Genet. 1998 Apr;62(4):800–9.
- Grønskov K, Ek J, Sand A, Scheller R, Bygum A, Brixen K, et al. Birth prevalence and mutation spectrum in danish patients with autosomal recessive albinism. Invest Ophthalmol Vis Sci. 2009 Mar;50(3):1058–64.
- 10.Hutton SM, Spritz RA. Comprehensive analysis of oculocutaneous albinism among non-Hispanic caucasians shows that OCA1 is the most prevalent OCA type. J Invest Dermatol. 2008 Oct;128(10):2442–50.
- 11.Rooryck C, Morice-Picard F, Elçioglu NH, Lacombe D, Taieb A, Arveiler B. Molecular diagnosis of oculocutaneous albinism: new mutations in the OCA1-4 genes and practical aspects. Pigment Cell Melanoma Res. 2008 Oct;21(5):583–7.
- 12. Human tyrosinase gene, mapped to chromosome 11 (q14---q21), defines second region of homology with mouse chromosome 7 PubMed [Internet]. [cited 2025 Mar 14]. Available from: https://pubmed.ncbi.nlm.nih.gov/3146546/
- 13.Giebel LB, Strunk KM, Spritz RA. Organization and nucleotide sequences of the human tyrosinase gene and a truncated tyrosinase-related segment. Genomics. 1991 Mar;9(3):435–45.
- 14.Giebel LB, Spritz RA. RFLP for MboI in the human tyrosinase (TYR) gene detected by PCR. Nucleic Acids Res. 1990 May 25;18(10):3103.
- 15. Cárdenas WA, Conley AB, Nagar SD, Núñez-Ríos DL, Jordan IK, Lattig MC. Ancestral origins of TYR and OCA2 gene mutations in oculocutaneous albinism from two admixed populations in Colombia. PLoS One. 2024 Nov 18;19(11):e0313777.
- 16.Cooksey CJ, Garratt PJ, Land EJ, Pavel S, Ramsden CA, Riley PA, et al. Evidence of the indirect formation of the catecholic intermediate substrate responsible for the autoactivation kinetics of tyrosinase. J Biol Chem. 1997 Oct 17;272(42):26226–35.
- 17.Khan J, Asif S, Ghani S, Khan H, Arshad MW, khan SA, et al. Mutational spectrum associated with oculocutaneous albinism and Hermansky-Pudlak syndrome in nine Pakistani families. BMC Ophthalmology. 2024 Aug 14;24(1):345.

- 18.Tomita Y, Miyamura Y. Oculocutaneous albinism and analysis of tyrosinase gene in Japanese patients. Nagoya J Med Sci. 1998 Oct;61(3–4):97–102.
- 19.Miller SA, Dykes DD, Polesky HF. A simple salting out procedure for extracting DNA from human nucleated cells. Nucleic Acids Res. 1988 Feb 11;16(3):1215.
- 20.Xiao Y, Zhou C, Xie H, Huang S, Wang J, Liu S. NGS-based targeted sequencing identified two novel variants in Southwestern Chinese families with oculocutaneous albinism. BMC Genomics. 2022 Apr 29;23(1):332.
- 21.Den Dunnen JT, Dalgleish R, Maglott DR, Hart RK, Greenblatt MS, McGowan-Jordan J, et al. HGVS Recommendations for the Description of Sequence Variants: 2016 Update. Human Mutation. 2016 June;37(6):564–9.
- 22.Prevalence of albinism in the South African negro PubMed [Internet]. [cited 2025 Mar 14]. Available from: https://pubmed.ncbi.nlm.nih.gov/7064008/
- 23.Ghodsinejad Kalahroudi V, Kamalidehghan B, Arasteh Kani A, Aryani O, Tondar M, Ahmadipour F, et al. Two Novel Tyrosinase (TYR) Gene Mutations with Pathogenic Impact on Oculocutaneous Albinism Type 1 (OCA1). PLoS One. 2014 Sept 12;9(9):e106656.
- 24. Sequence analysis of tyrosinase gene in ocular and

- oculocutaneous albinism patients: introducing three novel mutations PMC [Internet]. [cited 2025 Mar 14]. Available from: https://pmc.ncbi.nlm.nih.gov/articles/PMC4499471/
- 25.Saadat M, Ansari-Lari M, Farhud DD. Consanguineous marriage in Iran. Ann Hum Biol. 2004;31(2):263–9.
- 26.HGMD® home page [Internet]. [cited 2025 Mar 14]. Available from: https://www.hgmd.cf.ac.uk/ac/index.php
- 27. Chan KS, Bohnsack BL, Ing A, Drackley A, Castelluccio V, Zhang KX, et al. Diagnostic Yield of Genetic Testing for Ocular and Oculocutaneous Albinism in a Diverse United States Pediatric Population. Genes. 2023 Jan;14(1):135.
- 28.ClinVar [Internet]. [cited 2025 Mar 14]. Available from: https://www.ncbi.nlm.nih.gov/clinvar/
- 29. Schnur RE, Sellinger BT, Holmes SA, Wick PA, Tatsumura YO, Spritz RA. Type I oculocutaneous albinism associated with a full-length deletion of the tyrosinase gene. J Invest Dermatol. 1996 May;106(5):1137–40.
- 30.Oculocutaneous Albinism MalaCards [Internet]. [cited 2025 Mar 14]. Available from: https://www.malacards.org/card/oculocutaneous_albinism ?#Genes_Related_wrapper
- 31.Home OMIM [Internet]. [cited 2025 Mar 14]. Available from: https://www.omim.org/

Comparison Between HLA-B Allele Groups Among Peripheral Blood Stem Cell Donation Volunteers from Various Iranian Ethnicities

F. Yari^{1*}, F. Sabaghi^{1,2}, N. Bagheri¹, A. Teimurpour¹, M. Zaman-Vaziri¹, F. Mortezapour Barfi¹, M. Sobhani¹

¹ Blood Transfusion Research Center, High Institute for Research and Education in Transfusion, Tehran, Islamic Republic of Iran

Received: 1 July 2024 / Revised: 20 July 2025 / Accepted: 26 August 2025

Abstract

This research included 2064 individuals from various ethnic groups in Iran, all hematopoietic stem cell donors. The primary goal of this research was to establish an HLA database and assess genetic diversity across different ethnicities. DNA was extracted using the magnetic method, and HLA-typing was performed at a low-resolution level using the PCR-SSP method. The results were analyzed manually by independent experts as well as through software. HLA data from four ethnic groups, including Gilak (n=510), Lur (n=465), Kurdish (n=719), and Arab (n=370), were examined for associations between alleles and ethnicity. Allele frequencies were assessed through statistical methods to identify significant relationships, with the significance level set at 0.05. Additionally, standardized residuals were calculated to determine which ethnic groups exhibited allele frequencies that exceeded expected values based on assumptions of independence. Among HLA-B alleles, HLA-B*35 and HLA-B*51 were found to have the highest frequencies, while HLA-B*67, *78, *81, *82, and *83 were absent in this research. Significant differences were observed in 17 alleles across the ethnic groups for HLA-B, with P< 0.05. Standardized residuals exceeding a threshold of 2 indicated statistically significant deviations between observed and expected values at the 0.05 significance level. All analyses were conducted using R software. Determining HLA allele frequencies helps identify similarities and differences among ethnic groups. This information can assist in developing donor services strategies in Iran's diverse regions and establishing stem cell registries. In the future, this data may also contribute to clinical applications in transplantation, vaccine development, and infectious disease research.

Keywords: HLA, Hematopoietic Stem Cell; Donors; Ethnicity; Iran.

Introduction

Human Leukocyte Antigens (HLA) class I and II are

cell surface glycoproteins encoded by genes located on the short arm of chromosome 6. The genomic region housing these genes is called the major

² Hematology Department, Faculty of Allied Medicine, Iran University of Medical Science, Hemmat Highway, Tehran, Islamic Republic of Iran

^{*} Corresponding Author: Tel: +9821 82052115; Email: yarii.fatemeh@gmail.com

histocompatibility complex (MHC) and is typically inherited as a haplotype. The HLA system exhibits the most extraordinary genetic diversity in humans. Specifically, HLA-A, HLA-B, and HLA-C genes encode the corresponding class I antigens A, B, and C, while HLA-DRB1, HLA-DRB3, HLA-DRB4, HLA-DRB5, HLA-DQA1, HLA-DQB1, HLA-DPA1, and HLA-DPB1 encode class II antigens (1). New HLA alleles are continuously being discovered, with over 38,000 (HLA) identified (2).

Population migration and genetic mixing are critical drivers in the evolution and diversification of polymorphic HLA molecules. This wide diversity of alleles is shaped by natural selection and historical demographic events like migrations and population bottlenecks, contributing to human genetic variability. The adaptive importance of HLA variability is underscored by its critical role in the immune response, particularly in pathogen recognition and antigen presentation to T cells (3).

Hematopoietic stem cell transplantation (HSCT) has emerged as a critical treatment for severe blood disorders, and its demand has surged over the last decade as a viable therapeutic option for many malignancies. To minimize graft-versus-host disease (GVHD), matching HLA molecules between donors and recipients across multiple loci is essential, as the degree of compatibility directly influences transplantation outcomes.

Stem cell registries are designed to provide HLA-matched unrelated volunteers for patients awaiting transplantation. However, finding a HLA-compatible hematopoietic stem cell donor is challenging due to the high level of HLA polymorphism. A registry's size and genetic diversity are critical factors in determining the likelihood of finding a suitable donor (4).

Certain diseases are associated with specific HLA antigens in the population, highlighting the importance of investigating HLA-disease associations (5, 6). This research aims to determine the type and frequency of HLA allelic groups in four Iranian ethnic groups to expand the HLA database for patients. Moreover, understanding the prevalence of HLA alleles and haplotypes across different ethnicities is valuable for genetic investigations and insights into population relationships (7-9). Additionally, HLA polymorphism is a valuable tool in anthropological investigations (10, 11).

While HLA-compatible siblings are the preferred donors for transplantation, due to the low likelihood of genetic similarity among siblings and the declining number of family members in many societies, more than 70% of patients require HLA-compatible non-relative donors from stem cell registries. The greater the number of hematopoietic stem cell donors, the higher the chances

of finding a non-relative donor with identical HLA for a patient (12).

Materials and Methods

1. Sample preparation, DNA extraction and HLA-typing by PCR-SSP method

Blood samples were collected from all stem cell donation volunteers at the Iranian Blood Transfusion Organization. Each volunteer provided a 10 mL volume of whole blood, with EDTA as the anticoagulant. The samples were stored at temperatures between 1 and 10°C before being transported to the laboratory. DNA extraction was performed using the magnetic bead method with the MagCore Automated Nucleic Acid DNA Extractor (Switzerland). The PCR-SSP (polymerase chain reaction with sequence-specific primers) method was used for HLA typing. This technique uses sequence-specific primers to target and amplify a particular HLA DNA sequence. It comprises multiple PCR reactions, each specific to an allele or group of alleles. After amplification, the alleles are detected through agarose gel electrophoresis. Since SSP primers target particular DNA sequences, the amplification product confirms the presence of the allele containing that sequence (1). In this method, a kit is used for each sample, and each HLA-ABDR determination kit contains 96 microtubes, with primers specific to the HLA sequences and internal control primers.

For this research, HLA-typing kits from Olerup (Sweden) were the primary kits used, with Innotrain (Germany) kits employed to resolve ambiguities. Each kit contained 24 reactions for HLA-A, 48 reactions for HLA-B, and 24 reactions for HLA-DRB1 allele groups. After PCR, the samples were electrophoresed on a 1.5% agarose gel, and two independent experts analyzed the resulting images. If the image quality was adequate, the bands were counted and interpreted manually and by software.

2. Statistical analysis

This investigation employed the chi-square test to examine the association between ethnicity and allele frequency within the population sample. When applicable, Fisher's exact test was utilized. Standardized residuals were computed to identify notable deviations between the observed and expected allele frequencies under the null hypothesis of independence. A standardized residual with an absolute value greater than 2 indicated a meaningful discrepancy at the 0.05 threshold. All statistical analyses were conducted using R software.

Results

1. HLA-Typing results in the studied population of four Iranian ethnicities

Performing low-resolution HLA-typing tests on the samples of different ethnicities of Gilak (n=510), Lur (n=465), Kurdish (n=719), and Arab (n=370) led to the determination of allelic groups in HLA-A, -B and -DRB1 gene loci in the studied populations.

2. Frequency of Alleles in the Studied Population

The frequencies of allelic groups related to the HLA-A, HLA-B, and HLA-DRB1 gene loci were identified. The highest allelic frequencies for HLA-A in the entire

studied population were HLA-A*02 (19.6%), HLA-A*24 (15.2%), and HLA-A*03 (12.1%). For HLA-B, the most frequent alleles were HLA-B*35 (19%) and HLA-B*51 (14.2%) (Table 1). In terms of HLA-DRB1, the most frequent alleles were HLA-DRB1*11 (22.7%), HLA-DRB1*15 (11.7%), and HLA-DRB1*04 (11.1%). No alleles from the HLA-A*80 and HLA-B*67, *78, *81, *82, and *83 groups were detected in the studied population. Due to the volume of data, the allelic groups for HLA-B are exclusively presented in detail by ethnic group.

Table 1. Frequencies of allelic groups related to HLA-B in the entire studied population

		ntire studied popu		ILA-B III the entire	studied population
HLA-B		Frequency	Percent	Valid Percent	CumulativePercent
Valid	07	187	4.5	4.5	4.5
	08	164	4.0	4.0	8.5
	13	106	2.6	2.6	11.1
	14	85	2.1	2.1	13.1
	15	127	3.1	3.1	16.2
	18	219	5.3	5.3	21.5
	27	93	2.3	2.3	23.8
	35	786	19.0	19.0	42.8
	37	57	1.4	1.4	44.2
	38	153	3.7	3.7	47.9
	39	48	1.2	1.2	49.1
	40	122	3.0	3.0	52.0
	41	162	3.9	3.9	55.9
	42	10	.2	.2	56.2
	44	201	4.9	4.9	61.0
	45	16	.4	.4	61.4
	46	6	.1	.1	61.6
	47	11	.3	.3	61.8
	48	2	.0	.0	61.9
	49	99	2.4	2.4	64.3
	50	200	4.8	4.8	69.1
	51	586	14.2	14.2	83.3
	52	272	6.6	6.6	89.9
	53	37	.9	.9	90.8
	54	6	.1	.1	91.0
	55	189	4.6	4.6	95.5
	56	11	.3	.3	95.8
	57	51	1.2	1.2	97.0
	58	93	2.3	2.3	99.3
	59	1	.0	.0	99.3
	73	27	.7	.7	100.0
	Tot al	4128	100.0	100.0	

HLA-B* 67, *78, *81, *82, *83 allele groups were not detected.

Table 2. Comparison between the frequency distribution of allelic groups in the HLA-B gene locus in 4 ethnic groups of Iran: Lur,

Name	Ethnic	Allele	N (%)	Standardized Residuals	P-value
	Lur	Yes	36(3.87)	-0.18	
HLA-B*08		No	894(96.13)	0.18	
	Gilak	Yes	24(2.35)	-3.05	
		No	996(97.65)	3.05	
					< 0.001
	Arab	Yes	49(6.62)	4.07	
		No	691(93.38)	-4.07	
	Kurd	Yes	55(3.82)	-0.36	
		No	1383(96.18)	0.36	
HLA-B*14	Lur	Yes	16(1.72)	-0.83	
		No	914(98.28)	0.83	
	0.1.1	**	14(1.05)	1.50	
	Gilak	Yes	14(1.37)	-1.78	
		No	1006(98.63)	1.78	0.001
	A1	37	20(2.02)	2.02	0.001
	Arab	Yes	29(3.92)	3.93	
		No	711(96.08)	-3.93	
	VJ	V	26(1.91)	0.82	
	Kurd	Yes	26(1.81)	-0.83	
	T	No V	1412(98.19)	0.83	
ILA-B*15	Lur	Yes	23(2.47)	-1.21 1.21	
1LA-B"15		No	907(97.53)	1.21	
	Gilak	Yes	29(2.75)	-0.71	
	Gliak		28(2.75) 992(97.25)	0.71	
		No	992(97.23)	0.71	< 0.001
	Arab	Yes	45(6.08)	5.22	<0.001
	Alau	No	695(93.92)	-5.22	
		110	073(73.72)	-3.22	
	Kurd	Yes	31(2.16)	-2.5	
	Kuru	No	1407(97.84)	2.5	
	Lur	Yes	29(3.12)	2.02	
ILA-B*27	Lui	No	901(96.88)	-2.02	
		110	y01(y0.00)	2.02	
	Gilak	Yes	14(1.37)	-2.18	
	onui.	No	1006(98.63)	2.18	
			()		0.018
	Arab	Yes	11(1.49)	-1.55	
		No	729(98.51)	1.55	
			, ,		
	Kurd	Yes	39(2.71)	1.45	
		No	1399(97.29)	-1.45	
HLA-B*35	Lur	Yes	188(20.22)	1.04	
		No	742(79.78)	-1.04	
	Gilak	Yes	232(22.75)	3.47	
		No	788(77.25)	-3.47	
					< 0.001
	Arab	Yes	84(11.35)	-5.88	
		No	656(88.65)	5.88	
	Kurd	Yes	282(19.61)	0.68	
		No	1156(80.39)	-0.68	

3. Frequencies of HLA-B Alleles in Different Ethnic Groups

The HLA-B allele frequencies among the studied ethnic groups were also evaluated. As shown in Table 2, 31 allelic groups for HLA-B were compared, and significant differences (P-value < 0.05) were found in 17 of these allelic groups (Table 2).

It should be noted that the results for HLA-B*07, HLA-B*13, HLA-B*18, HLA-B*40, HLA-B*44, HLA-B*47, HLA-B*48, HLA-B*49, HLA-B*54, HLA-B*56, HLA-B*57, HLA-B*73, HLA-B*46, and HLA-B*59 were not statistically significant between the ethnic groups.

Table 2. Continued						
Name	Ethnic	Allele	N (%)	Standardized Residuals	P-value	
HLA-B*37	Lur	Yes	5(0.54)	-2.5		
		No	925(99.46)	2.5		
	0.1.1	**	25(2.45)	2.20		
	Gilak	Yes	25(2.45)	3.38		
		No	995(97.55)	-3.38	0.001	
	A	V	4(0.54)	2.16	0.001	
	Arab	Yes No	4(0.54)	-2.16 2.16		
		INO	736(99.46)	2.10		
	Kurd	Yes	23(1.60)	0.88		
	12010	No	1415(98.40)	-0.88		
HLA-B*38	Lur	Yes	33(3.55)	-0.29		
112.12.00	241	No	897(96.45)	0.29		
			()			
	Gilak	Yes	30(2.94)	-1.49		
		No	990(97.06)	1.49		
					0.016	
	Arab	Yes	42(5.68)	3.13		
		No	698(94.32)	3.13		
	Kurd	Yes	48(3.34)	-0.92		
	_	No	1390(96.66)	0.92		
HLA-B*39	Lur	Yes	12(1.29)	0.41		
		No	918(98.71)	-0.41		
	CT-1	37	20(1.06)	2.74		
	Gilak	Yes	20(1.96)	2.74		
		No	1000(98.04)	-2.74	0.0257	
	Arab	Yes	5(0.68)	-1.36	0.0237	
	Huo	No	735(99.32)	1.36		
		110	755(55.52)	1.50		
	Kurd	Yes	11(0.76)	-1.74		
		No	1427(99.24)	1.74		
	Lur	Yes	37(3.98)	0.1		
		No	893(96.02)	-0.1		
	Gilak	Yes	50(4.90)	1.85		
HLA-B*41		No	970(95.10)	-1.85	< 0.001	
	Arab	Yes	41(5.54)	2.5		
		No	699(94.46)	-2.5		
	171	V	24(2.20)	2.77		
	Kurd	Yes	34(2.36)	-3.77 2.77		
	Ι	No Yes	1404(97.64)	3.77 -0.95		
HLA-B*42	Lur	y es No	1(0.11)	-0.95 0.95		
11L/A-D"44		110	929(99.89)	0.73		
	Gilak	Yes	1(0.10)	-1.08		
	Gliak	No	1019(99.90)	1.08		
		110	1017(77.70)	1.00	0.018	
	Arab	Yes	6(0.81)	3.47		
		No	734(99.19)	-3.47		
			` /			
	Kurd	Yes	2(0.14)	-0.99		
		No	1436(99.86)	0.99		

Discussion

This research focused on HLA-A, HLA-B, and HLA-DRB1 loci polymorphism among four Iranian ethnic groups: Lur, Gilak, Kurd, and Arab. The study identified the frequencies of HLA allelic groups and observed

significant variations in the frequency of specific HLA-B alleles across the ethnicities (Table 2). When an important relationship was detected (P-value < 0.05), it indicated an association between the allele and the ethnicity. Further analysis using standardized residuals helped determine whether a specific ethnic group

Table 2. Continued						
Name	Ethnic	Allele	N (%)	Standardized Residuals	P-value	
HLA-B*45	Lur	Yes	3(0.32)	-0.36		
		No	927(99.68)	0.36		
	0.1.1	***	2(0.2)	1.12		
	Gilak	Yes	2(0.2)	-1.13		
		No	1018(99.8)	1.13	0.022	
	A	Yes	0(1.00)	2.25	0.022	
	Arab	No	8(1.08) 732(98.92)	3.35 -3.35		
		NO	132(96.92)	-3.33		
	Kurd	Yes	3(0.21)	-1.35		
	12414	No	1435(99.79)	1.35		
HLA-B*50	Lur	Yes	34(3.66)	-1.92		
		No	896(96.34)	1.92		
			,			
	Gilak	Yes	29(2.84)	-3.43		
		No	991(97.16)	3.43		
					< 0.001	
	Arab	Yes	57(7.7)	4		
		No	683(92.3)	-4		
	Kurd	Yes	80(5.56)	1.57		
TT 4 D4#4	.	No	1358(94.44)	-1.57		
HLA-B*51	Lur	Yes	170(18.28)	4.05		
		No	760(81.72)	-4.05		
	Gilak	Yes	95(9.31)	5 15		
	Gliak	No	925(90.69)	-5.15 5.15		
		NO	923(90.09)	5.15	< 0.001	
	Arab	Yes	69(9.32)	-4.19	\0.001	
	Huo	No	671(90.68)	4.19		
		110	071(50.00)	,		
	Kurd	Yes	252(17.52)	4.48		
		No	1186(82.48)	-4.48		
HLA-B*52	Lur	Yes	50(5.38)	-1.69		
		No	880(94.62)	1.69		
	Gilak	Yes	87(8.53)	2.88		
		No	933(91.47)	-2.88		
					0.029	
	Arab	Yes	46(6.22)	-0.45		
		No	694(93.78)	0.45		
	Kurd	Yes	80(6.10)	-0.76		
	Kuru	No	89(6.19) 1349(93.81)	0.76		
HLA-B*53	Lur	Yes	3(0.32)	-2.11		
IILA-D 33	Lui	No	927(99.68)	2.11		
		110	727(77.00)	2.11		
	Gilak	Yes	8(0.78)	-0.44		
		No	1012(99.22)	0.44		
			()		0.021	
	Arab	Yes	13(1.76)	2.74		
		No	727(98.24)	-2.74		
	Kurd	Yes	13(0.9)	0.04		
		No	1423(99.1)	-0.04		

exhibited a higher or lower allele frequency. Under the independence assumption, absolute values exceeding 2 for standardized residuals indicated significant differences between observed and expected frequencies. Positive residuals indicate that the observed frequency

exceeded the expected value, whereas adverse residuals suggest the observed frequency was lower than anticipated.

The HLA-B*67, B*78, B*81, B*82, and B*83 allelic groups were not observed in the overall population

Table 2. Continued

Name	Ethnic	Allele	N (%)	Standardized Residuals	P-value
HLA-B*55	Lur	Yes	42(4.52)	-0.1	- 133-0-0
TILLY D GG	Dui	No	888(95.48)	0.1	
	~				
	Gilak	Yes	82(8.04)	6.09	
		No	938(91.96)	-6.09	< 0.001
	Arab	Yes	9(1.22)	-4.83	
		No	731(98.78)	4.83	
	Kurd	Yes	56(3.89)	-1.54	
	11010	No	1382(96.11)	1.54	
	Lur	Yes	14(1.51)	-1.75	
HLA-B*58	Lui	No	916(98.49)	1.75	
	Gilak	Yes	22(2.14)	2.19	
	Gilak		32(3.14)		
		No	988(96.86)	-2.19	
					0.014
	Arab	Yes	23(3.11)	1.73	
		No	717(96.89)	-1.73	
	Kurd	Yes	24(1.67)	-1.85	
		No	1414(98.33)	1.85	

studied. The most common alleles for HLA-B were HLA-B*35 (19%) and HLA-B*51 (14.2%). Research conducted by Shaigan in 2011, which examined the allelic frequencies of HLA-A, HLA-B, and HLA-DRB1 in 244 individuals from the Fars ethnic group in Iran, reported results that aligned closely with the findings in the general population (13).

Abedini and colleagues performed a systematic review and meta-analysis of HLA allele frequencies in Iranian populations. Their reported frequencies were also similar to those of this research. For instance, the two most common alleles, HLA-B*35 and HLA-B*51, were observed at 19% and 14.2%, respectively, closely matching Abedini's 18% and 14% findings. However, differences were noted for rare alleles such as HLA-B*42 and HLA-B*45, which were absent (0%) in Abedini's research but appeared at 0.2% and 0.4% in this research. These discrepancies could be attributed to the larger sample size in this research (14).

An exciting aspect of this investigation was the variation in allele frequencies among different ethnic groups compared to the overall population. For instance, in the general population, HLA-B*35 had a frequency of 19%, and HLA-B*52 had a frequency of 14.2% (Table 1). However, in the Arab population, these frequencies were lower, with HLA-B*35 at 11.35% and HLA-B*52 at 9.32% (Table 2). Conversely, specific alleles, like HLA-B*15, had a higher frequency in the Arab population (6.08%) compared to the total population (3%). Similar trends were observed in other Arab populations. For instance, HLA-B*35 was highly

prevalent among Palestinians (20.3%) and Lebanese-Armenians (19.8%). In contrast, HLA-B*35 was found at varying frequencies in Iraqi Kurds (15.6%), Omanis (15.3%), Jordanians (14.9%), and Arab Emiratis (11.1%). The second most frequent allele, HLA-B*51, was also common among Saudis (19.3%), Omanis (17.5%), and Arab Emiratis (15.6%) (15).

In 2017, Shaheswar and colleagues conducted genomic research analyzing the distribution of HLA-A and HLA-B alleles in the Lak population of Lorestan Province. This research aimed to compare these findings with data from the broader Iranian population. Their results showed significant parallels with the Lur population in this research. For example, the frequency of HLA-B*35 was 20.22% among Lurs, compared to 24% among the Lak population (P< 0.05). Similarly, HLA-B*51 was found at 18.28% among Lurs and 16% in the Lak population (P< 0.05). Both investigations showed strong agreement in allele frequencies for common alleles; however, differences were observed in the less common alleles. For instance, HLA-B*48 and HLA-B*55 were found at 0.11% and 4.52%, respectively, compared to 1% for both alleles in Shaheswar's research (P-value < 0.05). These variations may result from the distinct subpopulations studied. Shaheswar's research focused exclusively on the Lak population, while this research included the Lur population. Furthermore, Shaheswar's research had a sample size of 100 individuals, while this research involved 465 participants (16).

Suarez-Trujillo and colleagues researched the

prevalence of HLA alleles in Saqqez-Baneh Kurds in Iran. Their findings reported frequencies for common alleles such as HLA-B*35:01 (21.67%), HLA-B*51:01 (9.17%), HLA-B*18:01 (5.83%), and HLA-B*50:01 (5.83%). This research yielded similar results to Suarez-Trujillo's research; however, there was a notable difference in the frequency of HLA-B*51 (P-value < 0.05). In the Kurdish population of this study, HLA-B*51 was recorded at 17.52%, compared to 9.17% in Suarez-Trujillo's research. This discrepancy may be attributed to the distinct Kurdish subpopulations examined in the two investigations. While Suarez-Trujillo's research focused solely on Saqqez-Baneh Kurds, this research included Kurds from various regions of Iran (17,18).

It is noteworthy that Hajighasemi and his team discovered prevalent HLA Class I and II alleles within the Iranian population through an immunoinformatic analysis of the database (www.allelefrequencies.net). This information could prove to be significant for vaccine development, organ transplantation, and donor matching. According to their research, the most frequently observed HLA-B alleles were HLA-B*35 (13%), B*51 (12%), and B*53 (13%). The findings of this study were consistent with Hajighasemi research (19).

Conclusion

Analyzing the distribution of HLA alleles across various ethnic populations reveals commonalities and distinctions within allelic groups. This analysis is critical in improving the efficiency of donor center programs in different regions and optimizing stem cell donation registries. The findings from this research can potentially drive groundbreaking clinical progress in fields like transplantation, vaccine creation, uncovering the genetic factors influencing drug responses, and combating infectious diseases.

Conflict of interest

No conflicts of interest were disclosed by the authors.

Acknowledgements

This article is the result of a research project approved and financially supported by the Iran Ministry of Health and Medical Education with the ethics code IR.TMI.REC.1397.026 obtained in the Blood Transfusion Research Center, High Institute for Research and Education in Transfusion Medicine, Tehran. We hereby thank the Ministry of Health and Medical Education for its financial support.

References

1. Eisenbrey AB. HLA System. Technical Manual. 20 ed:

- AABB; 2023. p. 479-99.
- Patel NN, Avlonitis VS, Jones HE, Reeves BC, Sterne JA, Murphy GJ. Indications for red blood cell transfusion in cardiac surgery: a systematic review and meta-analysis. The Lancet Haematology. 2015 Dec;2(12):e543-53. PubMed PMID: 26686409. Epub 2015/12/22. eng.
- Tokić S, Žižkova V, Štefanić M, Glavaš-Obrovac L, Marczi S, Samardžija M, et al. HLA-A,-B,-C,-DRB1,-DQA1, and-DQB1 allele and haplotype frequencies defined by next generation sequencing in a population of East Croatia blood donors. Scientific reports. 2020;10(1):5513.
- Gragert L, Eapen M, Williams E, Freeman J, Spellman S, Baitty R, et al. HLA match likelihoods for hematopoietic stem-cell grafts in the US registry. New England Journal of Medicine. 2014;371(4):339-48.
- Sarafnezhad A, Khosravi F, ALI MK, Dianat S, Ansaripour B, Moradi B, et al. HLA class II allele and haplotype frequencies in iranian patients with acute myelogenous leukemia and control group. 2006.
- Yari F, Sobhani M, Sabaghi F, Zaman-Vaziri M, Bagheri N, Talebian A. Frequencies of HLA-DRB1 in Iranian normal population and in patients with acute lymphoblastic leukemia. Archives of medical research. 2008;39(2):205-8.
- Farjadian S, Naruse T, Kawata H, Ghaderi A, Bahram S, Inoko H. Molecular analysis of HLA allele frequencies and haplotypes in Baloch of Iran compared with related populations of Pakistan. Tissue antigens. 2004;64(5):581-7.
- 8. Farjadian S, Ghaderi A. HLA class II similarities in Iranian Kurds and Azeris. International journal of immunogenetics. 2007;34(6):457-63.
- Farjadian S, Ghaderi A. HLA class II genetic diversity in Arabs and Jews of Iran. Iranian journal of Immunology. 2007;4(2):85-93.
- 10.Farjadian S, Ghaderi A. Iranian Lurs genetic diversity: an anthropological view based on HLA class II profiles. Iranian Journal of Immunology. 2006;3(3):106-13.
- 11.Farjadian S, Ota M, Inoko H, Ghaderi A. The genetic relationship among Iranian ethnic groups: an anthropological view based on HLA class II gene polymorphism. Molecular biology reports. 2009;36:1943-50.
- Shaiegan M, Zolgaghari Anaraki S. Unrelated stem cell donor registries in the world and Iran. Scientific Journal of Iran Blood Transfus Organ. 2014;11(2):164-76.
- 13. Shaiegan M, Yari F, Abolghasemi H, Bagheri N, Paridar M, Heidari A, et al. Allele frequencies of HLA-A, B and DRB1 among people of Fars ethnicity living in Tehran. مجله ی خون و سرطان ایران. ۲۰۱۱;۲۰۱۱ فون و سرطان ایران.
- 14. Abedini F, Rahmanian N, Heidari Z, Feizi A, Sherkat R, Rezaei M. Diversity of HLA class I and class II alleles in Iran populations: Systematic review and Meta-Analaysis. Transplant Immunology. 2021;69:101472.
- Hajjej A, Almawi WY, Arnaiz-Villena A, Hattab L, Hmida
 The genetic heterogeneity of Arab populations as inferred from HLA genes. PloS one. 2018;13(3):e0192269.
- 16.Shahsavar F, Varzi A-M, Ahmadi SAY. A genomic study on distribution of human leukocyte antigen (HLA)-A and HLA-B alleles in Lak population of Iran. Genomics Data. 2017;11:3-6.
- 17. Suarez-Trujillo F, Juarez I, Palacio-Gruber J, Martín-Villa

- JM, Amirzargar A, Arnaiz-Villena A. HLA genetic study in Iran Saqqez-Baneh Kurds: no genetic trace of Aryan invasions in Anatolian Turks and Kurds is found. Human Immunology. 2022;83(11):737-8.
- 18. Yari F, Teimourpour A, Zaman vaziri M, Sabaghi F, Bagheri N,Mortezapour Barfi F. The genetic diversity of the HLA-B*35 and HLA-B*51allele groups among ethnicities in Iran. Sci J Iran Blood Transfus Organ.
- 2024;21(3):207-13.
- 19.Hajighasemi F, Shirkavand A. Determination of most frequent major histocompatibility complex alleles in Iranian population by immunoinformatic. Journal of Basic and Clinical Pathophysiology. 2024;12(2):38-42.

On Projection Invariant Rickart Modules

Y. Maleki¹, A. Moussavi^{1*}, Y. Kara²

Department of Pure Mathematics, Faculty of Mathematical Sciences, Tarbiat Modares University, Tehran, Islamic Republic of Iran
Department of Mathematics, Bursa Uludağ University, Görükle, 16059 Bursa, Turkey

Received: 25 July 2025 / Revised: 11 August 2025 / Accepted: 16 September 2025

Abstract

This study examined π -Rickart modules, a module-theoretic analog of π -Rickart rings, from the perspective of their endomorphism rings. It is shown that π -Rickart conditions are located between π -e. Baer and p.q.-Baer conditions, and it is established that the corresponding endomorphism ring possesses the appropriate π -Rickart property. Besides, the notion of π -e.AIP modules is presented. Furthermore, connections to the aforementioned concepts of π -Rickart, endo-AIP, and π -e.AIP modules are examined.

Keywords: Baer modules; Rickart ring; Endomorphism rings; Annihilators; Rickart modules.

Introduction

This study operated within the ring and module theory framework, where R represents a ring with a non-zero identity, and M is a unitary right R-module. The notation S signifies the ring of R-endomorphisms of M. We further define, $l_S(X)$ and $r_M(X)$ as the left and right annihilators of a X within S and M, respectively, and I(R) as the subring of R generated by its idempotent elements.

Based on (1) and (2), a ring R is referred to as (quasi-)Baer if, for any nonempty subset (or ideal) Y of R, it holds that $r_R(Y) \leq_{\bigoplus} R_R$. Furthermore, R is designated right Rickart (3) if, given each $x \in R$, $r_R(x) \leq_{\bigoplus} R_R$. These classes of modules have applications in functional analysis. The concept of Rickart rings was initially introduced in (3) and has since been extensively studied by various researchers, including (4-9).

The aforementioned ring-theoretic concepts are naturally generalized to the module setting. Specifically, as delineated in (10), M_R is defined as (quasi-)Baer if, for every (fully invariant) submodule K of M_R , $l_S(K) \leq_{\bigoplus} {}_S S$. The notion of p.q.-Baer modules, as

introduced in (11), pertains to M_R where $r_M(\psi S) \leq_{\bigoplus} M_R$ for every $\psi \in S$. Moreover, based on (12), a module M_R is classified as Rickart if, for each $\psi \in S$, $Ker\psi = r_M(\psi) \leq_{\bigoplus} M_R$. The absence of symmetry in the Rickart ring property, unlike in the Baer and quasi-Baer conditions, motivates the introduction of \mathfrak{L} -Rickart modules. A module M_R is referred to as \mathfrak{L} -Rickart (13) if, for every $y \in M$, $l_S(y) \leq_{\bigoplus} SS$.

A right (or left) ideal A in a ring R is called *projection invariant* if, for every element e in R such that $e^2 = e$, ideal A remains unchanged when multiplied by e, i.e., $eA \subseteq A$. The concept of π -Baer rings is introduced in (14), is based on these kinds of ideals. A ring R is termed π -Baer if, for any projection-invariant left ideal X of R, $r_R(X) \leq_{\bigoplus} R_R$. Moreover, this idea extends to modules, where a submodule P of M_R is projection invariant if, for all idempotent elements $g \in S$, submodule satisfies $g(P) \subseteq P$, meaning it is preserved under multiplication by g. A module M_R is defined as π -e.Baer (15) if every projection-invariant submodule P of M_R satisfies $l_S(P) \leq_{\bigoplus} SS$. In recent studies, a more generalized form of π -Baer rings, called π -Rickart rings, was introduced.

^{*} Corresponding author: Tel: +98(21)82883446; Email: moussavi.a@modares.ac.ir and a.moussavi@gmail.com

As described in (16), a ring R is defined as left π -Rickart if, for any element $x \in R$, $l_R(I(R)x) \leq_{\bigoplus} {}_RR$. As with the Rickart ring condition, π -Rickart ring condition does not generally possess symmetry between the left and right aspects. For more results related to this concept, see (17-20).

Motivated by these studies, we aimed to explore the concepts of π -Rickart from rings to modules. We define M_R as π -Rickart if $r_M(\psi I(S)) \leq_{\bigoplus} M_R$ for all $\psi \in S$. It is apparent that R being a right π -Rickart ring is equivalent to R_R being a π -Rickart module. This new module classification is situated between p.q.-Baer modules and π -e.Baer modules. In our most recent study (21), we investigated π -endo.Rickart modules, which are an extension of the concept of left π -Rickart rings. The introduction of the concept of π -Rickart modules was motivated by the fact that the left and right π -Rickart properties are not necessarily symmetric, as previously mentioned. Thus, we found an interesting result stating that the endomorphism ring of a π -Rickart module is a right π -Rickart ring. However, this property does not generally hold for π -endo. Rickart modules.

In Section 1, we introduced π -Rickart modules and explored their fundamental properties. We established that a module M is π -Rickart if and only if, for every finitely generated left ideal Y of S, $r_M(YI(S)) \leq_{\bigoplus} M_R$ holds (Proposition 2.8). We showed that π -e.Baer modules are equivalent to π -Rickart modules satisfying FI-SSIP condition (Proposition 2.21). We investigate when the direct summand of a π -Rickart module retains this property (Theorem 2.10). Moreover, we established that the ring of endomorphisms of a π -Rickart module forms a right π -Rickart ring (Theorem 2.11). An analogous version of Chatters and Khuri's Theorem is derived for π -Rickart modules (Corollary 2.17). Therefore, for a right hereditary, right noetherian ring R, every injective right R-module M is π -e.Baer if and only if M is π -Rickart (Corollary 2.22). For an indecomposable artinian π -Rickart module M, the ring of endomorphisms of M is a division ring (Corollary 2.7). Furthermore, M is π -e.Baer if and only if M is π -Rickart and the set $\{Se | e \in S_r(S)\}$ is a complete lattice (Theorem 2.25).

In Section 2, we explore the concept of π -e.AIP modules, which encapsulated the definitions of π -Rickart and π -e.Baer modules, extending their applicability to a broader class of modules. The interconnections between π -Rickart, endo-AIP, and π -e.AIP modules are explored (Theorem 3.2). We investigated the conditions in which the characteristics of π -e.AIP, Rickart, and π -Rickart modules coincide (Proposition 3.4). Furthermore, we examine the theoretical characteristics of π -e.AIP modules. The characteristic of π -e.AIP is not preserved

by direct summands or direct sums, as seen in Example 3.8. We therefore investigated the circumstances under which the aforementioned property was inherited by direct summands and direct sums (Theorems 3.6 and 3.9). We also show that the ring of endomorphisms of a π -e.AIP module is left π -AIP (Theorem 3.11).

The notations $N \subseteq M$, $N \le M$, $N \le M$, $N \le_p M$, $N \le_{\bigoplus} M$, and $N \le_{\Longrightarrow} M$ signify that N is a subset, a right R-submodule, a fully invariant R-submodule, a projection invariant right R-submodule, a direct summand of M, and an essential submodule of M, respectively. Recall that an idempotent element $g \in R$ is termed left (right) semicentral if tg = gtg (gt = gtg) for all $t \in R$. The sets of left and right semicentral idempotents are denoted as $S_l(R)$ and $S_r(R)$, respectively. A ring R is abelian if its idempotents commute with all elements of R, and a module is abelian if the ring of its endomorphisms is abelian.

Results and Discussion

1 π - Rickart modules

The discussion on π -Rickart modules was initiated in this section, with an emphasis on their key attributes. Given the connections between Baer and Rickart modules, our objective was to explore the connections between π -e.Baer and π -Rickart modules. Additionally, we investigate the connections between extending modules and nonsingular modules by analyzing the properties of projection-invariant extending modules and projection-invariant nonsingular modules. Furthermore, we investigate the endomorphism ring of π -Rickart modules. The results that were employed throughout the investigation are summarized below for the sake of comprehensiveness.

Lemma 2.1 [(22), Lemma 1.1] The followings are equivalent for an idempotent element $f \in R$:

- (1) $f \in S_l(R)$.
- (2) $1 f \in S_r(R)$.
- (3) (1 f)Rf = 0.
- (4) $fR \leq R$.
- $(5) R(1-f) \le R.$
- (ii) $S_l(R) \cap S_r(R) = B(R)$, where B(R) is the set of central idempotents.

Lemma 2.2 [(15), Lemma 3.1](i) Let $M = \bigoplus_{i \in I} M_i$ and $N \preceq_p M$. Then, $N = \bigoplus_{i \in I} N \cap M_i$ and $N \cap M_i \preceq_p M_i$ for all $i \in I$.

(ii) Let M be a module. Then, $e \in S_l(S)$ if and only if $eM \trianglelefteq_p M$.

Definition 2.3 We call M_R is π -Rickart, if for any $\eta \in S$, there exists an idempotent element $f \in S$ such that $r_M(\eta I(S)) = fM$.

Note that the idempotent f in Definition 2.3 belongs

to $S_i(S)$ by Lemma 2.2.

Example 2.4(*i*) Every abelian von Neumann regular (strongly regular) ring is also π -Rickart.

- (ii) The module R_R is π -Rickart if and only if the ring R is a right π -Rickart ring.
- (iii) The classes of semisimple modules, Baer modules, and π -e.Baer modules are each examples of π -Rickart modules.
- (iv) Consider the ring R given by $R = \begin{pmatrix} A & H \\ 0 & \mathbb{C} \end{pmatrix}$, where A denotes a Banach subalgebra of the ring of bounded linear operators acting on a Hilbert space H, with the additional condition that A contains all rank 1 idempotents. As indicated in [(16), Example 3.12], R is a π -Baer ring and thus it is π -Rickart. Furthermore, by Theorem 2.10, it follows that eR also is a π -Rickart module, where $e = \begin{pmatrix} 1 & 0 \\ 0 & 0 \end{pmatrix}$.

 (v) \mathbb{Z}_p^{∞} is an injective \mathbb{Z} -module, but it does not
- (v) $\mathbb{Z}_{p^{\infty}}$ is an injective \mathbb{Z} -module, but it does not qualify as π -Rickart.

In the forthcoming theorem, we showed that π -Rickart modules constitute a discrete category situated between π -e.Baer and p.q.-Baer modules.

Proposition 2.5 M_R is π -e.Baer $\Rightarrow M_R$ is π -Rickart $\Rightarrow M_R$ is p.q.-Baer.

Proof. Assume M_R is a π -e.Baer module. For any $\psi \in S$, $S\psi I(S)$ constitutes a left ideal of S that is projection invariant. Consequently, we have $g^2 = g \in S$ for which $r_M(\psi I(S)) = r_M(S\psi I(S)) = gM$. Thus, M_R is π -Rickart. Now, suppose M_R is π -Rickart. Then, for any $\psi \in S$, we have $g^2 = g \in S$ such that $r_M(\psi I(S)) = gM$. As $\psi I(S) \subseteq \psi S$, it follows that $r_M(\psi S) \subseteq r_M(\psi I(S)) = gM$. Additionally, since $g \in S_l(S)$, we have $(\psi S)gM = (\psi g)(gSgM) \subseteq (\psi I(S))gM = 0$. Hence, $r_M(\varphi S) = gM$, and thus M is p.q.-Baer.

The subsequent example serves to show that the implications stated in Proposition 2.5 are not generally reversible.

Example 2.6 (i) Consider the subring T of $\prod_{n=1}^{\infty} A_n$, where $A_n = \mathbb{Z}$ for $n = 1, 2, \cdots$, defined as $T = \{(a_n) \in \prod_{n=1}^{\infty} A_n | a_n \text{ is eventually constant}\}$. Then T_T is a π -Rickart module, which is not π -e.Baer [(16), Example 1.6].

- (ii) The ring of endomorphisms of a π -e.Baer module is a π -e.Baer ring by [(15), Theorem 2.5]. Let B be a π -Rickart ring that is not a π -Baer ring (see, [(16), Example Example 1.6]). Consider the ring $R = \begin{bmatrix} B & B \\ 0 & B \end{bmatrix}$ and idempotent $g = \begin{bmatrix} 1 & 0 \\ 0 & 0 \end{bmatrix} \in R$. Then, based on Theorem 2.10, $M_R = gR$ is a π -Rickart module. However, since $End_R(M) \cong B$ is not a π -Baer ring, M_R is not a π -e.Baer module.
 - (iii) Suppose R is a simple ring that only has trivial

idempotents $\{0,1\}$, and is not a domain (see, (23)). Then, R is a quasi-Baer ring and therefore p.q-Baer. It can be easily verified that R does not satisfy the right π -Rickart property. Consequently, $M = R_R$ is not π -Rickart.

Proposition 2.7 (i) For an indecomposable module M_R , being π -Rickart, Baer, and π -e.Baer are equivalent properties.

(ii) If M_R is an indecomposable artinian π -Rickart module, then $End_R(M)$ is a division ring.

Proof. (i) It is straightforward, as M_R is indecomposable.

(ii) It follows from the part (i) and [(12), Corollary 4.11].

Proposition 2.8 The following conditions are equivalent for M_R .

- 1. M_R is π -Rickart.
- 2. For every finite subset $X = \{\varphi_1, ..., \varphi_n\}$ of S, $r_M(XI(S)) \leq_{\bigoplus} M$.
- 3. For each finitely generated left ideal Y of S, $r_M(YI(S)) \leq_{\bigoplus} M$.

Proof. (i) \Rightarrow (ii) It can be verified that $r_M(XI(S)) = r_M(\varphi_1I(S)) \cap \ldots \cap r_M(\varphi_nI(S))$. Since M is π -Rickart, we can find elements $g_j \in S_l(S)$ such that $r_M(\varphi_jI(S)) = g_jM$ for each $j \in \{1,2,\ldots\}$. Therefore, $r_M(XI(S)) = \bigcap_{i=1}^n g_iM = gM$, where $g = g_1g_2 \cdots g_n \in S_l(S)$.

- $(ii) \Rightarrow (iii)$ It is straightforward.
- $(iii) \Rightarrow (i)$ It is evident because every principal left ideal is finitely generated.

The following example shows that a direct summand of a π -Rickart module may not necessarily be π -Rickart, in general.

Example 2.9 Consider a prime ring R where R_R is uniform and $Z(R_R) \neq 0$. Now, let's consider the free module $A_R = \bigoplus_{i=1}^n R_i$ where $R_i \cong R$ for each $1 \leq i \leq n$. Based on [(15), Example 4.1], we can deduce that A_R is π -e.Baer. Using Proposition 2.5, we can further deduce that A_R is π -Rickart. However, since each one sided ideal of R is projection invariant and R is not Rickart, we can conclude that R_R is not π -Rickart.

The forthcoming theorem establishes the conditions under which a direct summand of a π -Rickart module is π -Rickart.

Theorem 2.10 Direct summands that are projection invariant in π -Rickart modules remain π -Rickart.

Proof. Let M be π -Rickart and N be a projection invariant direct summand of M_R . Then, there exist $e^2 = e \in S$ such that N = eM and $E \cong eSe$, where $E = End_R(N)$. Note that $e \in S_l(S)$, as $N \preceq_p M$. Observe that $\varphi = e\varphi e$, so I(E) = eI(S)e. For every $n \in r_N(\varphi I(E))$, n = en. So $\varphi I(S)n = e\varphi eI(S)en = \varphi(eI(S)e)n = \varphi I(E)n = 0$, and hence $r_N(\varphi I(E)) \subseteq r_M(\varphi I(S)) \cap N$. Now let $x \in r_M(\varphi I(S)) \cap N$ we have $x = ex \in N$ and

 $\varphi I(E)x = \varphi eI(S)ex = \varphi I(S)x = 0$. This implies that $r_N(\varphi I(E)) = r_M(\varphi I(S)) \cap N$. Since M is π -Rickart, $r_M(\varphi I(S)) = fM$ for some $f^2 = f \in S$. Hence $r_M(\varphi I(S)) \cap N = fM \cap eM = (efe)eM$, and efe is an idempotent of eSe. Therefore $r_N(\varphi I(E)) = (efe)eM \leq_{\oplus} eM = N$.

Theorem 2.11 The endomorphism ring of a π -Rickart module is a right π -Rickart ring.

Proof. Consider M as a π -Rickart module. For every $\psi \in S$, there is $g^2 = g \in S$ such that $r_M(\psi I(S)) = gM$. Consequently, $\psi I(S)g = 0$, implying $gS \subseteq r_S(\psi I(S))$. Now, let $\alpha \in r_S(\psi I(S))$. Hence, $\psi I(S)\alpha = 0$, which leads to $\alpha(M) \subseteq r_M(\psi I(S))$. This implies $\alpha = g\alpha$, so $r_S(\psi I(S)) = gS$. Therefore, S is right π -Rickart.

Corollary 2.12 Let R be a right π -Rickart ring and $e \in S_l(R)$. Then eRe is also a right π -Rickart ring.

Proof. Since $e \in S_l(R)$, it follows from Lemma 2.2 that $eR \trianglelefteq_p R$. Note that $End_R(eR) \cong eRe$. Thus, the conclusion is derived from Theorem 2.10 and 2.11.

The following example shows that the converse of Theorem 2.11 does not hold, in general.

Example 2.13 Let $C = \begin{bmatrix} \mathbb{Z} & \mathbb{Z}_2 \\ 0 & \mathbb{Z}_2 \end{bmatrix}$ and $g = \begin{bmatrix} 1 & 0 \\ 0 & 0 \end{bmatrix} \in \mathcal{C}$. Consider $M_C = gC$. Then $End_C(M)$ is a π -Rickart ring. However M_C is not a π -Rickart module.

As defined in [20], M_R is called *local-retractable* if, for each $\emptyset \neq A \subseteq S$ and for any $0 \neq m \in r_M(A)$, there exists a homomorphism $\psi_m : M \to r_M(A)$ with $m \in \psi_m(M) \subseteq r_M(A)$. Local-retractability paves the way for the establishment of the converse of Theorem 2.11.

Theorem 2.14 Let M_R be local-retractable module. Then, M_R is a π -Rickart module if and only if S is a right π -Rickart ring.

Proof. Let S be π -Rickart and $\varphi \in S$. Then, there exists $g^2 = g \in S$ such that $r_S(\varphi I(S)) = gS$. By [(13), Proposition 2.20], $r_M(\varphi I(S)) = r_S(\varphi I(S))(M)$. Thus, $r_M(\varphi I(S)) = gS(M) = gM$. Therefore, M is a π -Rickart module. The converse follows from Theorem 2.11.

Corollary 2.15 Consider \mathfrak{F} as a free R-module. Then, \mathfrak{F} is π -Rickart if and only if $\operatorname{End}_R(\mathfrak{F})$ is a right π -Rickart ring.

Proof. It is clear from [(13), Lemma 2.9] and Theorem 2.14.

Based on (13), M_R is identified as π -e.nonsingular if $r_M(A) \le ^{ess} gM$ where $g^2 = g \in S$ and $A \le_p S$, leading to $r_M(A) = gM$. Thus, M_R is termed \Re -nonsingular in (13), if, for any $\varphi \in S$, $Ker\varphi \le ^{ess} M$ implies $\varphi = 0$.

Proposition 2.16 Given a π -Rickart module M_R , we have the following properties:

- 1. M_R is π -e.nonsingular.
- 2. *S* is a semiprime ring if and only if every left semicentral idempotents of *S* is central.

3. M_R is \Re -nonsingular, if every essential submodule of M is an essential extension of a projection invariant submodule.

Proof. (i) Let M_R be π -Rickart, and let P be a projection invariant left ideal in S. Assume $r_M(P) \leq^{ess} gM$, with $g^2 = g \in S$. Since $r_M(P) = \bigcap_{\varphi \in I} r_M(\varphi I(S))$, for any $\varphi \in P$, it follows that $r_M(P) \leq r_M(\varphi I(S)) \cap gM \leq^{ess} gM$. As M is π -Rickart, there exists $h \in S_l(S)$ such that $r_M(\varphi I(S)) = hM$. Hence $hM \cap gM = ghM$, $ghM \leq^{ess} gM$. Since gh is an idempotent in S, ghM = gM. Thus, $gM \leq r_M(\varphi I(S))$ leading to $gM \leq \bigcap_{\varphi \in I} r_M(\varphi I(S)) = r_M(P)$. Therefore, $gM = r_M(P)$, so M is π -e.nonsingular.

(ii) Clearly, each left semicentral idempotents of a semiprime ring is central. Let M be a π -Rickart module and all left semicentral idempotents in S be central. Suppose $\varphi \in S$ and $\varphi S \varphi = 0$. Then, $\varphi I(S) \varphi = 0$. Consequently, for every $m \in M$, $\varphi(m) \in r_M(\varphi I(S)) = gM$ for some $g \in S_l(S)$. This implies $\varphi g = 0$ and $(1 - g)\varphi(m) = 0$ for each $m \in M$. As g is a central, we have $\varphi = g\varphi + (1 - g)\varphi = 0$. Hence, S is a semiprime ring.

(iii) suppose $\psi \in S$ and $Ker\psi \leq^{ess} M$. By assumption, there exists $N \trianglelefteq_p M$ such that $N \leq^{ess} Ker\psi \leq^{ess} M$. Consequently, $\psi I(S)N = \psi N = 0$. Thus, $N \subseteq r_M(\psi I(S))$. Since M is π -Rickart, $r_M(\psi I(S)) = gM$ for some $g^2 = g \in S$. As $N \leq^{ess} M$, g = 1. Consequently, $\psi = 0$, implying that M is a \Re -nonsingular module.

In their important 1980 publication, Chatters and Khuri demonstrated that a right nonsingular, right extending ring is accurately defined as a right cononsingular Baer ring. The objective of the forthcoming discussion was to further explore analogues of Chatters–Khuri Theorem, with insights to be drawn from the results presented in this paper. Based on (24), M_R is termed π -extending if for any $N \leq_p M$, we have $N \leq_{\bigoplus} gM$ where $g^2 = g$. As per (15), a module M_R satisfies the π -e.cononsingular property if, for all $P \leq_p M$, the condition $r_M(l_S(P)) \leq_{\bigoplus} M$ leads to $P \leq_{ess} r_M(l_S(P))$.

Corollary 2.17

- (i) Any abelian right π -Rickart ring is a semiprime ring.
- (ii) Any π -extending π -Rickart module is π -e.cononsingular and π -e.Baer.

Proof. Proposition 2.16 and [6, Theorem 4.16] yield the result.

A module M_R has IFP (Insertion of Factors Property), if for any element $\varphi \in S$, we have $r_M(\varphi) \trianglelefteq M$ (25). Following this idea, we define π -IFP module as a generalization of IFP modules. This new class of modules strengthen the condition for modules with IFP.

Definition 2.18 We call a module M_R is π -IFP, if for every $\phi \in S$, the submodule $r_M(\phi)$ is a projection invariant submodule of M. (or equivalently, for each $m \in M$, $l_S(m)$ is a projection invariant left ideal of S).

Note that every ring with *IFP* has π -*IFP*, but the converse is not true. For example, every simple abelian ring which is not a domain (see, (23)) has π -*IFP* but does not have *IFP*. Therefore, every abelian ring has π -*IFP*, but it does not have *IFP* in general [(26), Example 14].

Example 2.19 Let A be an abelian ring which does not have IFP. Consider $R = \begin{pmatrix} A & A \\ 0 & A \end{pmatrix}$ and $M_R = eR$ where $e = \begin{pmatrix} 1 & 0 \\ 0 & 0 \end{pmatrix} \in R$. Since $S = \begin{pmatrix} A & 0 \\ 0 & 0 \end{pmatrix}$ and A is abelian, M has π -IFP. On the other hand, since A does not satisfy IFP, there exist $x, y \in A$ such that xy = 0 and $xAy \neq 0$. Consequently, there exists $a \in A$ such that $xay \neq 0$. Set $m = \begin{pmatrix} y & y \\ 0 & 0 \end{pmatrix}$ and $\phi = \begin{pmatrix} x & 0 \\ 0 & 0 \end{pmatrix} \in S$. It follows that $\phi(m) = 0$, thus $\phi \in l_S(m)$. However, $\phi am \neq 0$ for $\begin{pmatrix} a & 0 \\ 0 & 0 \end{pmatrix} \in S$. Thus $l_S(m)$ is not a fully invariant left ideal of S. Hence, M fails to satisfy the IFP.

An additional example of a π -IFP module that is not IFP can be constructed by taking A as a simple abelian ring that is not a domain, as presented in Example 2.19.

Proposition 2.20 The following statements are equivalent.

- 1. M_R is both Rickart and abelian.
- 2. M_R is π -Rickart and fulfills the π -IFP.

Proof. (i) \Rightarrow (ii) It is evident that every abelian module satisfies π -IFP property. Let $\varphi \in S$. Since M_R is Rickart, there exists $f^2 = f \in S$ such that $r_M(\varphi) = fM$. For any $x \in r_M(\varphi I(S))$, we have $\varphi I(S)x = 0$. Thus, $x \in \ker(\varphi) = fM$. Since M is abelian, $\varphi I(S)fM = \varphi fI(S)M = 0$. Therefore, $r_M(\varphi I(S)) = fM$, indicating that M_R is π -Rickart.

 $(ii) \Rightarrow (i)$ Let $\varphi \in S$ and $x \in r_M(\varphi)$. Since M satisfies the π -IFP, we have $I(S)x \subseteq r_M(\varphi)$. This implied that $x \in r_M(\varphi I(S))$. Therefore, we conclude that $r_M(\varphi) = r_M(\varphi I(S))$. Since M_R is π -Rickart, one can find an element $f \in S$ satisfying $f^2 = f$ and $r_M(\varphi) = fM$. Now, we proceed to prove that M_R is abelian. Since M has π -IFP, $r_M(g) = (1-g)M \trianglelefteq_p M$ for any idempotent $g \in S$. Consequently, $g \in S_l(S)$ and similarly $g \in S_r(S)$. Therefore S is an abelian ring.

 M_R is said to possess the FI-strong summand intersection property (FI-SSIP) if every family of completely invariant direct summands of M_R has an intersection that is a direct summand of M_R . The following conclusion clarifies the conditions under which the π -e.Baer and π -Rickart modules are interchangeable.

Proposition 2.21 M_R is π -e.Baer if and only if M_R is π -Rickart and has the FI-SSIP.

Proof. Assume *M* is π-e.Baer and $\{N_{\gamma}\}_{\gamma \in \Gamma}$ is a family of fully invariant direct summands of *M*. For every $\gamma \in \Gamma$, there exist an element $e_{\gamma} \in S_{l}(S)$ such that $N_{\gamma} = e_{\gamma}M$. Let $J = \sum_{\gamma \in \Gamma} S(1 - e_{\gamma})$. Then *J* is a projection invariant left ideal of *S*, as $1 - e_{\gamma} \in S_{r}(S)$ for each $\gamma \in \Gamma$. Hence $r_{M}(J) \leq_{\bigoplus} M$. It follows that $\bigcap_{\gamma \in \Gamma} N_{\gamma} = \bigcap_{\gamma \in \Gamma} r_{M}(S(1 - e_{\gamma})) = r_{M}(J)$. Therefore, *M* has FI-SSIP. By Proposition 2.5, every π-e.Baer module is π-Rickart. Conversely, let *A* be a projection invariant left ideal of *S*. Then, we have $A = \sum_{\varphi_{i} \in A} \varphi_{i}I(S)$. So $r_{M}(A) = \bigcap_{\varphi_{i} \in A} r_{M}(\varphi_{i}I(S))$. Since M_{R} is π-Rickart, for each $\varphi_{i} \in A$, there is $e_{\varphi_{i}} \in S_{l}(S)$ such that $r_{M}(\varphi_{i}I(S)) = e_{\varphi_{i}}M$. As *M* has FI-SSIP, $r_{M}(A) = \bigcap_{\varphi_{i} \in A} e_{\varphi_{i}}M \leq_{\bigoplus} M$. Therefore *M* is π-e.Baer.

Corollary 2.22 Let R be a right hereditary, right noetherian ring. Then every injective module M_R is π -e.Baer if and only if M_R is π -Rickart.

Proof. [(27), Corollary 2.30] and Proposition 2.21 complete the result.

Lemma 2.23 Suppose M_R is a π -Rickart module and J is a nonzero projection invariant left annihilator in S. Then J contains a nonzero idempotent.

Proof. Let $0 \neq J = l_S(X)$ for some nonempty subset X of M and $\varphi \in J$. Due to π -Rickart property of M, $r_M(\varphi I(S)) = fM$, where $f^2 = f \in S$. Since J is projection invariant left ideal of S, it follows from (15) that $r_M(J) \leq_p M$. Consequently, $r_M(J) \subseteq r_M(\varphi I(S)) = fM$. Define e = 1 - f. Hence, $er_M(J) \subseteq efM = 0$, so $e \in l_S(r_M(J)) = J$.

Theorem 2.24 If S does not contain any infinite set of nonzero orthogonal idempotents, then M_R is the π -Rickart if and only if M_R is π -e.Baer if and only if M_R is π -e.Rickart.

Proof. Suppose $N \leq_p M$. By Lemma 2.23, $l_S(N)$ contains a nonzero idempotent. By assumption and [(12), Lemma 4.3], we can select an idempotent $f \in l_s(N)$ such that $S(1-f) = l_S(fM)$ is minimal. We aimed to prove that $l_S(N) \cap l_S(fM) = 0$. On the contrary, suppose $l_S(N) \cap l_S(fM) \neq 0$. Then $J = l_S(N \cup fM) \neq$ 0. Now, by Lemma 2.23, J must contain a nonzero idempotent g. Since gf = 0, h = f + (1 - f)g is also an idempotent in $l_S(N)$. As hg = g, $h \neq 0$. Additionally, $l_S(hM) \subseteq l_S(fM)$. However, gh = gf + $g(1-f)g = g \neq 0$. Consequently, $l_S(hM) \subset l_S(fM)$, contradicting the choice of f. Therefore, $l_S(N) \cap$ $l_S(fM) = 0$. Now, for any $\varphi \in l_S(N)$, we have $\varphi(1$ $f) = \varphi - \varphi f$. Since $f \in l_S(N)$, $\varphi(1 - f) \in l_S(N) \cap$ $l_S(fM) = 0$. Thus, $\varphi = \varphi f \in Sf$. This implies that $l_S(N) = Sf$, and hence M_R is π -e.Baer. The converse is deduced from Proposition 2.5. The other equivalent comes from [(21) Theorem 3.7].

Theorem 2.25 A module M_R possesses the π -e.Baer property if and only if it is π -Rickart and the set L=

 $\{Se | e \in S_r(S)\}\$ forms a complete lattice in terms of inclusion.

Proof. Let M_R be π -Rickart, $L = \{Se | e \in S_r(S)\}$ a complete lattice under inclusion, and X a projection invariant left ideal of S. Since X is projection invariant, $X = \sum_{\gamma \in \Gamma} x_{\gamma} I(S)$ for each $x_{\gamma} \in X$. Given M_R is π -Rickart, for each $\gamma \in \Gamma$, there exists an idempotent $e_{\gamma} \in$ $S_l(S)$ such that $r_M(x_{\nu}I(S)) = e_{\nu}M$. Thus, we have $r_M(X) = \bigcap_{\gamma \in \Gamma} r_M(x_{\gamma}I(S))$, implying $r_M(X) = \bigcap_{\gamma \in \Gamma} e_{\gamma}M$. Hence, $l_S(r_M(x_{\gamma}I(S))) = S(1 - e_{\gamma})$ for each $\gamma \in \Gamma$. Since L is a complete lattice under inclusion, and 1 $e_{\gamma} \in S_r(S)$, there exists an element $e \in S_r(S)$ such that $Se \subseteq \cap_{v \in \Gamma} S(1 - e_v)$. Consequently, $Se \subseteq l_S(r_M(X))$, $r_M(X) = r_M(l_S(r_M(X))) \subseteq r_M(Se) = (1$ e)M. As $e \in l_S(r_M(x_{\nu}I(S)))$ for each $\gamma \in \Gamma$, em = 0 for each $m \in r_M(X)$. Therefore, for each $m \in r_M(X)$, m =(1-e)m, implying $r_M(X) \subseteq (1-e)M$. Thus, M_R is π e. Baer. Conversely, by Proposition 2.5, M_R is π -Rickart. Additionally, as M_R is π -e.Baer, by [(15), Theorem 5.1], S is a π -Baer ring and hence by [(16), Theorem 2.7], S is a complete lattice under inclusion.

2 π-endo.AIP Modules

A new class of modules, referred to as π -e.AIP, is introduced in this section. This class of modules extends its applicability to a considerably wider class by including the classes of π -Rickart and π -e.Baer modules. The interconnections between π -Rickart, endo-AIP, and π -e.AIP modules are explored. Moreover, the present work aimed to investigate potential connections between π -e.AIP module and the ring of its endomorphisms.

As defined in (28), a left ideal A of R is right s-unital if for every $x \in A$, there is some $y \in A$ for which xy = x

Definition 3.1 We say M_R is a π -endo.AIP module, denoted by π -e.AIP, if $l_S(L)$ forms a right s-unital ideal of S for all $L \leq_p M$. A ring R is considered left π -AIP, if R_R is a π -e.AIP module.

If $K \le M$ and for all right R-module L, the map $L \bigotimes_R K \to L \bigotimes_R M$ is a monomorphism, then K is called pure. Whenever $l_S(K)$ stands as a pure left ideal for any fully invariant submodule K of M, it is recalled from (29) that M_R is termed *endo-AIP*.

Theorem 3.2 The following implications holds true.

- (i) M_R is π -e.AIP $\Rightarrow M_R$ is endo-AIP.
- (ii) M_R is Rickart $\Rightarrow M_R$ is π -e.AIP.
- (iii) M_R is π -e.Baer $\Rightarrow M_R$ is π -Rickart $\Rightarrow M_R$ is π -e.AIP.

Proof. (*i*) Assume M is π -e.AIP and $K \subseteq M$. For $x \in l_S(K)$, since $K \subseteq_p M$, there exist $c \in l_S(K)$ such that x = xc. Consequently, $l_S(K)$ is right s-unital. According to [(30), Proposition 11.3.13], $l_S(K)$ is pure as a left ideal. Therefore, M_R is endo-AIP.

(ii) Suppose M is Rickart, $P ext{ } ext{$\supseteq$}_p M$ and $\varphi \in l_S(P)$. Then, $P \subseteq r_M(\varphi)$. As M_R is Rickart, there exists $g^2 = g \in S$ such that $r_M(\varphi) = gM$. Consequently, $1 - g \in l_S(P)$ and $\varphi(1 - g) = \varphi$. Therefore, M is π -e.AIP.

(iii) By Proposition 2.5, π -e.Baer implies π -Rickart. Let M_R be π -Rickart, $P \unlhd_p M$ and $\psi \in l_S(P)$. Then $\psi(P) = 0$, so $\psi I(S)P = 0$. Consequently, $P \subseteq r_M(\psi I(S))$. Since M is a π -Rickart module, there exists $c^2 = c \in S$ such that $P \subseteq r_M(\psi I(S)) = cM$. This implies that $1 - c \in l_S(P)$ and $\psi(1 - c) = \psi$. Hence, M is π -e.AIP.

The following example illustrates that the converse of Theorem 3.2 does not necessarily hold in general.

Example 3.3 (*i*) endo-AIP $\Rightarrow \pi$ -e.AIP: Based on [(16), Example 1.6], there exists a right p.q.-Baer ring R with trivial idempotents that is not right π -Rickart. By [(29), Theorem 2.5], every right p.q.-Baer ring is endo-AIP. Thus, R_R is endo-AIP. Since R_R has π -IFP, R_R is π -e.AIP if and only if R_R is π -Rickart by Proposition 3.4. Therefore, R_R is not π -e.AIP.

(ii) π -e.AIP $\Rightarrow \pi$ -Rickart: Let R be the ring in [(22), Example 1.6]. Then, R is a right Rickart ring that is not right π -Rickart by [(16), p.5]. Consider $M = R_R$. Then, M is a π -e.AIP module, but not π -Rickart By Theorem 3.2(ii).

(iii) π -e.AIP \Rightarrow Rickart: Let $R = \begin{pmatrix} \mathbb{Z} & \mathbb{Z} \\ 0 & \mathbb{Z} \end{pmatrix}$ and $M = R_R$. By [(31), Proposition 3.12], M_R is endo-AIP. Note that I(S) = S, so M is π -e.AIP. However, M_R is not a Rickart module [(12), Example 2.9].

Proposition 3.4 The following conditions are equivalent for module M with π -IFP.

- 1. M_R is π -e.AIP.
- 2. M_R is Rickart.
- 3. M_R is π -Rickart.

Proof. (i) \Rightarrow (ii) Consider $\eta \in S$ and $X = r_M(\eta)$. Given that M has π -IFP, $r_M(\eta) \trianglelefteq_p M_R$. Since M is π -e.AIP and $\eta \in l_S(X)$, there exists $\psi \in l_S(X)$ such that $\eta \psi = \varphi$. Consequently, $\eta(1 - \psi) = 0$ and $r_M(\eta) \subseteq r_M(\psi)$. Hence, $\psi(1 - \psi) = 0$, implying $\psi^2 = \psi \in S$. Let $e = 1 - \psi$, then X = eM. Thus, M_R is Rickart.

 $(ii) \Rightarrow (iii)$ Let M_R be Rickart. Then, for any $\psi \in S$, there exists $g^2 = g \in S$ such that $r_M(\psi) = gM$. It is evident that $r_M(\psi I(S)) \subseteq r_M(\psi)$. As M has π -IFP, for every $m \in r_M(\psi)$, it follows that $m \in r_M(\psi I(S))$. Thus, we can deduce that $r_M(\psi I(S)) = gM$. Consequently, M_R is π -Rickart.

 $(iii) \Rightarrow (i)$ follows directly from Theorem 3.2.

The necessity of π -IFP condition in Proposition 3.4 is illustrated by the following example. Notably, there is a module M within π -e.AIP class that lacks both the Rickart property and the π -IFP property.

Example 3.5 (i) Consider R and M_R as described in

Example 3.3 (ii). M_R is a π -e.AIP module but not Rickart. Now, let e_{ij} denote a 2×2 matrix with the element 1 in (i,j)-position and 0 elsewhere. Define φ as $\varphi = \begin{pmatrix} 1 & 0 \\ 0 & 0 \end{pmatrix}$ and f as $e_{11} + e_{12}$. Note that $f^2 = f$. Since $\varphi e_{22} = 0$ while $\varphi f e_{22} \neq 0$, M fails to satisfy π -IFP.

(ii) Let $R = M_2(\mathbb{Z}[x])$ and $M = R_R$. since $\mathbb{Z}[x]$ is a domain, it is π -Rickart. Utilizing [(16), Proposition 3.10], we conclude that M is π -Rickart. Nonetheless, M is not Rickart as seen in [(32), Example 3.1.28]. Similar to the part (i), M_R fails to satisfy π -IFP.

A straight summand of a π -e.AIP module doesn't always inherit the π -e.AIP property. Example 2.9 shows that the module M_R meets the π -e.AIP requirement, which is supported by Theorem 3.2. However, the direct summand R_R does not fit this criterion, as shown in Example 3.3. The following discussion investigated the specific conditions under which a direct summand of a π -e.AIP module also retains the π -e.AIP property.

Theorem 3.6 In a π -e.AIP module, any direct summand that remains invariant under projection also fulfills the π -e.AIP condition.

Proof. Consider M to be a π -e.AIP module, and let $P = gM \leq_p M$ for some $g^2 = g \in S$, with $A \leq_p P$. Then, $g \in S_l(S)$ and $E = \operatorname{End}_R(P) = gSg$. For any $\eta \in l_E(A)$, it follows that $\eta(A) = 0$, and one can find $\psi \in S$ with the property $\eta = g\psi g$. Observe from Lemma 2.2 that $A \leq_p M$. Since $\eta \in l_S(A)$ and M is π -e.AIP, we have $a \in l_S(A)$ with $\eta = \eta a$. Note that $gag \in l_E(A)$ and $\eta(gag) = (g\psi g)(gag) = g\psi g = \eta$. It follows that P is π -e.AIP module.

Corollary 3.7 (i) Given that M is a π -e.AIP module with an abelian endomorphism ring, it follows that all direct summands of M are also π -e.AIP.

(ii) Let R_R be π -e.AIP and $e \in S_l(R)$. Then eR is a π -e.AIP module.

The example below shows that direct sums of π -e.AIP modules may not inherit the π -e.AIP property.

Example 3.8 Consider the \mathbb{Z} -module $M = \mathbb{Z} \oplus \mathbb{Z}_2$. It is evident that both \mathbb{Z} and \mathbb{Z}_2 are π -e.Baer, implying they are π -e.AIP. Nevertheless, M itself is not π -e.AIP, as shown in [(29), Example 2.13].

Theorem 3.9 Let $M = \bigoplus_{\gamma \in \Gamma} M_{\gamma}$ such that each M_{γ} meets π -e.AIP criterion while also being subisomorphic to M_{η} for all $\gamma \neq \eta \in \Gamma$. Then, M_R is a π -e.AIP module.

Proof. For every $\gamma \in \Gamma$, let S_{γ} denote the ring of endomorphisms of M_{γ} . The ring of endomorphisms of M, denoted by S, is structured as a matrix ring. In this ring, the entry in the (γ, γ) -position comes from S_{γ} , and the entry in (γ, η) -position (for $\gamma, \eta \in \Gamma$ with $\gamma \neq \eta$) corresponds to a map from M_{η} to M_{γ} . Let $P \leq_p M_R$. Then $P = \bigoplus_{\gamma \in \Gamma} P \cap M_{\gamma} = \bigoplus_{\gamma \in \Gamma} P_{\gamma}$ and $P_{\gamma} = P \cap R_{\gamma}$

 $M_{\gamma} \trianglelefteq_{p} M_{\gamma}$ for all $\gamma \in \Gamma$ by Lemma 2.2. Consider $\varphi \in l_{S}(P)$. since $\varphi(P) = 0$, it follows that $\varphi_{\gamma\gamma} \in l_{S_{\gamma}}(P_{\gamma})$ for $\gamma \in \Gamma$. As M_{η} and M_{γ} are subisomorphic, there exists a monomorphism $\psi_{\gamma\eta} : M_{\eta} \to M_{\gamma}$. Clearly, for $\gamma \neq \eta \in \Gamma$, $\psi_{\gamma\eta}\varphi_{\eta\gamma}(P_{\gamma}) = 0$. Since M_{γ} satisfies the π -e.AIP property, $l_{S_{\gamma}}(P_{\gamma})$ is right s-unital, and there exists a finite subset $\{\eta_{1}, ..., \eta_{n}\}$ of Γ such that $\varphi_{\eta\gamma} \neq 0$. Hence there is $u_{\gamma} \in l_{S_{\gamma}}(P_{\gamma})$ such that $\varphi_{\gamma\gamma}u_{\gamma} = \varphi_{\gamma\gamma}$ and $\psi_{\gamma\eta}\varphi_{\eta\gamma}u_{\gamma} = \psi_{\gamma\eta}\varphi_{\eta\gamma}$ for $\gamma \neq \eta \in \Gamma$. Since $\psi_{\gamma\eta}$ is a monomorphism for $\gamma \neq \eta \in \Gamma$, $\varphi_{\eta\gamma}u_{\gamma} = \varphi_{\eta\gamma}$. We construct an element $x = (u_{\gamma\eta})_{\gamma,\eta\in\Gamma}$, where $u_{\gamma\gamma} = u_{\gamma}$ and $u_{\gamma\eta} = 0$, if $\gamma \neq \eta$. Then $\varphi x = \varphi$. Thus, M exhibits the π -e.AIP property.

Corollary 3.10 If a module is π -e.AIP, then its direct sum with any number of copies also preserves the π -e.AIP condition.

Theorem 3.11 For a π -e.AIP module M_R , then the ring of its endomorphisms, denoted $End_R(M)$, is a left π -AIP ring.

Proof. Assume A is a projection invariat right ideal in S. For every $\varphi \in l_S(A)$, $\varphi A(M) = 0$. Then, $\varphi \in l_S(AM)$. Since $AM \leq_p M$ and M is π -e.AIP, there is $\psi \in l_S(AM)$ such that $\varphi \psi = \varphi$. It follows that $\psi A = 0$, so $\psi \in l_S(A)$. Therefore, we can deduce that S is left π -AIP ring.

The subsequent example indicates that the converse of Theorem 3.11 is not necessarily valid. It shows that a module having a left π -AIP endomorphism ring does not ensure that the module itself is π -e.AIP.

Example 3.12 Let's consider \mathbb{Z} -module $M = \mathbb{Z}(p^{\infty})$, where p is a prime number. The endomorphism ring $End(M_{\mathbb{Z}})$ is a commutative domain, specifically the ring of p-adic integers. Therefore, $End(M_{\mathbb{Z}})$ is a π -Baer ring, and by Theorem 3.2, it is π -AIP. From [(33), Theorem 1.2], it follows that $M_{\mathbb{Z}}$ being a duo module implies that it satisfies the π -IFP condition. However, as illustrated in [(12), Example 2.17], $M_{\mathbb{Z}}$ does not possess the Rickart property. Thus, based on Proposition 3.4, $M_{\mathbb{Z}}$ does not fulfill the condition of being π -e.AIP.

For the converse of Theorem 3.11 to be valid, the concept of being locally π -quasi-retractable is exactly the required condition.

Definition 3.13 We say that M_R is locally π -quasiretractable if for each $\gamma \in S$ where $r_M(S\gamma I(S)) \neq 0$, there is a nonzero element $\beta \in S$ satisfying $\beta(M) = r_M(S\gamma I(S))$.

Proposition 3.14 Given that M_R is locally π -quasi-retractable and S is a left π -AIP ring, it follows that M_R is π -e.AIP.

Proof. Suppose $0 \neq X \leq_p M$ and $\gamma \in l_S(X)$. Because $X \leq_p M$, it follows that $S\gamma I(S) \subseteq l_S(X)$. Therefore, $0 \neq X \subseteq r_M(S\gamma I(S))$. Based on the concept of π - quasi-

retractability, there exists a nonzero $\beta \in S$ such that $\beta(M) = r_M(S\gamma I(S))$. Consequently, $X \subseteq r_M(S\gamma I(S)) = \beta(M)$ and $\gamma \in l_S(I(S)\beta S)$, where $I(S)\beta S$ is a projection invariant right ideal of S. Given that S is a left π -AIP ring, $l_S((I(S)\beta S))$ is right s-unital. Therefore, there exists $\gamma' \in l_S(I(S)\beta S)$ such that $\gamma = \gamma \gamma'$. Since $X \subseteq \beta(M)$, it follows that $\gamma'(I(S)X) \subseteq \gamma'(I(S)\beta(M)) = 0$. Hence, $\gamma' \in l_S(X)$, considering $X \preceq_p M_R$. Consequently, M is a π -e.AIP module.

According to [(16), Definition 2.1], a ring R is defined as *right* ρ -*regular* if, for each $\gamma \in R$ there exists $\eta = \eta^2 \in R$ such that $R\gamma I(R) = R\eta$.

Proposition 3.15 A right ρ -regular ring S ensures that M_R possesses the π -e.AIP condition.

Proof. Based on [(16), Lemma 2.2], S is right π -Rickart. Consequently, S is is a left π -AIP ring by Theorem 3.2. For any $\gamma \in S$, since S is right ρ -regular, there exists a central idempotent $g \in S$ such that $S\gamma I(S) = gS$ as per [(16), Proposition 2.4]. Note that $g \neq 1$ and $0 \neq \beta = 1 - g \in S$. Given that $g \neq 1$ is central, we have $g(M) = r_M(S\gamma I(S))$. As a result, M is locally π -quasi-retractable. Consequently, Proposition 3.14 concludes the proof.

Corollary 3.16 The ring of endomorphisms of a free module over a ρ -regular ring is a left π -AIP ring.

Proof. Tis conclusion is derived from Corollary 3.10 and Theorem 3.11.

Acknowledgment

The authors are grateful to the referees for careful reading of the paper and valuable suggestions and comments.

References

- Kaplansky I. Rings of Operators New York: Benjamin; 1965.
- Clark WE. Twisted matrix units semigroup algebras. Duke Math J. 1967; 34(3): 417–23.
- 3. Maeda S. On a ring whose principal right ideals generated by idempotents form a lattice. J Sci Hiroshima Univ Ser A. 1960; 24: 509-25.
- Armendariz EP. A note on extensions of Baer and P.P.rings. J Austra Math Soc. 1947; 18: 470-73.
- Berberian K. Baer *-Rings New York-Berlin: Springer Berlin, Heidelberg.
- Bergman GM. Hereditary commutative rings and centres of hereditary rings. Proc London Math Soc. 1971; 23(4): 214-36
- Evans M. On commutative P.P. rings. Pacific J Math. 1972; 41(3): 687–97.
- Hattori A. A foundation of torsion theory for modules over general rings. Nagoya Math J. 1960; 17: 147-58.
- Jondrup S. p.p. rings and finitely generated flat ideals. Proc Ame. Math Soc. 1971; 28(2): 431-35.
- 10.Rizvi ST, Roman CS. Baer and quasi-Baer modules. Comm Algebra. 2004; 32(1): 103-23.

- 11.Lee G. Principally quasi-Baer modules and their generalizations. Comm Algebra. 2019; 47(10): 4077-94.
- Lee G, Rizvi ST, Roman CS. Rickart Modules. Comm Algebra. 2010; 38(11): 4005-27.
- Lee G, Rizvi ST, Roman CS. 2-Rickart Modules. Comm Algebra. 2015; 43(5): 2124-51.
- 14.Birkenmeier GF, Kara Y, Tercan A. π-Baer rings. J Algebra Appl. 2018; 17(2).
- 15.Birkenmeier GF, Kara Y, Tercan A. π-endo Baer modules. Comm Algebra. 2020; 48(3): 1132-49.
- 16.Birkenmeier GF, Kara Y, Tercan A. π-Rickart rings. J Algebra Appl. 2021; 20(8).
- 17.Birkenmeier GF, Kara Y, Tercan A. Primitive and prime rings with s.Baer or related modules. J Algebra Appl. 2024; 23(03).
- 18.Birkenmeier GF, Kilic N, Mutlu, Tastan, Tercan, Yasar. Connections between Baer annihilator conditions and extending conditions for nearrings and rings. J Algebra Appl. 2025.
- 19.Kara Y. Weak π-Rickart rings. Comm Algebra. 2025;: 1-
- 20.KESKIN TÜTÜNCÜ D. A Study on the π-Dual Rickart Modules. J. Iran. Math. Soc. 2023 july; 4(2): 235-45.
- 21.Maleki Y, Moussavi A, Kara Y. On π-Endo.Rickart Modules. Iran J Sci. 2024.
- Birkenmeier GF, Kim JY, Park JK. Principally quasi-Baer rings. Comm Algebra. 2001; 29(2): 638-60.
- 23.Lorenz M. K0 of Skew Group Rings and Simple Noetherian Rings without idempotents. J Lond Math Soc. 1985; 32(5): 41-50.
- 24.Birkenmeier GF, Tercan A, Yucel CC. The extending condition relative to sets of submodules. Commun Algebra. 2014; 42(2): 764-78.
- 25. Liu Q, Ouyang B, Wu T. Principally quasi-Baer modules. J Math Res Appl. 2009; 29(5): 823-30.
- Huh C, Lee Y, Smoktunowicz A. Armendariz rings and semicommutative rings. Commun Algebra. 2002; 30(2): 751-61.
- 27.Lee G, Rizvi ST, Roman CS. Dual Rickart Modules. Comm Algebra. 2011; 39(11): 4036-58.
- Tominaga H. On s-unital rings. Mathematical Journal of Okayama University. 1976; 18(2): 117-34.
- 29.Amirzadeh Dana P, Moussavi A. Modules in which the annihilator of a fully invariant submodule is pure. Comm Algebra. 2020; 48(11): 4875-88.
- 30. Wolfson KG. Baer rings of endomorphisms. Math Ann. 1961; 143(1): 19-28.
- 31.Majidinya A, Moussavi A, Paykan K. Rings in which the annihilator of an ideal is pure. Algebra Colloq. 2015; 22(01): 947-68.
- 32.Birkenmeier GF, Park JK, Rizvi ST. Extensions of Rings and Modules New York: Birkhauser; 2013.
- 33.Ozcan AC, Harmanci A, Smith PF. Duo modules. Glasg Math J. 2006; 48(03): 533-45.
- 34. Chatters AW, Khuri SM. Endomorphism rings of modules over nonsingular CS rings. J London Math Soc. 1980; 21(2): 434-44.
- 35.Birkenmeier GF, Kara Y, Tercan A. Primitive and prime rings with s.Baer or related modules. J Algebra Appl. 2024; 23(03).

A New Bivariate Shock Model Covering All Degrees of Dependencies

H. A. Mohtashami-Borzadaran, H. Jabbari*, M. Amini

Department of Statistics, Faculty of Mathematical Sciences, Ferdowsi University of Mashhad, Mashhad, Islamic Republic of Iran

Received: 3 December 2024 / Revised: 26 August 2025 / Accepted: 7 September 2025

Abstract

This paper presents a bivariate distribution that improves the Marshall-Olkin exponential shock model. The new construction method enhances the model's capacity to include a common joint shock across components, making it especially suitable for reliability and credit risk assessments. The model features a single component and supports negative dependence structures. We investigate the key dependence properties and conduct a stress-strength analysis. After evaluating the performance of the parameter estimator, chemical engineering data is analyzed.

Keywords: Dependence; Marshall-Olkin model; Shock model. **Mathematics Subject Classification (2010):** 60E05, 60E15, 62N05.

Introduction

The univariate exponential distribution is known for its applications in different fields such as reliability, telecommunication, hydrology, medical sciences and environmental science; see, e.g., Balakrishnan (1). Several bivariate and multivariate extensions have been proposed in the literature (Lai and Balakrishnan (2), Chapter 10), with a significant multivariate extension introduced Marshall and Olkin (3) through a shock model. For three independent exponential random variables $T_1 \sim E(\theta_1)$, $T_2 \sim E(\theta_2)$, and $T_{12} \sim E(\theta_{12})$, the Marshall-Olkin (MO) shock model is derived from the stochastic representation

$$(X,Y) = (\min\{T_1, T_{12}\}, \min\{T_2, T_{12}\}),$$
 (1) with the joint survival function given by $S(x,y) = \exp\{-\theta_1 x - \theta_2 y - \theta_{12} \max(x,y)\}.$ (2) Due to the common shock identified by T_{12} in (1), we

Due to the common shock identified by T_{12} in (1), we have $P(X = Y) = \frac{\theta_{12}}{\theta_1 + \theta_2 + \theta_{12}}$, if $\theta_{12} > 0$, the distribution

(1), has a singular component along the line $\{x = y\}$.

Therefore, the MO exponential distribution has both singular and continuous parts in its density and covers a positive dependence structure.

Numerous studies have examined models and modifications based on the foundational work of Marshall and Olkin (3), particularly in reliability, finance, actuarial science, and credit risk (e.g., Cherubini et al. (4), Lindskog and McNeil (5)). Recently, Cherubini and Mulinacci (6) emphasized the MO model's importance and adaptability for analyzing systemic crises in credit risk and financial contexts. They noted that the MO model captures unobserved shocks affecting individuals either independently or collectively, using common shocks to explain simultaneous defaults within clusters influenced by the same factor. The model also maintains the marginal exponential distribution for observed default times.

Several bivariate and multivariate extensions of the exponential distribution have been developed for reliability applications. For instance, Esary and Marshall

^{*} Corresponding Author: Tel: +98 9151778318; Email: Jabbarinh@um.ac.ir

(7) characterized a multivariate exponential distribution and established conditions for positive dependence among distributions with exponential minima. Raftery (8) introduced a continuous multivariate exponential distribution that accommodates various correlation structures while achieving Fréchet bounds in the bivariate case. A multivariate exponential distribution based on the limiting behavior of normalized maxima or minima was introduced by Tawn (9). Lin et al. (10) examined a shared-load model of the multivariate exponential distribution for dependent redundancies. Constant failure rate multivariate exponential distributions were defined by Basu and Sun (11), while Gomez et al. (12) introduced the multivariate power exponential distribution. An analytical method for assessing the reliability of coherent systems with dependent components based on the MO model was proposed by Cui and Li (13). Additionally, Fan et al. (14) developed a multivariate exponential survival tree procedure utilizing a score test statistic from a parametric exponential frailty model, and Kundu and Gupta (15) presented parameter estimation for a new bivariate exponential distribution using an EM algorithm. Generalized bivariate MO distributions, with the common MO model as a special case, were investigated by Li and Pellerey (16). Bayesian estimation for the MO bivariate Weibull distribution was conducted by Kundu and Gupta (17), and Bayramoglu and Ozkut (18) applied the MO model considering system structure. A multivariate proportional reversed hazard model derived from the MO copula was discussed by Kundu et al. (19), while Cha and Badia (20) proposed a multivariate exponential distribution model based on dependent dynamic shock models. A multivariate weighted exponential distribution for failure time data analysis was developed by Al-Mutairi et al. (21). Recently, Mohtashami-Borzadaran et al. (22) enhanced the MO shock model by incorporating a distortion function, broadening its applicability. Additionally, El Ktaibi et al. (23) introduced a bivariate copula based on a bivariate exponential distribution with negative dependence, Bentoumi et al. (24) developed by using the countermonotonic shock model. Lee and Cha (25) developed a new class of continuous bivariate distributions based on a shock model. Agrawal et al. (26) proposed a bivariate distribution for modelling competing risks data with singularity originating from a shock model. A variant of the bivariate Poisson common shock model was presented in Genest et al. (27).

From a shock model perspective, the MO model (1) has limitations due to the assumption of shock equality in the common shock T_{12} , suggesting that T_{12} is likely equal for components X_1 and X_2 . Our new model

addresses this limitation by allowing for a random percentage of common stock on each component. Most existing bivariate and multivariate exponential distribution extensions exhibit positive dependence structures, with negative dependence structures being rare.

In this paper, which was first posted at arXiv Mohtashami-Borzadaran et al. (28), we propose a new bivariate exponential shock model that accommodates negative dependence structures as well. Section 2 presents the new shock model and its flexibility compared to the MO model. Section 3 outlines the model's main properties, including dependence structure, association measures, tail dependence measures, and stress-strength index. Section 4 focuses on parameter estimation for the new model, which poses challenges due to its singular component, followed by a performance analysis of the estimators. Section 5 applies the model to real data, demonstrating its superior fit.

Materials and Methods

Consider three independent exponential random variables $T_1 \sim E(\theta_1)$, $T_2 \sim E(\theta_2)$, and $T_{12} \sim E(\theta_{12})$, along with an independent uniform random variable $U \sim U(0,1)$, which is independent of T_1 , T_2 , and T_{12} . Let α_{12} (taking values ± 1) be the dependence structure of the model where $\alpha_{12} = +1$ concludes positive and $\alpha_{12} = -1$ gives negative dependence structure. When $\alpha_{12} = +1$, set $T_{12}^*(\alpha_{12}) = T_{21}^*(\alpha_{12}) = F_{12}^{-1}(U)$ or $T_{12}^*(\alpha_{12}) = T_{21}^*(\alpha_{12}) = F_{T_{12}}^{-1}(U)$. If $\alpha_{12} = -1$, put $T_{12}^*(\alpha_{12}) = F_{T_{12}}^{-1}(U)$, $T_{21}^*(\alpha_{12}) = F_{T_{12}}^{-1}(1-U)$ or $T_{12}^*(\alpha_{12}) = F_{T_{12}}^{-1}(1-U)$, $T_{21}^*(\alpha_{12}) = F_{T_{12}}^{-1}(U)$ where $F_{T_{12}}$ is the corresponding distribution function of T_{12} . Then, the bivariate MO random vector $T_{12}^*(\alpha_{12})$ covering all degree of dependence is

 $(R, S) = (\min\{T_1, T_{12}^*(\alpha_{12})\}, \min\{T_2, T_{21}^*(\alpha_{12})\}).$ (3) Clearly, when $\alpha_{12} = +1$, the vector (R, S) reduces to $(R, S) = (\min\{T_1, T_{12}\}, \min\{T_2, T_{12}\}),$

which is the well-known MO model given in Marshall and Olkin (3) that has positive dependence structure. When $\alpha_{12} = -1$, the random vector (R,S) gives a new MO model with negative dependence structure (see Proposition 2.2) which is called the bivariate negative MO model, denoted by $BNMO(\theta_1, \theta_2, \theta_{12})$. This model is obtained by

 $(R,S) = \left(\min\{T_1, F_{T_{12}}^{-1}(U)\}, \min\{T_2, F_{T_{12}}^{-1}(1-U)\}\right), (4)$ or

 $(R,S) = (\min\{T_1, F_{T_{12}}^{-1}(1-U)\}, \min\{T_2, F_{T_{12}}^{-1}(U)\}).$ (5) Throughout this paper, we focus on the (R,S) given in (4).

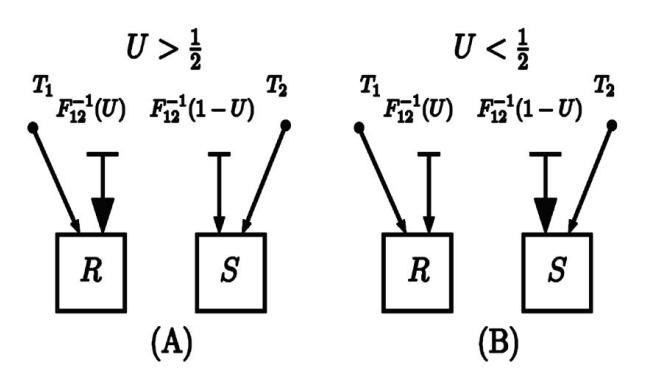


Figure 1. Shock models based on the construction in (4)

A similar construction for a bivariate Poisson model has been given by Genest et al. (27).

The interpretation for this construction is different from the well-known MO model. Consider Figure 1 given based on the relation (4). If $U > \frac{1}{2}$, then the dependent shock is more likely to be powerful on the first component R (Figure 1 (A)) and, if $U < \frac{1}{2}$, the dependent shock is more likely to be powerful on S (Figure 1 (B)). The survival function of both vectors (4) and (5) for $\theta_1, \theta_2, \theta_{12} > 0$ is

$$\tilde{F}_{R,S}(r,s) = P\left(T_1 > r, T_2 > s, F_{T_{12}}(r) < U < 1 - F_{T_{12}}(s)\right),
= e^{-\theta_1 r} e^{-\theta_2 s} \max\{e^{-\theta_{12} r} + e^{-\theta_{12} s} - 1, 0\}.$$
(6)

This model has a singular part at $e^{-\theta_{12}r} + e^{-\theta_{12}s} = 1$. The probability density function of (4) when $e^{-\theta_{12}r} + e^{-\theta_{12}s} > 1$ is

$$f_{R,S}(r,s) = e^{-\theta_1 r - \theta_2 s} (\theta_2(\theta_1 + \theta_{12})e^{-\theta_{12}r} + \theta_1(\theta_2 + \theta_{12})e^{-\theta_{12}s} - \theta_1\theta_2).$$
(7)

The following statement gives the probability of the singular part.

 $\begin{array}{ll} \textbf{Proposition} & \textbf{2.1.} & \text{Suppose} & (R,S) \sim \\ BNMO(\theta_1,\theta_2,\theta_{12}) & \text{and let } \alpha := \frac{\theta_{12}}{\theta_1+\theta_{12}}, \; \beta := \frac{\theta_{12}}{\theta_2+\theta_{12}}. \end{array}$ Then

$$P(e^{-\theta_{12}R} + e^{-\theta_{12}S} = 1) = Beta\left(\frac{1}{\beta}, \frac{1}{\alpha}\right),$$

where $Beta(a, b) = \int_0^1 x^{a-1} (1-x)^{b-1} dx$.

Proof. Based on (Joe (29), Theorem 1.1, p. 15), for $e^{-\theta_{12}r} + e^{-\theta_{12}s} = 1$, we have

$$1 - \int_{0}^{g(r)} f_{S|R}(s|r)ds = \frac{\theta_{12}}{\theta_{1} + \theta_{12}} (1 - \exp\{-\theta_{12}r\})^{\theta_{2}/\theta_{12}},$$
where $g(r) = \frac{-1}{\theta_{12}} \ln(1 - \exp\{-\theta_{12}r\})$. Let $h(r) =$

 $1 - \int_0^{g(r)} f_{S|R}(s|r) ds$. By using the construction in (4) and Theorem 1.1 in Joe (27), we get

(8)

Remark 2.1. If $\theta_1 = \theta_2 = \theta_{12}$ or equivalently $\alpha = \beta = \frac{1}{2}$, then

$$P(e^{-\theta_{12}R} + e^{-\theta_{12}S} = 1) = \frac{1}{6}$$

The survival copula associated with (6) is achieved

$$\hat{C}(u, v) = u^{1-\alpha} v^{1-\beta} \max\{u^{\alpha} + v^{\beta} - 1, 0\}, \quad \alpha, \beta, u, v \in (0, 1),$$
(9)

and the corresponding copula density is given as $c(u,v) = (1-\alpha)u^{-\alpha} + (1-\beta)v^{-\beta} - (1-\alpha)(1-\beta)u^{-\alpha}v^{-\beta}I_{\{u^{\alpha}+v^{\beta}-1>0\}}(u,v) + Beta\left(\frac{1}{\alpha},\frac{1}{\beta}\right)I_{\{u^{\alpha}+v^{\beta}-1=0\}}(u,v), \quad \alpha,\beta,u,v \in (0,1),$

(10)

where $I_A(u, v)$ is an indicator function getting 1 if $(u, v) \in A$ and zero elsewhere.

Remark 2.2. El Ktaibi et al. (23) introduced only the survival copula (9) in parallel with this paper in an almost similar way to the present study by defining $\theta := \alpha = \beta$. They used four independent exponential random variables that have a common parameter, which is the factor that creates the dependency. One part of this parameter ultimately appears as the dependence parameter of the survival copula. Instead, this paper uses three independent exponential random variables with different parameters, and one of them is included as a factor for establishing dependence in the model (1). Therefore, unlike, El Ktaibi et al. (23) the present study uses a common random variable instead of a parameter to develop the dependency. So, the results of El Ktaibi et al. (23) are a special case of the present study with only one dependence parameter.

1. Some distributional properties

In this section, we present some properties of BNMO model such as dependence structure, association measures, tail dependence measures and stress-strength

1.1. Dependence structure

Let (X,Y) be a random vector with a survival function \bar{F} . The pair (X,Y) is said to be the right corner set decreasing, denoted by RCSD(X,Y), whenever for any $x_1 < x_2$ and $y_1 < y_2$ we have

 $\bar{F}(x_1,y_1)\bar{F}(x_2,y_2) - \bar{F}(x_1,y_2)\bar{F}(x_2,y_1) \le 0,$ that is equivalent to

$$\frac{\partial^2}{\partial r\,\partial s}\ln\left(\tilde{F}(r,s)\right)\leq 0.$$

RCSD(X,Y) implies negative dependence structures like RTD(X|Y), RTD(Y|X) and NQD(X,Y) (for more information see Nelsen (30)). The following statement specifies the dependence structure of the proposed model.

Proposition 2.2. If $(R,S) \sim BNMO(\theta_1, \theta_2, \theta_{12})$, then we have RCSD(R, S).

$$\begin{split} & \textit{Proof.} \text{ For all } \theta_1, \theta_2, \theta_{12} \in \textit{R}, \text{ we obtain} \\ & \frac{\partial^2}{\partial r \, \partial s} \ln \left(\tilde{F}_{\textit{R},\textit{S}}(r,s) \right) = \frac{-\theta_{12}^2 e^{-\theta_{12} r - \theta_{12} s}}{(1 - e^{-\theta_{12} r} - e^{-\theta_{12} s})^2} \leq 0, \end{split}$$

which implies RCSD(R, S) and the proof is complete. The random vectors (X_1, Y_1) and (X_2, Y_2) can be compared in terms of their dependence structure via the

upper orthant (UO) order. For any two vectors such as $(X_1, Y_1), (X_2, Y_2),$ we say (X_1, Y_1) is less than (X_2, Y_2) in UO order and write $(X_1, Y_1) \prec_{UO} (X_2, Y_2)$ whenever

$$\bar{F}_{X_1,Y_1}(x,y) \le \bar{F}_{X_2,Y_2}(x,y)$$
 for all x,y .

$$\begin{split} \bar{F}_{X_1,Y_1}(x,y) &\leq \bar{F}_{X_2,Y_2}(x,y) \text{ for all } x,y. \\ \textbf{Proposition 2.3. Let } (R,S) &\sim BNMO(\theta_1,\theta_2,\theta_{12}) \end{split}$$
and $(R',S') \sim BNMO(\theta_1,\theta_2,\theta_{12}')$. If $\theta_{12} \leq \theta_{12}'$ then $(R',S') \prec_{UO} (R,S).$

Proof. For every $r, s, \theta_1, \theta_2 > 0$ and $\theta_{12} \le \theta'_{12}$, we

$$\begin{split} \tilde{F}_{R,S}(r,s) &= e^{-\theta_1 r} e^{-\theta_2 s} \big(e^{-\theta_{12} r} + e^{-\theta_{12} s} - 1 \big) \\ &\geq e^{-\theta_1 r} e^{-\theta_2 s} \big(e^{-\theta'_{12} r} + e^{-\theta'_{12} s} - 1 \big) \\ &\geq \tilde{F}_{R',S'}(r,s). \end{split}$$
 Hence, $(R',S') \prec_{UO} (R,S)$ and this completes the

1.2. Association measures and tail dependence

Two common measures of concordance between continuous random variables X and Y are Kendall's tau (τ) and Spearman's rho (ρ_s) . In the following, after some elementary (but tedious) algebra, we provide explicit expressions for these measures based on the survival function (6).

Proposition 2.4. If $(R, S) \sim BNMO(\theta_1, \theta_2, \theta_{12})$ with the survival function $\bar{F}_{R,S}$ in (6), then we have

$$\tau = 4E\left(\bar{F}_{R,S}(R,S)\right) - 1$$
$$= -2ab,$$

and
$$\rho_{s} = 12 \int_{(0,\infty)^{2}} \left[\tilde{F}_{R,S}(r,s) - \tilde{F}_{R}(r) \tilde{F}_{S}(s) \right] f_{R}(r) f_{S}(s) dr ds$$

$$= -3ab,$$
where $a = \frac{\theta_{12}}{2\theta_{1} + \theta_{12}}$ and $b = \frac{\theta_{12}}{2\theta_{2} + \theta_{12}}$.

The plots of τ and ρ_s with respect to a and b are

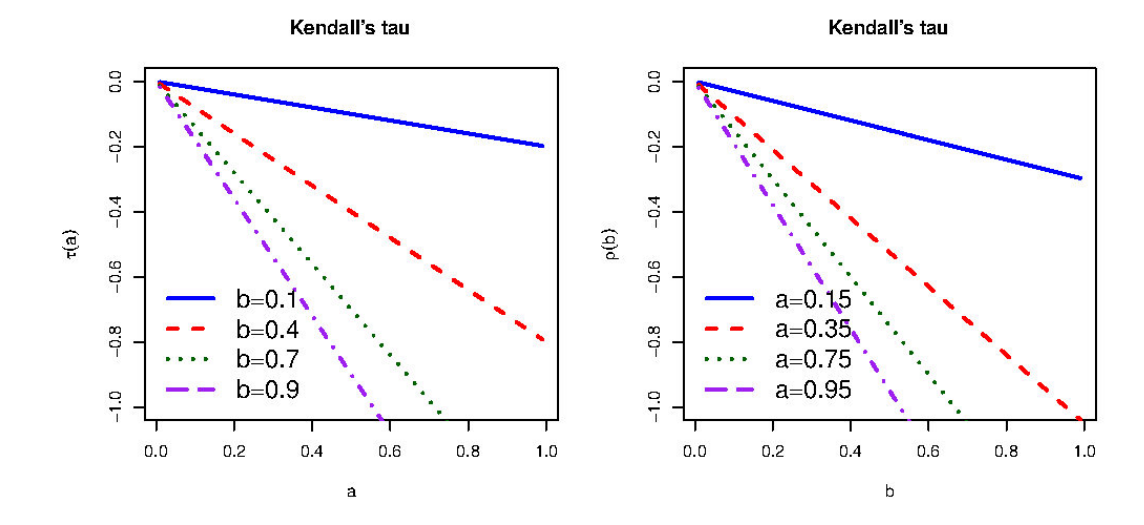


Figure 2. Kendall's τ plots against a and b

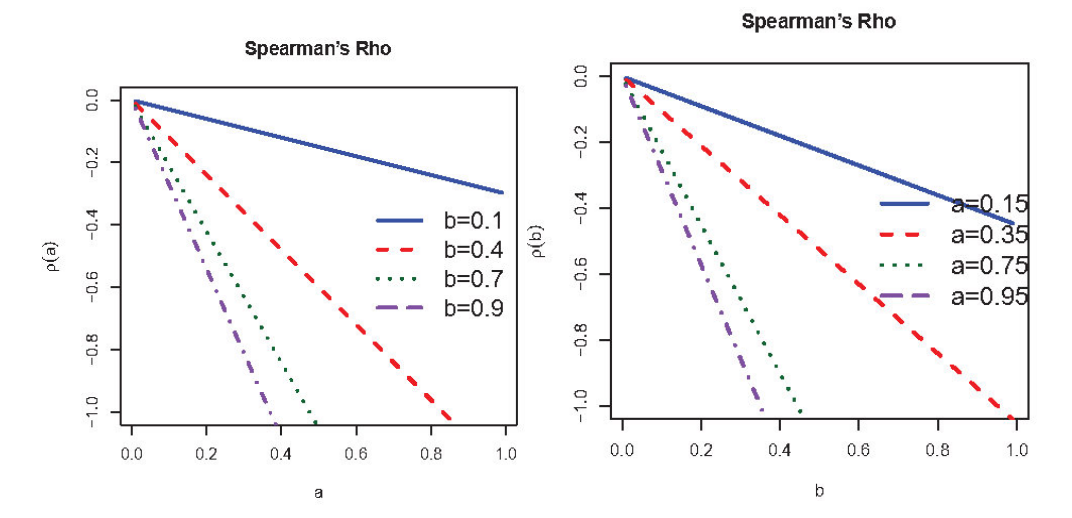


Figure 3. Spearman's ρ_s plots against α and b

shown in Figures 2 and 3, respectively. Based on Figure 2, as the value of a and b tend to 1, the value of dependence measure τ decreases to -1 and the dependency becomes stronger. Also, Figure 3 illustrates that the strength of dependence increases to $\rho_s = -1$ as a and b become large.

The lower and upper tail dependence coefficients λ_L and λ_U are another dependence measures that are defined by $\lambda_L = \lim_{t \to 0^+} P(R \le F_R^{-1}(t) | S \le F_S^{-1}(t))$ and $\lambda_U = \sum_{t \to 0} P(R \le F_R^{-1}(t) | S \le F_S^{-1}(t))$ $\lim_{t\to 1^-} P(R > F_R^{-1}(t)|S > F_S^{-1}(t))$, respectively (see Nelsen (28)). The following proposition presents the tail dependence coefficients for $\bar{F}_{R,S}$ in (6).

Proposition 2.5. If $(R,S) \sim BNMO(\theta_1, \theta_2, \theta_{12})$,

then $\lambda_L = \lambda_U = 0$. Proof. Let $\alpha = \frac{\theta_{12}}{\theta_1 + \theta_{12}}$ and $\beta = \frac{\theta_{12}}{\theta_2 + \theta_{12}}$ as defined in Proposition 2.1. For every $\alpha, \beta \in (0,1)$, we have

$$\begin{split} \tilde{F}_{R,S}\left(F_R^{-1}(t), F_S^{-1}(t)\right) \\ &= (1-t)^{2-\alpha-\beta} \Big((1-t)^\alpha + (1-t)^\beta - 1 \Big). \end{split}$$

So,

$$\lambda_{L} = \lim_{t \to 0^{+}} P\left(R \le F_{R}^{-1}(t) | S \le F_{S}^{-1}(t)\right)$$

$$= \lim_{t \to 0^{+}} \frac{1}{t} \left(2t - 1 + \tilde{F}_{R,S}\left(F_{R}^{-1}(t), F_{S}^{-1}(t)\right)\right)$$

$$= \lim_{y \to 1^{-}} \frac{1}{1 - y} \left(1 - 2y + y^{2 - \alpha - \beta} \left(y^{\alpha} + y^{\beta} - 1\right)\right) = 0.$$
Also,

$$\begin{split} \lambda_U &= \lim_{t \to 1^-} P \big(R > F_R^{-1}(t) | S > F_S^{-1}(t) \big) \\ &= \lim_{t \to 1^-} \frac{1}{1 - t} \Big(\tilde{F}_{R,S}(F_R^{-1}(t), F_S^{-1}(t) \Big) \\ &= \lim_{y \to 0^+} \frac{1}{y} \Big(y^{2 - \alpha - \beta} \big(y^{\alpha} + y^{\beta} - 1 \big) \Big) = 0. \end{split}$$

So, the proof is complete.

1.3. Stress-strength index

In reliability analysis, the stress-strength model evaluates a system's reliability using random variables R for stress (supply) and S for strength (demand). The system fails when stress exceeds strength, leading to the reliability expression P(R < S). The stress-strength index can be calculated using competing risk models, where failure times R and S are considered latent. We define the failure time as $T = \min(R, S)$ and the failure cause C = 1, if R < S and C = 2, if R > S. The corresponding sub-distribution functions are given by:

$$F^*(1,t) = P(C = 1, T \le t) = \int_0^t f^*(1,z)dz,$$
nd

$$F^*(2,t) = P(C=2,T \le t) = \int_0^t f^*(2,z)dz,$$

 $f^*(1,t) = -\partial \bar{F}(x,y)/\partial x|_{x=y=t}$ where $f^*(2,t) = -\partial \tilde{F}(x,y)/\partial y|_{x=y=t}$ are sub-density functions. Consequently, the stress-strength index is defined as $P(R < S) = F^*(1, \infty)$ and P(R > S) = $F^*(2,\infty)$. According to the competing risk model, the stress-strength index for the proposed model is expressed

Proposition 2.6. Let $(R,S) \sim BNMO(\theta_1, \theta_2, \theta_{12})$,

then

$$P(R < S) = \frac{2\theta_1 + \theta_{12}}{\theta_1 + \theta_2 + \theta_{12}} - \frac{\theta_1}{\theta_1 + \theta_2},$$
 or equivalently
$$P(R < S) = \frac{2\beta - \alpha\beta}{\beta + \alpha - \alpha\beta} - \frac{\beta - \alpha\beta}{\beta + \alpha - 2\alpha\beta}.$$
 Proof. Based on (6), we have
$$f^*(1, t) = -\frac{\partial \tilde{F}_{R,S}(r, s)}{\partial r}|_{r=s=t}$$
$$= \theta_1 e^{-(\theta_1 + \theta_2)t} \left(2e^{-\theta_{12}t} - 1\right) + \theta_{12} e^{-(\theta_1 + \theta_2 + \theta_{12})t}.$$

Thus,

$$F^{*}(1,t) = \int_{0}^{t} f^{*}(1,u)du$$

$$= \frac{2\theta_{1} + \theta_{12}}{\theta_{1} + \theta_{2} + \theta_{12}} \left(1 - e^{-(\theta_{1} + \theta_{2} + \theta_{12})t}\right) - \frac{\theta_{1}}{\theta_{1} + \theta_{2}} \left(1 - e^{-(\theta_{1} + \theta_{2})t}\right).$$
Therefore,
$$P(R < S) = \lim_{t \to +\infty} F^{*}(1,t)$$

$$= \frac{2\theta_{1} + \theta_{12}}{\theta_{1} + \theta_{2} + \theta_{12}} - \frac{\theta_{1}}{\theta_{1} + \theta_{2}}.$$

Using $\alpha = \frac{\theta_{12}}{\theta_1 + \theta_{12}}$ and $\beta = \frac{\theta_{12}}{\theta_2 + \theta_{12}}$, we obtain the second statement.

As a result, the obtained stress-strength parameter can be estimated as follows:

$$\hat{P}(R < S) = \frac{2\hat{\theta}_1 + \hat{\theta}_{12}}{\hat{\theta}_1 + \hat{\theta}_2 + \hat{\theta}_{12}} - \frac{\hat{\theta}_1}{\hat{\theta}_1 + \hat{\theta}_2}.$$

Remark 2.3. If $\theta_1 = \theta_2$ or equivalently $\alpha = \beta$, then $P(R < S) = \frac{1}{2}$.

Figure 4 illustrates the stress-strength index for different values of α and β . According to this figure, we conclude that as α increases, the estimated stressstrength index decreases approximately. Also, if β increases, then $\hat{P}(R < S)$ increases approximately.

Results and Discussion

In this section, we introduce the generation of random data from the proposed model $BNMO(\theta_1, \theta_2, \theta_{12})$ and estimate of its parameters.

1. Random number generation

Simulating random numbers is essential for understanding the behavior of a model. To generate the random numbers from $BNMO(\theta_1, \theta_2, \theta_{12})$, the following algorithm is introduced.

Algorithm 3.1. Random number generation from $BNMO(\theta_1, \theta_2, \theta_{12})$

The algorithm is carried out in the following three

- Step 1: Generate three independent random variables $T_i \sim E(\theta_i)$ for i = 1,2 and $U \sim U(0,1)$.
- Step 2: Set $R = \min\{T_1, F_{T_{12}}^{-1}(U)\}$ and S = $\min\{T_2, F_{T_{12}}^{-1}(1-U)\}\$, where $F_{T_{12}}^{-1}(.)$ is the quantile function of $T_{12} \sim E(\theta_{12})$.
 - Step 3: The desired pair is (R, S).

Figure 5 shows scatterplots of 750 generated data from Algorithm 3.1. As the dependence parameter θ_{12} increases, the dependence increases.

2. Estimation method

Here, we estimate the parameters using the maximum likelihood (ML) method. Consider the random sample of size m, namely $\{(r_1, s_1), ..., (r_m, s_m)\}$ distributed from $BNMO(\theta_1, \theta_2, \theta_{12})$. Let m_1 and m_2 be the number of observations for which $e^{-\theta_{12}r} + e^{-\theta_{12}s} > 1$ and $e^{-\theta_{12}r} + e^{-\theta_{12}s} = 1$, respectively, such that $m_1 + m_2 =$ m. Then, the log-likelihood function for a given sample of observations is obtained by

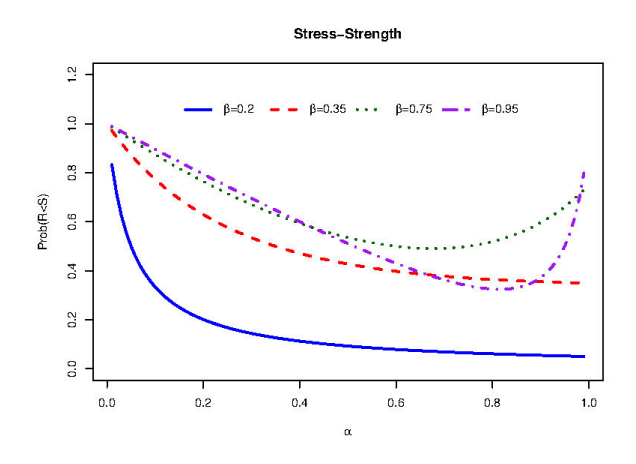


Figure 4. Stress-strength index for varying dependence parameters, α and β

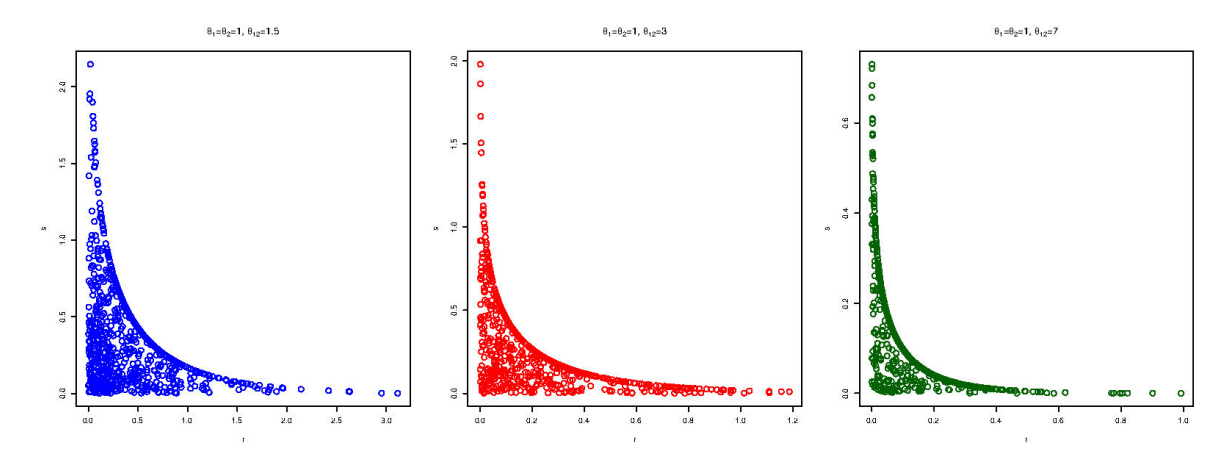


Figure 5. Scatterplot of 750 generated data using Algorithm 3.1 for different values of dependence parameter $\theta_{12} = 1.5,3,7$ (from left to right) and fixed marginal parameters $\theta_1 = \theta_2 = 1$

$$\begin{split} l(\theta_{1},\theta_{2},\theta_{12}) &= & -\theta_{1} \sum_{j=1}^{m_{1}} r_{j} - \theta_{2} \sum_{j=1}^{m_{1}} s_{j} \\ &+ \sum_{j=1}^{m_{1}} \ln \left(\theta_{2}(\theta_{1} + \theta_{12})e^{-\theta_{12}r_{j}} + \theta_{1}(\theta_{2} + \theta_{12})e^{-\theta_{12}s_{j}} - \theta_{1}\theta_{2}\right) \\ &+ m_{2} \ln \left(\frac{\theta_{12}}{\theta_{1} + \theta_{12}}\right) + \frac{\theta_{2}}{\theta_{12}} \sum_{j=m_{1}+1}^{m} \ln \left(1 - e^{-\theta_{12}r_{j}}\right), \end{split}$$

where the observations are classified such that $\{(r_1,s_1),\ldots,(r_{m_1},s_{m_1})\}\in A$ and $\{(r_{m_1+1},s_{m_1+1}),\ldots,(r_m,s_m)\}\in A^c$ and $A=\{(r_i,s_i)|e^{-\theta_{12}r}+e^{-\theta_{12}s}>1\}$.

Based on the normal equations (given in the Appendix), if either m_1 or m_2 are zero, then the ML estimator may lack uniqueness. However, this will not pose a problem since

$$P(m_1 = 0) = [P(e^{-\theta_{12}R} + e^{-\theta_{12}S} > 1)]^m \to 0 \text{ as } m \to \infty,$$
 and

 $P(m_2=0) = \left[P(e^{-\theta_{12}R} + e^{-\theta_{12}S} = 1)\right]^m \to 0 \ as \ m \to \infty.$ For moderate sample size m, the events $[m_1=0]$ and $[m_2=0]$ are rare. When $m_1, m_2 > 0$, the normal equations (detailed in the Appendix) cannot be solved analytically, necessitating numerical methods. However, we found these methods to be less efficient than directly maximizing the log-likelihood function in (11). This maximization can be executed using the optim function in R. Initial values for optimization are obtained through the global non-linear optimization package "Rsolnp" in R version 3.6.1 (Ghalanos et al. (31)). We consider the constraints $\theta_1, \theta_2, \theta_{12} > 0$ and identified local maxima for various values of $\theta_1, \theta_2, \theta_{12}$. The global maximum is selected using the relation:

$$(\hat{\theta}_1, \hat{\theta}_2, \hat{\theta}_{12}) = \operatorname{argmax}_{\theta_1, \theta_2, \theta_{12} \in \Theta} l(\theta_1, \theta_2, \theta_{12}).$$
 (12)

3. Performance analysis

Next, a finite sample performance of the estimators

for marginal parameters (θ_1, θ_2) and dependence parameter θ_{12} is given. The performance is evaluated according to the bias and mean squared error (MSE) of the ML estimators introduced in the previous section. A specific sample size m has been taken from BNMO(1,3,0.8) and MSEs have been calculated based on 10,000 iterations. The results are shown in Figure 6. The ML estimator performs very well for small sample sizes. Notably, after some fluctuations, the bias values stabilize around zero as the sample size increases. It is important to mention that the MLE consistently found a unique global maximum that did not lie on the boundary of the parameter space. The computational time to determine this global maximum, after testing all initial value combinations, was under 7 hours.

4. A real data analysis

This section illustrates the results of applying the BNGM distribution to a dataset on mercury (Hg) concentration in large-mouth bass, as explored by Mohsin et al. (32). Data were collected from 53 Florida lakes to study the factors affecting mercury levels in bass. Water samples were collected from the surface middle of each lake on specific dates, where measurements of alkalinity (mg/l), calcium (mg/l), and chlorophyll (mg/l) were taken, using averages from August and March. Fish samples, ranging from 4 to 44 individuals per lake, were then analyzed for minimum mercury concentration $(\mu g/g)$. Lange et al. (33) noted that mercury bioaccumulation in large-mouth bass is significantly influenced by the lakes' chemical characteristics, making calcium and minimum mercury concentration key variables of interest. We apply the proposed distribution

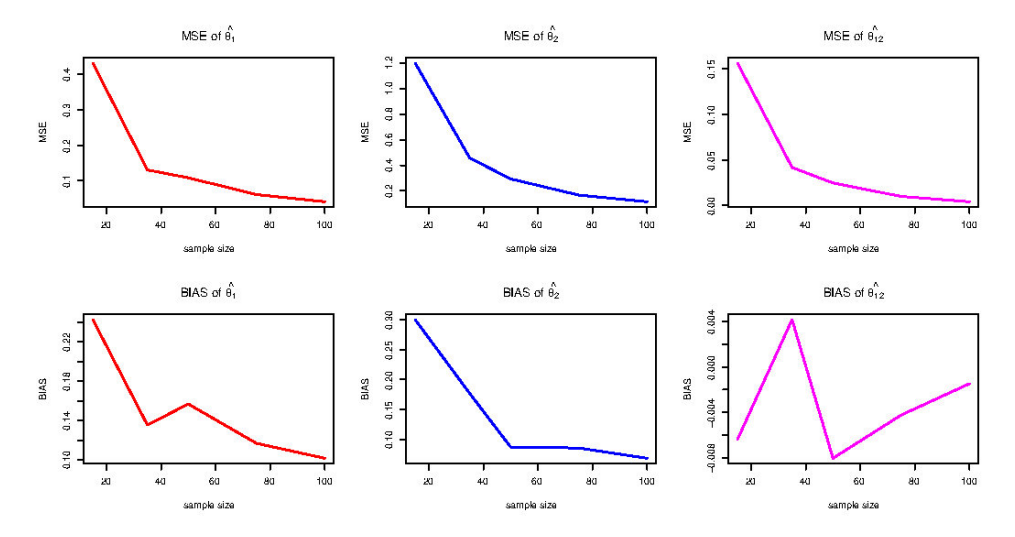


Figure 6. Performance analysis of ML estimators based on MSE and bias for $(\theta_1, \theta_2, \theta_{12})=(1,3,0.8)$ using 10,000 independent replications

to model this data, noting that the 40th row, considered an outlier, was omitted as stated by Mohsin et al. (32). A summary of the data is presented in Table 1. The dependency values of ρ_s and τ indicate a moderate relationship between the variables. We have fitted an exponential distribution to the marginal data, which are summarized in Table 2 and illustrated in Figure 7. Clearly the marginal distributions are well fitted to the data. With the confirmation that the marginal data follows an exponential distribution, we will fit the joint model to the Mercury and Calcium data and compare it to the results in Mohsin et al. (32). These results are shown in Table 3. The BNMO model outperforms the BALE model from Mohsin et al. (32). Both models fit the data well according to the Kolmogorov-Smirnov goodness-of-fit criteria. Figure 8 illustrates the scatter plot of actual versus simulated Mercury and Calcium data derived from the fitted BNMO model.

Conclusion

In practical applications, systems of components are frequently subjected to various shocks, which impact their reliability. According to the well-known MO bivariate shock model in (1), it is challenging to assign the probability of a common shock (T_{12}) to each component $(X_1 \text{ and } X_2)$. We address this limitation by proposing a new MO shock model, which offers beneficial properties such as dependency characteristics and a closed-form formula for the strength parameter, enhancing its applicability. There are few bivariate exponential distributions with a negative dependence structure, making our model particularly appealing. However, the presence of a singular component complicates parameter estimation. We have developed an estimation method and conducted a performance analysis to assess its effectiveness. Applying our model to real data demonstrates that it outperforms existing models.

Table 1. Descriptive statistics of data vectors Mercury and Calcium

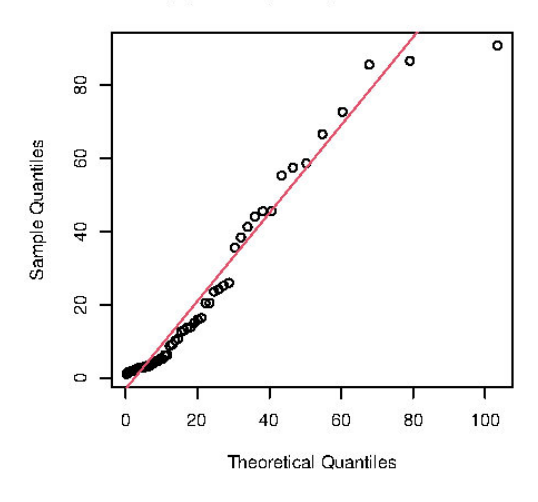
Statistics	Mercury	Calcium
Minimum	0.04	1.1
1 st -Quantile	0.09	3.3
Median	0.25	12.6
Mean	0.27	22.2
3 rd -Quantile	0.33	35.6
Maximum	0.92	90.7
SD	0.22	24.93
Spearman's rho	-0.5	536
Kendall's tau	-0.3	392

Table 2. Marginal goodness-of-fit for Mercury and Calcium

Variables	Distribution	MLE	Log-likelihood	K-S p-value
Mercury	Exponential	3.573	14.502	0.195
Calcium	Exponential	0.045	-217.309	0.232

Exp(0.04504) Q-Q plot for Calcium

Exp(3.5738) Q-Q plot for Mercury



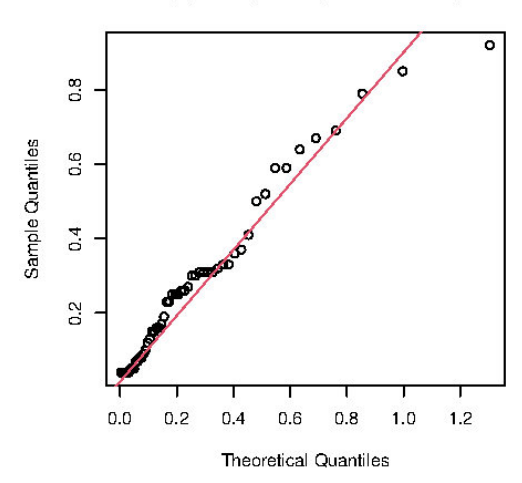


Figure 7. Q-Q plots of Calcium (left) and Mercury (right) for their fitted distributions

Table 3. Goodness-of-fit for the joint vector (Mercury, Calcium)

Model	MLE	Log-Likelihood	K-S p-value
BNMO	$\hat{\theta}_1 = 0.01, \hat{\theta}_2 = 3.67, \hat{\theta}_{12} = 0.038$	-194.0028	0.28
BALE (Mohsin et al. (32))	$\hat{\alpha} = 3.63, \hat{\beta} = 0.01, \hat{\gamma} = 0.25$	-3887.665	0.16

Acknowledgements

The authors thank the editor and anonymous reviewer for their insightful comments on an earlier version of this paper, which significantly improved its quality. This

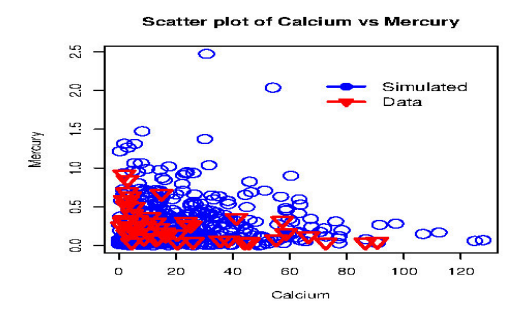


Figure 8. Scatterplot of Mercury versus Calcium for generated data, which are from the best BNMO model

research was funded by grant No. 3/38530 from Ferdowsi University of Mashhad.

References

- Balakrishnan, K. Exponential Distribution: Theory, Methods and Applications. Taylor and Francis, Routledge. 2018.
- Lai, CD, and Balakrishnan, N. Continuous Bivariate Distributions. Springer-Verlag, New York. 2009.
- 3. Marshall, AW, and Olkin, I. A multivariate exponential distribution. Journal of the American Statistical Association. 1967;62(317):30–44.
- Cherubini, U, Durante, F, and Mulinacci, S. Marshall-Olkin distributions. in Advances in Theory and Applications. Springer Proceedings in Mathematics and Statistics, Springer. 2015.
- Lindskog, F, and McNeil, A.J. Common Poisson shock models: Applications to insurance and credit risk modeling. ASTIN Bulletin: The Journal of the IAA. 2003;33(2):209–

- 238.
- Cherubini, U, and Mulinacci, S. The Gumbel-Marshall-Olkin distribution. In Copulas and Dependence Models with Applications, Springer. 2017.
- Esary, JD, and Marshall, AW. Multivariate distributions with exponential minimums. The Annals of Statistics. 1974;2(1):84–98.
- 8. Raftery, AE. A continuous multivariate exponential distribution. Communications in Statistics-Theory and Methods. 1984;13(8):947–965.
- 9. Tawn, JA. Modeling multivariate extreme value distributions. Biometrika. 1990;77(2):245–253.
- 10.Lin, H-H, Chen, K, and Wang, R-T. A multivariant exponential shared-load model. IEEE Transactions on Reliability. 1993;42(1):165–171.
- 11.Basu, AP, and Sun, K. Multivariate exponential distributions with constant failure rates. Journal of Multivariate Analysis. 1997;61(2):159–170.
- 12.Gómez, E, Gomez-Viilegas, M, and Marin, J. A multivariate generalization of the power exponential family of distributions. Communications in Statistics-Theory and Methods. 1998;27(3):589–600.
- 13.Cui, L, and Li, H. Analytical method for reliability and MTTF assessment of coherent systems with dependent components. Reliability Engineering and System Safety. 2007;92(3):300–307.
- 14.Fan, J, Nunn, ME, and Su, X. Multivariate exponential survival trees and their application to tooth prognosis. Computational Statistics and Data Analysis. 2009;53(4):1110–1121.
- 15.Kundu, D, and Gupta, RD. Bivariate generalized exponential distribution. Journal of Multivariate Analysis. 2009;100(4):581–593.
- 16.Li, X, and Pellerey, F. Generalized Marshall-Olkin distributions and related bivariate aging properties. Journal of Multivariate Analysis. 2011;102(10):1399–1409.
- 17.Kundu, D, and Gupta, AK. Bayes estimation for the Marshall–Olkin bivariate Weibull distribution. Computational Statistics and Data Analysis. 2013;57(1):271–281.
- 18.Bayramoglu, I, and Ozkut, M. The reliability of coherent systems subjected to Marshall–Olkin type shocks. IEEE Transactions on Reliability. 2014;64(1):435–443.
- Kundu, D, Franco, M, and Vivo, J-M. Multivariate distributions with proportional reversed hazard marginals. Computational Statistics and Data Analysis. 2014;77:98– 112.
- 20.Cha, JH, and Badía, F. Multivariate reliability modeling

- based on dependent dynamic shock models. Applied Mathematical Modelling. 2017;51:199–216.
- 21.Al-Mutairi, D, Ghitany, M, and Kundu, D. Weighted Weibull distribution: Bivariate and multivariate cases. Brazilian Journal of Probability and Statistics. 2018;32(1):20–43.
- 22.Mohtashami-Borzadaran, HA, Jabbari, H, and Amini, M. Bivariate Marshall-Olkin exponential shock model. Probability in the Engineering and Informational Sciences. 2021;35(3):745–765.
- 23.El Ktaibi, F, Bentoumi, R, Sottocornola, N, and Mesfioui, M. Bivariate copulas based on counter-monotonic shock method. Risks. 2022; 10:202–222.
- 24.Bentoumi, R, El Ktaibi, F, and Mesfioui, M. A new family of bivariate exponential distributions with negative dependence based on counter-monotonic shock method. Entropy. 2021;23:548–565.
- 25.Lee, H, and Cha, JH. New continuous bivariate distributions generated from shock models. Statistics. 2024;58(2):437–449.
- 26.Agrawal, A, Ganguly, A, and Mitra, D. Modelling competing risks data by a bivariate model with singularity originating from a shock model using the Lehmann family of distributions. Research in Statistics. 2025;3(1):1–13.
- 27.Genest, C, Mesfioui, M, and Schulz, J. A new bivariate Poisson common shock model covering all possible degrees of dependence. Statistics and Probability Letters. 2018;140:202–209.
- 28.Mohtashami-Borzadaran, HA, Amini, M, Jabbari, H, and Dolati, A. Marshall-Olkin exponential shock model covering all ranges of dependence. arXiv preprint arXiv: 2004.11241. 2020.
- 29.Joe, H. Multivariate Models and Multivariate Dependence Concepts. Chapman and Hall/CRC, New York. 1997.
- Nelsen, RB. An Introduction to Copulas. Springer-Verlag, New York. 2007.
- 31.Ghalanos, A, Theussl, S, and Ghalanos, MA. Package "Rsolnp". 2012.
- 32. Mohsin, M, Kazianka, H, Pilz, J, and Gebhardt, A. A new bivariate exponential distribution for modeling moderately negative dependence. Statistical Methods and Applications. 2014;23(1):123–148.
- 33.Lange, TR, Royals, H, and Connor, LL. Influence of water chemistry on mercury concentration in largemouth bass from Florida lakes. Transactions of the American Fisheries Society. 1993;122(1):74–84.

Appendix

Let
$$\tilde{\theta} = (\theta_1, \theta_2, \theta_{12})$$
 and for all j :

$$\Delta_{i} = \theta_{2}(\theta_{1} + \theta_{12})e^{-\theta_{12}r_{j}} + \theta_{1}(\theta_{2} + \theta_{12})e^{-\theta_{12}s_{j}} - \theta_{1}\theta_{2}.$$

The normal equations for estimating parameters are as follows:

$$\begin{split} \frac{\partial l(\tilde{\theta})}{\partial \theta_1} &= -\sum_{j=1}^{m_1} r_j + \sum_{j=1}^{m_1} \frac{1}{J_j} \left(\theta_2 e^{-\theta_{12} r_j} + (\theta_2 + \theta_{12}) e^{-\theta_{12} s_j} - \theta_2\right) - \frac{m_2}{\theta_1 + \theta_{12}}, \\ \frac{\partial l(\tilde{\theta})}{\partial \theta_2} &= -\sum_{j=1}^{m_1} s_j + \sum_{j=1}^{m_1} \frac{1}{J_j} \left((\theta_1 + \theta_{12}) e^{-\theta_{12} r_j} + \theta_1 e^{-\theta_{12} s_j} + \theta_1\right) \\ &+ \frac{1}{\theta_{12}} \sum_{j=m_1+1}^{m} \log\left(1 - \exp\{-\theta_{12} r_j\}\right), \end{split}$$

$$\begin{split} \frac{\partial l(\tilde{\theta})}{\partial \theta_{12}} &= \sum_{j=1}^{m_1} \frac{-1}{\Delta_j} \Big(\theta_2(\theta_1 + \theta_{12}) e^{-\theta_{12} r_j} r_j + \theta_1(\theta_2 + \theta_{12}) e^{-\theta_{12} s_j} s_j \Big) \\ &+ \frac{m_2}{\theta_{12}} - \frac{m_2}{\theta_1 + \theta_{12}} - \frac{\theta_2}{\theta_{12}^2} \sum_{j=m_1+1}^m \log \left(1 - \exp\{-\theta_{12} r_j\} \right) \\ &+ \frac{\theta_2}{\theta_{12}} \sum_{j=m_1+1}^m \frac{r_j e^{-\theta_{12} r_j}}{1 - \exp\{-\theta_{12} r_j\}}. \end{split}$$

Modeling Mortality in Heart Failure Patients: Considering Time-Varying Effects - A Bayesian Survival Analysis Utilizing Bayesian AFT Model with the INLA Method

S. Vijayan, S. Kavitha*, V. Saranaya

Department of Statistics, Periyar University, Salem, Tamil Nadu, India

Received: 23 July 2024 / Revised: 27 January 2025 / Accepted: 2 February 2025

Abstract

Heart failure and disease ranks among the most common illnesses globally. Heart failure is a condition where the heart cannot pump blood efficiently, posing a growing global public health challenge with a high mortality rate. This study aimed to identify factors influencing the survival time of heart failure patients. Using secondary data, 299 heart failure patients were studied based on medical records from a 12-month enrollment period. The analysis employed Kaplan-Meier plots and Bayesian parametric survival models, utilizing SPSS and R software, with Integrated Nested Laplace Approximation methods. The Bayesian lognormal accelerated failure time model was deemed appropriate based on model selection criteria. The results indicated that factors such as age, gender, height, systolic and diastolic blood pressure, smoking, alcohol consumption, and the presence of heart disease significantly affected survival times. Cholesterol levels notably impacted survival outcomes in older patients. The Bayesian Weibull accelerated failure time model also described the survival data well. The study's findings suggested that the age groups 59 to 95 and above were most affected by heart failure, significantly impacting survival time.

Keywords: Heart Failure; Kaplan-Meier; Bayesian; Survival time; INLA.

Introduction

Individuals suffering from heart failure often face a steady clinical decline over time. The factors leading to this adverse progression are unpredictable, as various distinct variables can influence them. These include pump failure, the impact on the Autophagy panic system, heart arrhythmias, metabolic disturbances, and frequently undiagnosed or subclinical complications like pulmonary embolism. These potential complications can

arise despite current therapeutic approaches, and their predictability over time remains limited. Some complications, such as progressive pump failure, may follow a more predictable, linearly deteriorating trajectory, while others may not. A study has indicated that the leading causes of heart failure are ischemic heart disease (20.05%), rheumatic valvular heart disease (22.25%), cardiomyopathy (23.72%), and hypertensive heart disease (25.43%). The rest of the causes make up 8.55% of the cases, with these sources contributing

^{*} Corresponding Author: Tel: +919791650315; Email: pustatkavitha@gmail.com

significantly to the total number of combinations of heart failure (1). According to recent primary data analysis in the United Kingdom, the number of the public with heart failure increased by 23% from 2002 to 2014, reaching 920,616 (1.4% of the population) (2). Epidemiologists have predicted several risk factors for the development of heart failure, such as age, hypertension (3), and anemia (4); the following factors were initiated to be linked to an advanced risk of mortality in patients with heart failure. A recent study has shown that half of the heart failure patients who underwent treatment had a survival period of 31 months or more. It was found that around 59.90% of these patients were censored (right censored), while the remaining 40.10% passed away during the study. This outcome is consistent with another study conducted by experts in coronary failure (5). The study found that 31.3% of patients with heart failure had died, while the remaining 68.7% were still alive at the end of the study. Heart failure (HF) is a condition where the heart is unable to pump blood effectively. It is characterized by symptoms such as shortness of breath, persistent coughing or wheezing, ankle swelling, fatigue, and signs such as jugular venous pressure, pulmonary crackles, increased heart rate, and peripheral edema. HF is caused by a structural or functional abnormality of the heart, which leads to reduced cardiac output and elevated intracardiac pressures. Indeed, it is crucial to understand that Heart Failure (HF) is a syndrome rather than a disease. Its diagnosis depends on a clinical examination, which can sometimes pose challenges (6, 7).

Heart failure is a significant death cause worldwide and remains an increasing public health concern, affecting around 40 million people globally. Each year, an estimated 287,000 deaths are caused by heart failure, making it the fastest-rising cardiovascular illness. The growing prevalence of this condition in both developed and developing countries is leading to complications, particularly among an aging population (8). In the United States of America, there are nearly 6.5 million people with heart failure (HF). Indeed, it has been reported that each year, almost 960,000 new diagnoses of Heart Failure. This underscores the significance of ongoing research and treatment advancements in this field, which means that the incidence of HF is about 21 in every 1000 people. Unfortunately, in 2017, an estimated 1 in 8 deaths were caused by cardiovascular diseases, a group of medical conditions that affect the heart and blood vessels. Some examples of these conditions include coronary heart disease. Which can cause heart attacks, a cerebrovascular disease that can lead to strokes, heart failure (also known as HF), and other forms of pathology

The study's main objective is to assess the survival

time of heart failure patients at the Jimma University Medical Center in Jimma, Ethiopia. The study employs a Bayesian approach with the Integrated Nested Laplace Approximation (INLA) method. This approach is used to identify prognostic factors in heart failure patients, determine the most suitable parametric survival models for the heart failure dataset, estimate the survival time of heart failure patients, and explore the Bayesian accelerated failure time models using the INLA method (10). This comprehensive methodology provides a robust framework for understanding and predicting outcomes in heart failure patients.

Materials and Methods

1. Data collection

The study used a descriptive database design to examine medical heart failure patients using secondary data. Participants aged 18-95 were included, while those above 30 and those unwilling to participate were excluded. Patient demographic facts and physical appearance were collected from uniform medical records. Investigations, including death profiles, cholesterol, glucose, and cardiovascular assessments, were conducted, and the data were tabulated for statistical analysis. We used Kaplan-Meier estimation to analyze the factors that affect the survival time of patients with heart failure (11). The 'Starting Time' refers to the commencement of the intermission, measured in days. 'Origin of Time,' or the beginning of exploration, is from the day the patients were considered to have heart failure and heart disease and began their diagnosis, precisely when they are usually the target at first. The 'ending time' denotes the time (in days) the event transpired, either once the patient with heart failure passed away or survived until the study's conclusion. This indicates that the survival information is a right-censored type.

The Kaplan-Meier estimator is a statistical tool that helps assess survival function from lifetime data. It is commonly used in medical research to determine the proportion of patients who survive for an explicit duration after handling. The Kaplan-Meier formula calculates this estimation.

calculates this estimation.

$$\hat{S}(t) = \prod_{t_i \le t} \left(1 - \frac{d_i}{n_i} \right)$$
(1)

- i) The variables t_i represent the times of the events,
- ii) The text looks clear and error-free. It states that di refers to the no. of events, such as deaths that occurred at a specific time ti.
- iii) ni represents the number of individuals who have survived up to time $t_{\rm i}$ without an event or being censored.

We can use the Kaplan-Meier estimator to determine

the survival probability group of individuals over time. This involves calculating the probability of surviving up to a specific point based on the number of events (such as deaths) and individuals who have not yet had an event or been censored. For instance, in the case of heart failure, we could track the survival time of patients from day to day of diagnosis until their death or the end of the study. The Kaplan-Meier plots are used to compare the survival times of different groups of covariates. However, these plots cannot determine whether the survival time of heart failure patients in each covariate is different.

 H_{θ} : There is no difference in survival between the two groups.

 H_I : There is a difference in survival between the two groups.

2. Bayesian AFT Model Using INLA

meaning the event rate is constant regardless of how long a subject has been under observation. Suitable for modeling time-to-event data with a constant hazard rate. Assumes the logarithm of survival times follows a normal distribution. This allows for a variable hazard rate that can change over time. Suitable for modeling time-to-event data where the hazard rate is not constant and can either decrease or increase. Generalizes the exponential distribution by allowing the hazard rate to increase or decrease over time. This provides more flexibility in modeling survival data. Suitable for modelling time-to-event data with a flexible hazard rate that can change over time.

3. Exponential Distribution

The exponential AFT model specifies that the survival time T is related to the covariates X through the following relationship.

$$\log(T) = \beta' X + \epsilon \tag{2}$$

In the study, β represents the vector of regression coefficients, X denotes the vector of covariates, and ϵ is the variance. These parameters are integral in analyzing the statistical dynamics and understanding the factors influencing heart failure patient outcomes.

4. Log-Normal Distribution

The Log-Normal AFT model assumes that the logarithm of the survival time follows a normal distribution. The formula for the log-likelihood function is

$$\ell(\beta, \sigma^{2}; t) = -\frac{n}{2}\log(2\pi\sigma^{2}) - \frac{1}{2\sigma^{2}}\sum_{i=1}^{n} (\log(t_{-}i) - \beta'X_{-}i)^{2}$$
(3)

In this study, t_i represents the observed survival time, β denotes the vector of regression coefficients, Xi is the vector of covariates, and σ^2 is the variance. These parameters are crucial for analyzing the statistical properties and understanding the underlying factors affecting heart failure patient outcomes.

5. Weibull Distribution

The Weibull AFT model assumes that the survival time follows a Weibull distribution. The likelihood function is

$$\ell(\beta, \lambda; t) = nlog(\lambda) + (\lambda - 1) \sum_{i=1}^{n} \log(t_i) - \lambda \sum_{i=1}^{n} \left(\frac{t_i}{exp(\beta'Xi)}\right)^{\lambda}$$
(4)

In the context of this study, t_i represents the observed survival time, β denotes the vector of regression coefficients, X_i is the vector of covariates, and σ^2 is the shape parameter of the distribution. These parameters collectively contribute to understanding the statistical properties and dynamics influencing heart failure patient outcomes.

6. Posterior Distribution

The formula for the adequate number of parameters, often denoted as p_D , in the context of the Deviance Information Criterion (DIC)

$$p_D = D(\theta) - D(\theta) \tag{5}$$

i) $D(\theta)$ is the mean deviance, calculated as the average of the deviance values over the posterior samples.

ii) $D(\theta)$ is the deviance evaluated at the posterior mean of the parameters.

This measure helps understand the difficulty of the model by accounting for the number of parameters well used in fitting it. Lower values of p_D indicate a simpler model, while higher values suggest a more complex model. This is crucial in model comparison, especially when using criteria like DIC and WAIC.

7. Follow-up Method

Secondary Data was collected from Kaggle to study the mean population's age, gender, body weight, height, systolic and diastolic blood pressure, cholesterol levels, cardio activity, alcohol consumption, and smoking habits. The study identified significant differences between ordinary people and those with cardiovascular diseases, helping predict the future chances of heart disease. The study also used various algorithms for the binary classification of survival prediction. The feature

ranking unit shows all patients' follow-up time, and the Kaplan-Meier algorithm was implemented to predict survival. Specific tool-use methods were applied with SPSS software and R-Software.

8. Integrated Nested Laplace Approximation Method

Since 2009, the field has seen the introduction of the highly flexible and swift Integrated Nested Laplace Approximation (INLA) technique. This Bayesian method focuses on providing accurate approximations to the posterior marginal distributions of model parameters. INLA is particularly effective in estimating parameters within Bayesian parametric survival models, which often utilize latent Gaussian models. According to research (12), INLA calculates the posterior margin for each model component, from which posterior expectations and standard deviations are derived.

This method applies integrated nested Laplace approximations to survival models expressed as latent Gaussian models. Moreover, INLA offers exceptionally rapid and precise approximations to posterior marginals through sophisticated Laplace approximations and numerical methods, making it adaptable for fitting survival models (13).

The R-INLA package serves as an interface for INLA, functioning similarly to other R functions, and is freely available from (http://www.r-inla.org). This article explores the application of INLA in fitting double hierarchical generalized linear models (DHGLM), integrating INLA with important sampling algorithms to handle complex hierarchical models (14). Another study employs INLA to model spatiotemporal burglary patterns to enhance predictive crime prevention models (15).

Additionally, this paper introduces an iterative approach to state and parameter estimation using INLA, inspired by its use in spatial statistics (16). Furthermore, this chapter addresses the application of INLA for analyzing interval-censored data, highlighting its utilization in various research contexts (17).

h(t|x): The hazard function at time t, given covariates x.

 $h_0(t)$: The baseline hazard function, representing the hazard when all covariates are zero.

 $exp(x^{T}\beta)$: The effect of the covariates on the baseline hazard, ensuring the hazard remains positive.

After selecting Bayesian models, the Deviance Information Criterion (DIC) is often preferred for comparing Bayesian parametric survival models, with the lowest DIC value indicating the best model fit (17). Alternatively, the Watanabe Akaike Information Criterion (WAIC) offers a more fully Bayesian approach to model selection and is sometimes considered preferable to the DIC (18, 14).

Results and Discussion

The frequency procedure provides helpful statistics and graphics because many variables can be described. Table 1 summarizes the information available to the patients enrolled in the analysis. Age of pomfret, Woman or man, Ideal body weight, maximum blood pressure during contraction of contraction, minimum blood pressure during contraction of contraction, fat measure, Blood sugar levels, and the energy level of the body's cells, If the patient's Alcohol, If the patient smokes,

Table 1. Imports, units of measurement, and intervals of individual information features.

Feature	Description	Dimension	Array
Age	Patient age	int (days)	[5995]
Gender	Woman or man	categorical code	1,2
Height	The distance from the bottom of the feet to the top of the	int (cm)	
	head in a human body		[148,181]
Weight	Ideal body weight	float (kg)	[47,115]
Systolic blood	Maximum blood pressure during contractions	Mm Hg	[100,170]
pressure			
Diastolic blood	Minimum blood pressure during contractions	Mm Hg	[70,110]
pressure			
Cholesterol	Fat measure	mg/dl	1,2,3
Glucose	Blood sugar levels and the energy level of the body's cells	Mmol/dl	1,2,3
Smoke	If the patient smokes	Boolean	0,1
Alcohol	If the patient's Alcohol	Boolean	0,1
Activity	Physical Activity	Boolean	1,2,3
Cardio	Less heart disease /Failure and More than heart	Boolean	0,1
	disease/Failure		
Time	Follow-up period	Days	[2,288]
Death to event	If the patient died during the follow-up period	Boolean	0,1

Table 2. Statistical quantitative description of the category features

Risk factors	Number of cases	Percentage	P-value
Age			
59-66 years	110	37%	
67-75 years	124	42%	.001**
76-95 years	65	21%	
Total	299	100%	
Smoking			
Yes	32	11%	
No	267	89%	.000***
Total	299	100%	
Alcohol			
Yes	12	4%	
No	287	96%	.610
Total	299	100%	
Active			
Yes	229	77%	
No	70	23%	.515
Total	299	100%	
Cardio			
Yes	159	53%	.01*
No	140	47%	
Total	299	100%	

Significant Codes: 0 '***' 0.001 '**' 0.01 '*' 0.05 '.' 0.1 ' 1'.

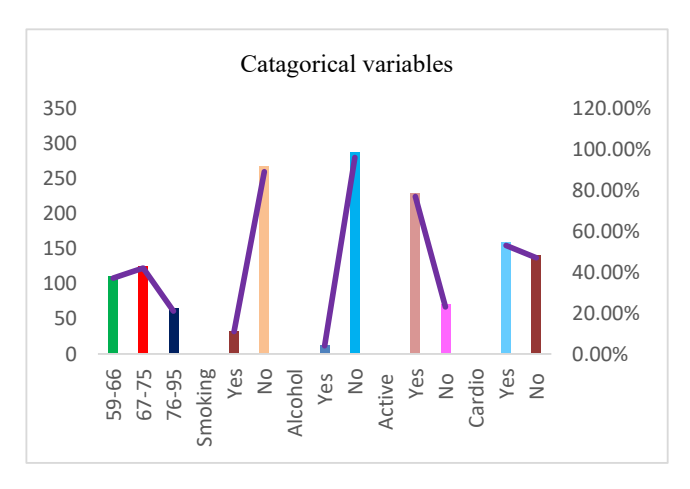


Figure 1. Information about respondents with heart failure reasons

Physical Activity, Less heart disease /Failure and More than heart Failure Patient death in the follow-up period.

Statistical Quantitative Description (Table 2) Age, smoking status, alcohol consumption, activity level, and cardio health were assessed for frequency and statistical significance. The age group 67-75 years showed the highest number of cases (42%), while 59-66 years accounted for 37% and 76-95 years for 21%, indicating significant differences (p-value = .001). Smoking status and cardio health showed substantial differences (p-

values .000 and .01*, respectively). Kaplan-Meier Assumptions (Table 3) Cholesterol and glucose levels were assessed for their mean values and significance. Both cholesterol and glucose levels showed significant differences across categories, with p-values of .002* and .001*, respectively.

Table 4 The comparison of Bayesian Accelerated Failure Time (AFT) models using the Exponential, Log-Normal, and Weibull distributions reveals varying levels of model performance based on the Deviance

Table 3. Shows a test of the assumption in the Kaplan-Meier.

Categorical variables	Mean	St. Error	P-Value
Cholesterol			
Normal	206.158	7.807	.002*
Above Normal	222.189	14.178	
Well Above Normal	155.094	17.986	
Glucose			
Normal	205.458	7.011	.001*
Above Normal	203.721	19.158	
Well Above Normal	151.750	30.290	

Table 4. Presents the comparison of Bayesian AFT models using INLA methods.

Model	Pd	DIC	WAIC
Exponential	-10302.020	-19594.042	543.694
Log-Normal	-8372.022	-15834.042	393.694
Weibull	-6642.025	-12474.052	333.937

Information Criterion (DIC) and Watanabe-Akaike Information Criterion (WAIC) values. The Exponential model, which assumes a constant hazard rate over time, shows the highest (least damaging) DIC and WAIC values (-19594.042 and 543.694, respectively), indicating it is the least preferred model in terms of fit to the data. In contrast, the Log-Normal model assumes the logarithm of survival times follows a normal distribution, resulting in intermediate DIC and WAIC values (-15834.042 and 393.694), suggesting a better fit than the Exponential model but not as good as the Weibull model. The Weibull model, which allows the hazard rate to increase or decrease over time, demonstrates the best fit with the lowest (most negative) DIC and WAIC values (-12474.052 and 333.937). Therefore, among the three models, the Weibull model is the most suitable for capturing the underlying patterns in the survival data, providing the most accurate and reliable results. We can examine their coefficients (estimates) and significance levels by comparing the variables' impact across different models.

Age, Gender, Height, Weight, Systolic and Diastolic, Smoke and Alcohol. Comparison of Variables (Table 5).

A detailed comparison of coefficients across

Exponential, Log-Normal, and Weibull models highlighted consistent trends in the impact of various risk factors. Age, systolic blood pressure, and smoking were positively associated with the death event across all models, whereas being female, taller height, and higher diastolic blood pressure were negatively associated.

Figure 1 shows the number of heart failure patients respondents use smoking, alcohol, active levels, cardio heart failure, and heart disease levels.

Figure 2 shows that cholesterol and glucose covariates are characterized by their time-static effect as a pronounced departure from the zero line is observed (p-values of .002 and .001, respectively).

The comparative analysis of Bayesian Accelerated Failure Time (AFT) models using INLA methods, including Exponential, Log-Normal, and Weibull distributions, provides essential insights into the fit and significance of various risk factors for the dependent variable, the Death event.

1. Model Comparison

The Weibull model best fits the data with the lowest DIC (-12474.052) and WAIC (333.937) values. This indicates its superior flexibility and accuracy in modeling

Table 5. Comparison of the variables of the coefficient

Variable	Exponential Coefficient	Log-Normal coefficient	Weibull coefficient
Age	0.010	0.015	0.020
Gender (Female)	-0.250	-0.200	-0.180
Height	-0.002	-0.003	-0.004
Weight	0.015	0.020	0.025
Systolic	0.020	0.025	0.030
Diastolic	-0.015	-0.010	-0.005
Smoke (Yes)	0.500	0.400	0.300
Alcohol (Yes)	0.100	0.120	0.130

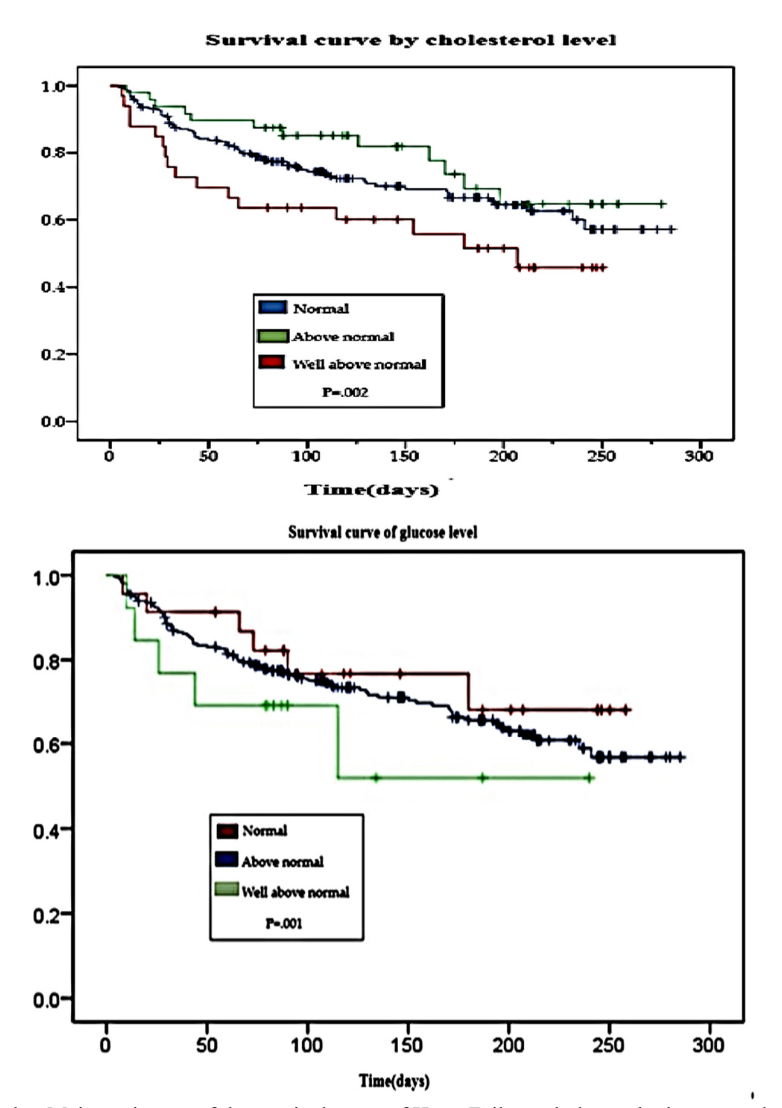


Figure 2. Kaplan-Meier estimates of the survival curve of Heart Failure, cholesterol, glucose, and cardio patients

the survival data compared to the Exponential and Log-Normal models. Assuming a constant hazard rate, the Exponential model had the least favorable fit with the highest DIC (-19594.042) and WAIC (543.694) values. The Log-Normal model provided an intermediate fit with DIC (-15834.042) and WAIC (393.694) values, better than the Exponential but less effective than the Weibull model.

2. Variable Impact

Positive coefficients for variables such as Age, Weight, Systolic Blood Pressure, and Smoking consistently indicated that increases in these factors are associated with a higher likelihood of death. Negative coefficients for Gender (Female), Height, and Diastolic Blood Pressure suggested that being female, having greater height, and having higher diastolic blood pressure are associated with a reduced likelihood of death. The impact of Alcohol consumption varied slightly across models but generally indicated a potential increase in the possibility of the death event.

Conclusion

This analysis evaluates various Bayesian Accelerated

Failure Time (AFT) models using INLA methods to identify the factors influencing the Death event in a patient dataset. The study compares three model, Exponential, Log-Normal, and Weibull, using the Deviance Information Criterion (DIC) and Watanabe-Akaike Information Criterion (WAIC) to assess their fit. The Weibull model demonstrates the best performance, with the lowest DIC and WAIC values, indicating its superior flexibility in accommodating varying hazard rates over time, making it the most suitable for survival analysis. Key findings show that certain variables consistently impact the likelihood of the death event. Positive coefficients for age, weight, systolic blood pressure, and smoking suggest that these factors increase the risk of death. Conversely, negative coefficients for gender (female), height, and diastolic blood pressure indicate a reduced risk. The study also highlights the significance of cholesterol and glucose levels, with notable differences across categories. Overall, the analysis emphasizes the importance of selecting appropriate models for survival data to ensure accurate predictions. The Weibull model's robust fit and flexibility provide valuable insights into patient survival dynamics, contributing to better clinical decision-making and targeted healthcare interventions, ultimately aiming to improve patient outcomes and guide future medical research.

Acknowledgments

The authors acknowledge that no financial support for this work could have influenced its outcome. They would like to thank the Editor-in-Chief, section editors, and anonymous reviewers for their comments and suggestions, which helped to improve the quality of this work.

References

- Ahmad T, Munir A, Bhatti SH, Aftab M, Raza MA. Survival analysis of heart failure patients: A case study. PloS One. 2017 Jul 20;12(7):e0181001.
- Akerkar R, Martino S, Rue H. Implementing approximate Bayesian inference for survival analysis using integrated nested Laplace approximations. Prepr Stat Nor Univ Sci Technol. 2010 Jan 13; 1:1-38.
- Hailay A, Kebede E, Mohammed K. Survival during treatment period of patients with severe heart failure admitted to intensive care unit (ICU) at gondar university hospital (GUH), Gondar, Ethiopia. American Journal of Health Research. 2015 Jul;3(5):257-69.
- 4. Tamrat Befekadu Abebe TB, Eyob Alemayehu Gebreyohannes EA, Yonas Getaye Tefera YG, Tadesse Melaku Abegaz TM. Patients with HFpEF and HFrEF have different clinical characteristics but similar prognosis: a

- retrospective cohort study.
- Benjamin EJ, Muntner P, Alonso A, Bittencourt MS, Callaway CW, Carson AP, Chamberlain AM, Chang AR, Cheng S, Das SR, Delling FN. Heart disease and stroke statistics—2019 update: a report from the American Heart Association. Circulation. 2019 Mar 5;139(10):e56-2.
- Habte B, Alemseged F, Tesfaye D. The pattern of cardiac diseases at the cardiac clinic of Jimma University specialised hospital, South West Ethiopia. Ethiopian journal of health sciences. 2010;20(2).
- Weng SF, Reps J, Kai J, Garibaldi JM, Qureshi N. Can machine learning improve cardiovascular risk prediction using routine clinical data? PloS one. 2017 Apr 4:12(4):e0174944.
- Gottlieb SS. Prognostic indicators: useful for clinical care?.
 Journal of the American College of Cardiology. 2009 Jan 27:53(4):343-4.
- Boqué P, Saez M, Serra L. Need to go further: using INLA to discover limits and chances of burglaries' spatiotemporal prediction in heterogeneous environments. Crime Science. 2022 Sep 10;11(1):7.
- 10.Ashine T, Tadesse Likassa H, Chen DG. Estimating Timeto-Death and Determining Risk Predictors for Heart Failure Patients: Bayesian AFT Shared Frailty Models with the INLA Method. Stats. 2024 Sep 23;7(3):1066-83.
- 11. Aalen OO. Survival and Event History Analysis: A Process Point of View. Springer-Verlag; 2008.
- Maller RA, Zhou X. Survival analysis with long-term survivors. (No Title). 1996.
- 13.Anderka R, Deisenroth MP, Takao S. Iterated INLA for State and Parameter Estimation in Nonlinear Dynamical Systems. arXiv preprint arXiv:2402.17036. 2024 Feb 26.
- 14.Gelman A, Hwang J, Vehtari A. Understanding predictive information criteria for Bayesian models. Statistics and computing. 2014 Nov; 24:997-1016.
- 15. Núñez J, Garcia S, Núñez E, Bonanad C, Bodí V, Miñana G, Santas E, Escribano D, Bayes-Genis A, Pascual-Figal D, Chorro FJ. Early serum creatinine changes and outcomes in patients admitted for acute heart failure: the cardio-renal syndrome revisited. European Heart Journal: Acute Cardiovascular Care. 2017 Aug 1;6(5):430-40.
- 16.Morales-Otero M, Gómez-Rubio V, Núñez-Antón V. Fitting double hierarchical models with the integrated nested Laplace approximation. Statistics and Computing. 2022 Aug;32(4):62.
- 17.Chopin N. Approximate Bayesian inference for latent Gaussian models by using integrated nested Laplace. JR Stat. Soc. Ser. B Stat. Methodol. 2009 Apr;71:319-92.
- 18.Tripoliti EE, Papadopoulos TG, Karanasiou GS, Naka KK, Fotiadis DI. Heart failure: diagnosis, severity estimation and prediction of adverse events through machine learning techniques. Computational and structural biotechnology journal. 2017 Jan 1;15:26-47.
- 19.van Niekerk J, Rue H. Use of the INLA approach for the analysis of interval-censored data. In Emerging topics in modeling interval-censored survival data 2022 Jul 15 (pp. 123-140). Cham: Springer International Publishing.
- 20. Watanabe S, Opper M. Asymptotic equivalence of Bayes cross validation and widely applicable information criterion in singular learning theory. Journal of machine learning research. 2010 Dec 1;11(12).

21.Yancy CW, Jessup M, Bozkurt B, Butler J, Casey DE, Drazner MH, Fonarow GC, Geraci SA, Horwich T, Januzzi JL, Johnson MR. 2013 ACCF/AHA guideline for the management of heart failure: executive summary: a report of the American College of Cardiology

Foundation/American Heart Association Task Force on practice guidelines. Journal of the American College of Cardiology. 2013 Oct 15;62(16):1495-539.of Cardiology, 62(16), e147-e239.

Preparation of Polymer Nanocomposites Containing Multiwall Carbon Nanotubes Functionalized by Chloroform Plasma

F. Pourfayaz*, A. Gholami

School of Energy and Sustainable Resources Engineering, College of Interdisciplinary Science and Technology, University of Tehran, Tehran, Islamic Republic of Iran

Received: 23 October 2023 / Revised: 27 August 2024 / Accepted: 24 May 2025

Abstract

The carbon nanotubes (CNTs) can more efficiently enhance the polymer properties than the other nanofillers due to their unique physical and chemical properties. However, the good dispersion of carbon nanotubes into the polymer matrices is challenging because the CNTs tend to form bundles and agglomerate due to strong van der Waals interactions between the nanotubes. The functionalization of carbon nanotubes can help solve this problem and lead to the good dispersion of CNTs in polymers. In this study, the multiwall carbon nanotubes (MWCNTs) were functionalized using dielectric barrier discharge plasma in helium saturated with chloroform. Then, the functionalized MWCNTs were used to prepare the polymer nanocomposites with a good dispersion state of nanotubes. Fourier transform infrared spectroscopy (FTIR) results showed that the MWCNTs' surfaces are functionalized with the chlorinated group due to exposure of the MWCNTS to the plasma. Moreover, the optical microscopy images and measured rheological properties of the nanocomposites indicated that the plasma-functionalized MWCNTs are better distributed into the polymer matrix than the unfunctionalized MWCNTs. This confirmed that the plasma functionalization enhances the interactions between the MWCNTs and the polymer matrices.

Keywords: Polymer nanocomposites; Carbon nanotubes; Functionalization; Plasma.

Introduction

Composites are solid materials comprising two or more components. The properties of the composite material should differ from each component's properties. Composites usually include a continuous phase, primarily a polymer, ceramic, or metal, and a dispersed phase, such as fiberglass, carbon particles, silica powder, and clay (1, 2). The recent advances in nanotechnology have led to the emergence of a new class of composites

known as nanocomposites. According to a widely accepted definition, nanocomposites are composite materials containing at least one dispersed component with at least one nanoscale dimension. Adding these nanocomponents, called nanofillers, as a dispersed phase (or reinforcing phase) to materials like polymers as a continuous phase leads to composites with excellent properties and diverse potential applications (3, 4).

Polymeric nanocomposites are one of the most important subclasses of nanocomposites, which have

^{*} Corresponding author; Tel: +982161115775; Email: pourfayaz@ut.ac.ir

attracted much attention and have been the focus of many pieces of research (5, 6). Some polymeric nanocomposites have been commercialized and used in industry (7). In polymeric nanocomposites, the continuous phase, called the matrice phase, is a polymer, and the dispersed phase, or reinforcing phase, comprises one or more mineral nanofillers (8). Polymers have diverse applications in industry owing to their unique properties, such as facile synthesis, lightness, and flexibility. However, polymers have lower strength, chemical, and thermal stability than metals and ceramics and are usually nonconductors. Nanofillers like activated carbon, nano-silica, nano-clay, carbon nanofibers, and carbon nanotubes can be added to these materials to enhance polymers' mechanical, electrical, and thermal properties. These nanoscale fillers can reinforce polymers much better than common fillers due to their large specific surface area and aspect ratio (9, 10).

Carbon nanotubes (CNTs) are one of the most important nanofillers that can be employed as an ideal reinforcing nanocomponent to synthesize multi-task polymeric nanocomposites (11). Compared to other nanofillers, CNTs can improve polymers' properties more effectively due to their excellent properties and high length-to-diameter ratio (12, 13).

Generally, CNTs have great potential in many applications owing to their electrical, mechanical, thermal, optical, and chemical properties. The electronic properties of CNTs have gained particular attention. The nanometer size and completely symmetrical structure of nanotubes lead to interesting quantum effects and electronic, magnetic, and lattice properties. Numerous theoretical calculations and experimental measurements have confirmed the abnormal electronic properties of nanotubes (for instance, the quantum wire property of a single-wall nanotube, a group of single-wall and multiwall nanotubes, and semiconducting and metal characteristic of a single-wall nanotube). Since the discovery of nanotubes, these unique properties have resulted in various applications of these materials in detection, catalysis, composites, absorption, drug delivery, biology, and nanoelectronics (14).

To maximize the reinforcing effect of CNTs on polymers, they must be well dispersed in the polymeric matrix (15). CNTs tend to aggregate and form bundles due to the strong van der Waals interactions between nanotubes, making their uniform distribution in polymeric matrix cumbersome. One crucial method to overcome this challenge is surface modification or functionalization of CNTs. Functionalization significantly improves CNTs' performance in many applications (16-18).

Several approaches are used to functionalize or

modify CNTs' surface, including covalent bonding of chemical groups to the end or side wall of the CNTs, noncovalent absorption, or covering the CNTs with various functional molecules (16). Compared to the methods based on non-covalent interactions, covalent chemical functionalization has considerable potential in adjusting CNTs' properties and is expected to encompass diverse applications of nanotubes. The standard methods for functionalizing CNTs are usually based on wet chemistry. In this method, CNTs and reactants often interact in a solution (predominantly at high temperatures). The methods based on wet chemistry usually cause damage to the graphite structure of CNTs and shorten their length. Compared to this approach, modification of CNTs using plasma is a practical lowtemperature process with less pollution. Moreover, various functional groups can be grafted on the nanotubes' surface by adjusting plasma parameters such as power, applied gases, pressure, and processing time. This technique also considerably reduces the reaction time compared to other chemical methods (19, 20).

The synthesis methods of nanotube/polymer nanocomposites are primarily focused on the dispersion of nanotubes in polymer matrices (21, 22). One of the synthesis techniques is a solution method based on phase inversion (23). In this approach, multiwall carbon nanotubes (MWCNTs) are first dispersed in the solvent using ultrasonication. The polymer is then solved in the solvent, and the nanotubes are dispersed again through ultrasonication. Finally, water or acetone (insoluble) is added to the mixture so that the polymer is quickly precipitated and the polymeric nanocomposite is formed (24).

In this study, to sufficiently disperse the MWCNTs, they were first functionalized using a Dielectric Barrier Discharge (DBD) Plasma system at atmospheric pressure. Chloroform-saturated helium was used as the plasma gas. The plasma-synthesized polymeric nanocomposites containing functionalized CNTs were fabricated and characterized. An optical microscope was employed to measure the dispersion of nanotubes in the polymer. The rheological properties of the as-synthesized polymeric nanocomposites were determined and investigated.

Materials and Methods

A dielectric barrier discharge plasma reactor at atmospheric pressure was used to functionalize MWCNTs. Figure 1 depicts the plasma reactor. The reactor is made of a quartz tube, with an inner diameter of 16 mm, an outer diameter of 20 mm and a height about 30 cm. It has two electrodes: the electrode connected to

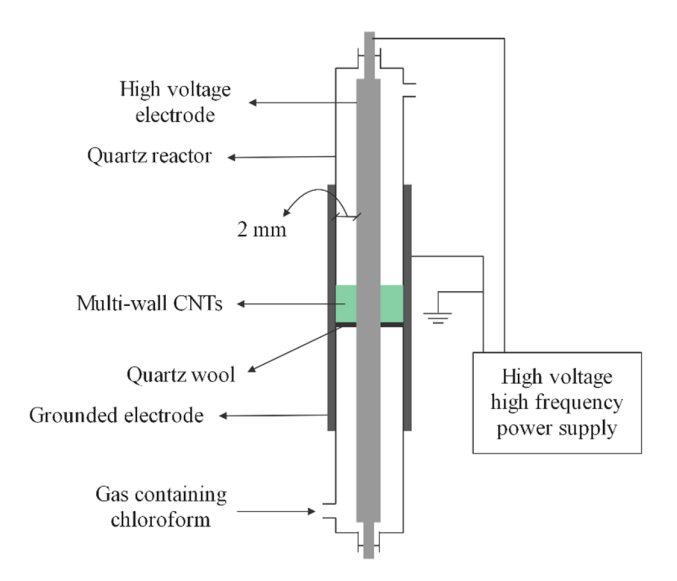


Figure 1. Plasma set-up for functionalization of MWCNTs

high voltage is made of stainless steel, and the electrode connected to the ground is a metal sheet made of stainless steel (or aluminum) wrapped around the quartz tube. First, a helium flow whose mass flow rate is controlled by a mass flow rate controller passes through a chloroform container. The helium saturated with chloroform then enters the plasma reactor, and the plasma reactor is turned on. In this study, the plasma voltage and frequency were 9 kV and 2.6 kHz, respectively. The sample was exposed to plasma for 4 min.

Polypropylene bonded with maleic anhydride was

employed as the polymer matrix to investigate the effect of plasma functionalization. Nanocomposites containing 0.5 wt.% carbon nanotubes were synthesized using functionalized and non-functionalized nanotubes. As depicted in Figure 2, carbon nanotubes were first added to toluene to synthesize these nanocomposites and dispersed through ultrasonication. Then, a solution of polypropylene-maleic anhydride in toluene was added to the mixture. The polymer-nanotube-toluene mixture was exposed to ultrasonication for 80 min. Finally, an equimolar of acetone was added to the mixture to recover the composite. The composite was clotted as a result of

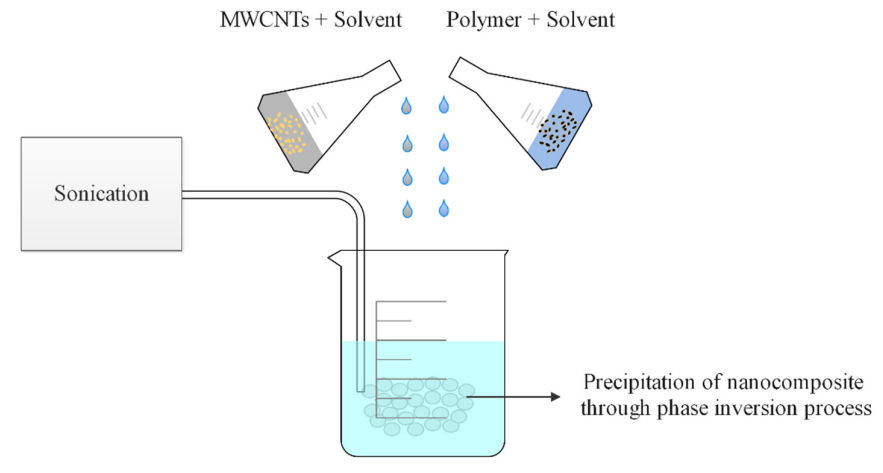


Figure 2. Synthesis process of polymer/MWCNTs nanocomposites

phase inversion. The obtained composite gel was filtered and dried at 120 °C. The dispersion of nanotubes in the polymer matrices was studied through optical microscopy. The nanocomposites' rheological properties were also measured.

Results and Discussion

The chloroform plasma was used to create chlorine functionalities on the surface of carbon nanotubes. The helium gas was passed through a chloroform-containing vessel to be saturated with chloroform. The chloroform-saturated helium entered the plasma reactor and turned the plasma system on. The plasma voltage was adjusted at 9 kV, as in all previous studies, this voltage resulted in the formation of the highest number of functional groups on the nanotubes' surface. The plasma frequency was set at approximately 2.5 kHz. The functionalization of nanotubes with chlorine groups was confirmed by FTIR

spectroscopy of the nanotubes exposed to the plasma for 3 min.

The FTIR spectroscopy for non-functionalized and functionalized nanotubes is shown in Figure 3. There are almost no peaks in the spectrum of non-functionalized nanotubes, indicating the elimination of nearly all the defects and functionalities on the surface due to annealing of nanotubes up to 1000 °C. As can be seen from the spectrum of functionalized nanotubes, the functionalization led to a peak at 1520 cm⁻¹, which implies structural defects on the nanotubes' surface due to plasma or functionalization. There is another peak at around 657 cm⁻¹, which can be attributed to the C-Cl bonds, confirming the formation of chlorinated groups on the surface of functionalized nanotubes.

Optical microscopy images of nanocomposites synthesized by non-functionalized and plasma-functionalized CNTs are shown in Figure 4. As can be

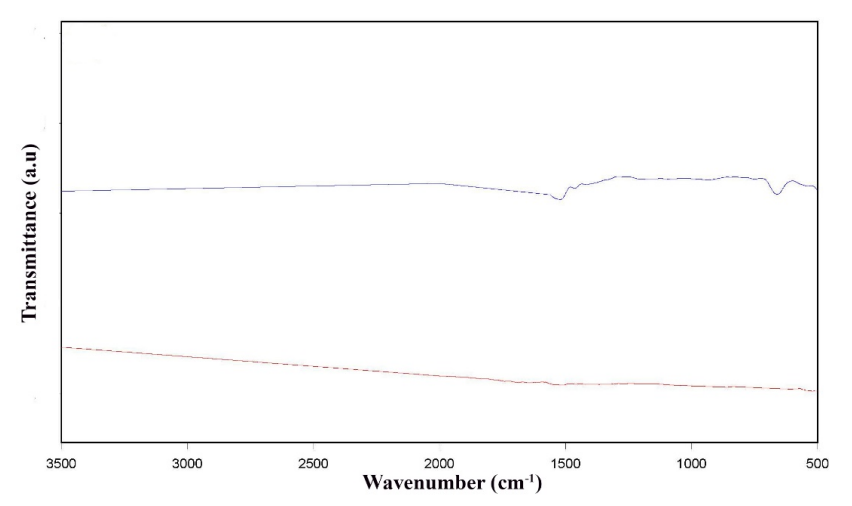


Figure 3. FTIR spectroscopy of non-functionalized and functionalized nanotubes

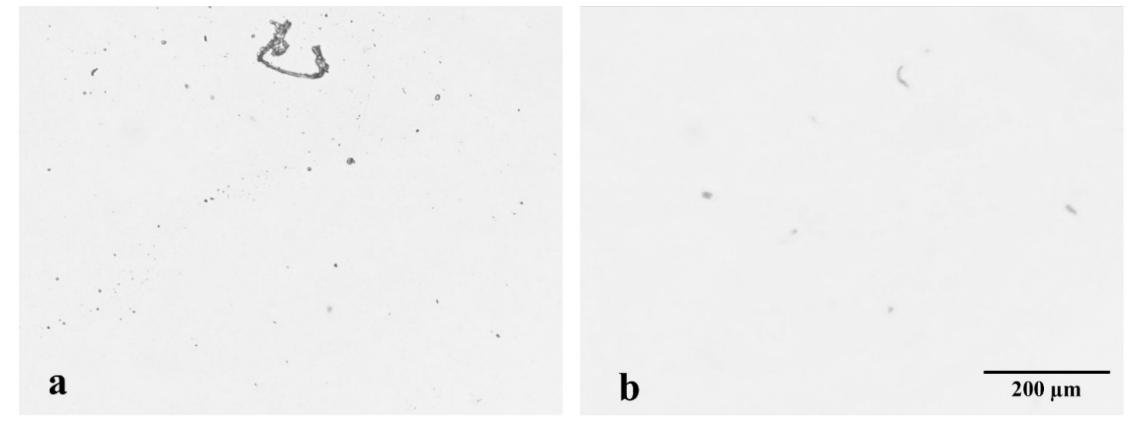


Figure 4. Optical microscopy images of nanocomposites provided by: a. non-functionalized MWCNTs; b. MWCNTs functionalized with chloroform.

observed, the non-functionalized MWCNTs show worse dispersion than the plasma-functionalized MWCNTs. This may be due to the fact that functionalization of MWCNTs by plasma leads to an increased interaction between CNTs and polymer matrix, thus improving the dispersion of CNTs in the polymer matrix.

Figure 5 plots the storage modulus of nanocomposites fabricated through non-functionalized MWCNTs and plasma-functionalized MWCNTs against frequency. Given the better dispersion of plasma-functionalized nanotubes in the polymer matrix, their resultant nanocomposites have greater storage modulus in different frequencies (especially in low frequencies). Generally, the enhanced storage modulus resulting from the inclusion of carbon nanotubes in a polymer matrix can be explained by the effect of carbon nanotubes on the

microstructure of the polymer matrix. In this regard, the strong CNT-polymer and CNT-CNT may link carbon nanotubes and form a semi-lattice structure. This structure may prevent the polymer chain movements and lead to semi-solid rheological behavior. Moreover, the higher the dispersion of nanotubes in nanotube/polymer nanocomposite, the greater the storage modulus. This is ascribed to the complete formation of a nanotube network when there is a more uniform distribution of CNTs in a nanotube/polymer nanocomposite. The appearance of a complete nanotube network creates more limitations for the movement of polymer chains, resulting in more similar rheological behavior to solids (24).

The complex viscosity of nanocomposites based on non-functionalized MWCNTs and plasma-functionalized MWCNTs is depicted in Figure 6. The functionalized

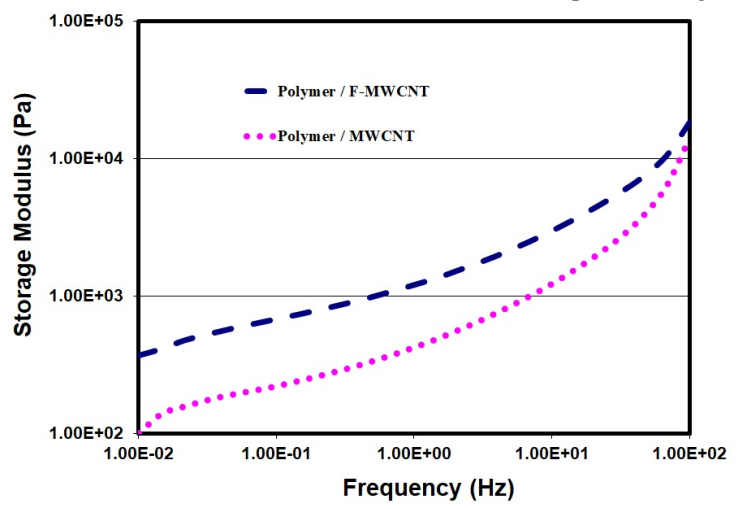


Figure 5. The storage modulus plot of nanocomposites formed by non-functionalized MWCNTs and plasma-functionalized MWCNTs against frequency

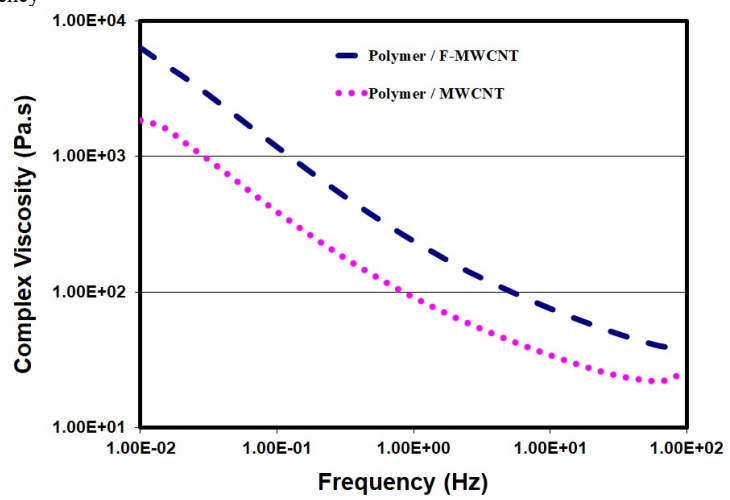


Figure 6. The complex viscosity plot of nanocomposites based on non-functionalized MWCNTs and plasma-functionalized MWCNTs against frequency

MWCNT-based nanocomposites have higher complex viscosities in different frequencies than their non-functionalized counterparts. This implies that the plasma-functionalization of CNTs led to their improved distribution in the polymer matrix.

Overall, the rheological behavior of polymers can be divided into two regions. The first region, including low frequencies, is called the Newtonian region. In this region, the storage and loss modulus heavily depend on frequency, while complex viscosity is slightly dependent on frequency. The storage and loss modulus gradually rise, and complex viscosity slowly falls linearly with an increase in frequency. In high frequencies where non-Newtonian behavior is observed, the frequency dependence is inversed. Adding nanotubes to polymers considerably affects their rheological behavior. Nanotubes increase the storage modulus and complex viscosity of nanocomposites. Also, the higher distribution of CNTs in the polymer matrix translates into their greater impact (8).

Conclusions

Due to their outstanding mechanical, electrical, and thermal properties, CNTs can be employed as the reinforcing phase in polymeric nanocomposites. However, using these nanomaterials as the reinforcing phase is accompanied by some challenges, the most serious of which is their non-uniform distribution in the matrix phase. Functionalizing CNTs can improve their distribution in the polymer matrices. Plasmafunctionalization of CNTs, among other methods, is a low-temperature and practical approach with less pollution. This study used dielectric barrier discharge plasma with chloroform-saturated helium functionalize multiwall carbon nanotubes. The properties of the plasma-functionalized CNTs-based polymeric nanocomposites were also investigated. nanocomposites were prepared using a solution method based on phase inversion.

The results of FTIR analysis showed that chlorinated groups were grafted on the MWCNTs' surface. The optical microscopy images of the CNTs/polymer nanocomposites indicated that the plasma-functionalized MWCNTs had better distribution in the polymer matrix than non-functionalized MWCNTs. The rheological studies of the polymeric nanocomposites also proved that functionalizing MWCNTs led to an enhanced distribution of nanotubes in the polymer matrix.

References

1. Naser M, Hawileh R, Abdalla J. Fiber-reinforced polymer

- composites in strengthening reinforced concrete structures: A critical review. Eng Struct. 2019;198:109542.
- Shcherbakov AB, Reukov VV, Yakimansky AV, Krasnopeeva EL, Ivanova OS, Popov AL, et al. CeO₂ nanoparticle-containing polymers for biomedical applications: A review. Polymers. 2021;13(6):924.
- 3. Hassan T, Salam A, Khan A, Ullah Khan S, Khanzada H, Wasim M, et al. Functional nanocomposites and their potential applications: A review. J Polymer Res. 2021;28:1-22
- Murugesan S, Scheibel T. Copolymer/clay nanocomposites for biomedical applications. Adv Func Mat. 2020;30(17):1908101.
- Abubakre OK, Medupin RO, Akintunde IB, Jimoh OT, Abdulkareem AS, Muriana RA, et al. Carbon nanotubereinforced polymer nanocomposites for sustainable biomedical applications: A review. J Sci. 2023:100557.
- Darwish MS, Mostafa MH, Al-Harbi LM. Polymeric nanocomposites for environmental and industrial applications. Int J Mol Sci. 2022;23(3):1023.
- McWilliams A. Nanocomposites, Nanoparticles, Nanoclays and Nanotubes: Global Markets to 2022, in BBC Research. 2018: Norwalk, CT USA.
- Pourfayaz F, Khodadadi AA, Jafari SH, Mortazavi Y, Khonakdar HA. Ultra-low electrical and rheological percolation thresholds in PMMA/plasma-functionalized CNTs nanocomposites. Polymer-Plastics Technology and Engineering. 2014;53(14):1450-1455.
- 9. Wang M, Tang XH, Cai JH, Wu H, Shen JB, Guo SY. Construction, mechanism and prospective of conductive polymer composites with multiple interfaces for electromagnetic interference shielding: A review. Carbon. 2021;177:377-402.
- 10.Yang X, Fan S, Li Y, Guo Y, Li Y, Ruan K, et al. Synchronously improved electromagnetic interference shielding and thermal conductivity for epoxy nanocomposites by constructing 3D copper nanowires/thermally annealed graphene aerogel framework. Composites Part A: Applied Science and Manufacturing. 2020;128:105670.
- 11. Pourfayaz F, Khodadadi AA, Mortazavi Y, Jafari SH. Plasma functionalization of MWCNTs in He followed by NH3 treatment and its application in PMMA based nanocomposites. Plasma Processes and Polymers. 2010;7(12):1001-1009.
- 12.Coleman JN, Khan U, Blau WJ, Gun'ko YK. Small but strong: a review of the mechanical properties of carbon nanotube–polymer composites. Carbon. 2006;44(9):1624-1652.
- Sahoo NG, Rana S, Cho JW, Li L, Chan SH. Polymer nanocomposites based on functionalized carbon nanotubes. Progress in Polymer Science. 2010;35(7):837-867.
- 14. Schnorr JM, Swager TM. Emerging applications of carbon nanotubes. Chemistry of Materials. 2011;23(3):646-657.
- 15.Xie XL, Mai YW, Zhou XP. Dispersion and alignment of carbon nanotubes in polymer matrix: a review. Materials science and engineering: R: Reports. 2005;49(4):89-112.
- 16.Abousalman-Rezvani Z, Eskandari P, Roghani-Mamaqani H, Salami-Kalajahi M. Functionalization of carbon nanotubes by combination of controlled radical polymerization and "grafting to" method. Adv Colloid

- Interface Sci. 2020;278:102126.
- 17.Pourfayaz F, Ahmadi-Avval P, Haji Tarverdi MS, Maleki A, Ahmadi MH. A study of effects of different surface modifications of MWCNTs on their adsorption capacity of benzene and toluene. Iranian Journal of Chemistry and Chemical Engineering (IJCCE). 2017;36(6):107-114.
- 18.Sezer N, Koç M. Oxidative acid treatment of carbon nanotubes. Surfaces and Interfaces. 2019;14:1-8.
- 19. Pourfayaz F, Mortazavi Y, Khodadadi A, Jafari SH, Boroun S, Naseh MV. A comparison of effects of plasma and acid functionalizations on structure and electrical property of multiwall carbon nanotubes. Appl Surface Sci. 2014;295:66-70.
- 20.Pourfayaz F, Mortazavi Y, Khodadadi AA, Jafari SH. Rapid and enhanced functionalization of MWCNTs in a dielectric barrier discharge plasma in presence of diluted CO₂. Applied Physics A. 2012;106:829-836.
- 21.Kamal A, Ashmawy M, SS, Algazzar AM, Elsheikh AH. Fabrication techniques of polymeric nanocomposites: A comprehensive review. Proceedings of the Institution of Mechanical Engineers, Part C: Journal of Mechanical

- Engineering Science. 2022;236(9):4843-4861.
- 22. Mohd Nurazzi N, Asyraf MRM, Khalina A, Abdullah N, Sabaruddin FA, Kamarudin SH. Fabrication, functionalization, and application of carbon nanotube-reinforced polymer composite: An overview. Polymers. 2021;13(7):1047.
- 23.Pourfayaz F, Jafari SH, Mortazavi Y, Khodadadi AA, Khonakdar HA. Combination of plasma functionalization and phase inversion process techniques for efficient dispersion of MWCNTs in polyamide 6: assessment through morphological, electrical, rheological and thermal properties. Polymer-Plastics Technology and Engineering. 2015;54(6):632-638.
- 24.Pourfayaz F, Jafari SH, Khodadadi AA, Mortazavi Y, Khonakdar HA. On the dispersion of CNTs in polyamide 6 matrix via solution methods: assessment through electrical, rheological, thermal and morphological analyses. Polymer Bullet 2013;70:2387-2398.

J. Sci. I. R. Iran Vol.35 No.4 Autumn 2024

PERSIAN TRANSLATION OF ABSTRACTS

چکیدههای فارسی

Identification of *TYR* Whole Gene Deletion in a Patient with Oculocutaneous Albinism by Next Generation Sequencing

M. R. Pourreza^{1,5}, Gh. Dargahi^{2,5}, M. Hoseinzadeh^{1,5}, N. Tabibi^{3,5} M.A. Tabatabaiefar^{1,4,5*}

شناسایی حذف کامل ژن TYR در یک بیمار مبتلا به آلبینیسم چشمی_پوستی با استفاده از توالییابی نسل جدید

محمدرضا پوررضا ۱٬۰، غزاله درگاهی ۲٬۰ مرضیه حسین زاده ۱٬۰ نسیبه طبیبی ۲٬۰ محمد امین طباطبایی فر ۱٬۰۰۰

اگروه ژنتیک و بیولوژی مولکولی، دانشگاه علوم پزشکی اصفهان، اصفهان، جمهوری اسلامی ایران

* گروه ژنتیک و بیولوژی مولکولی، دانشگاه آزاد اسلامی نجف آباد، نجف آباد، جمهوری اسلامی ایران

* گروه ژنتیک پزشکی، دانشکده ی علوم پزشکی، دانشگاه تربیت مدرس، تهران، جمهوری اسلامی ایران

* مرکز تحقیقات بیماریهای ارثی کودکان، پژوهشکده پیشگیری بنیادین بیماریهای غیرواگیر، دانشگاه علوم پزشکی اصفهان، اصفهان، جمهوری

اسلامی ایران

° گروه تحقیق و توسعه، آزمایشگاه هارمونیک ژنتیک پزشکی، اصفهان، جمهوری اسلامی ایران

حكىدە

آلبینیسم چشم-پوستی (OCA) یک اختلال اتوزوم مغلوب ژنتیکی با هتروژنیسی بالا است که با کاهش یا عدم وجود کامل رنگدانه در مو، پوست و چشمها مشخص می شود و با اختلالات بینایی همراه است. در این مطالعه ، چندین ژن در یک نوزاد پسر ایرانی مبتلا به OCA مورد بررسی قرار گرفت. ارزیابیهای بالینی و آزمایشگاهی برای فرد مبتلا انجام شد و نمودار شجره نیز ترسیم گردید. DNA ژنومی از فرد مبتلا و والدین او استخراج شد. آنالیز جهش با استفاده از فناوری توالییابی نسل جدید بر روی مجموعهای از ژنها انجام گرفت. حذف اگزونهای TYR در ژن TYR در فرد مبتلا شناسایی شد. منطقی است که والدین به صورت هتروزیگوت حامل این جهش باشند. نتایج این مطالعه نشاندهنده کارایی توالییابی هدفمند با توان بالا در تشخیص بیماریهای هتروژن مانند OCA و شناسایی بازآراییهای بزرگ ژنومی است. این جهش حذف ممکن است ناشی از کراسینگ اور نابرابر در یکی از تبارهای اجدادی باشد.

واژههای کلیدی: آلبینیسم چشمی-پوستی (OCA)؛ حذف ژن TYR؛ توالییابی نسل جدید (NGS)

¹ Department of Genetics and Molecular Biology, Isfahan University of Medical Sciences, Isfahan, Islamic Republic of Iran.

² Department of Genetics and Molecular Biology, Najafabad Branch, Islamic Azad University, Najafabad, Islamic Republic of Iran.

³Department of Medical Genetics, Faculty of Medical Sciences, Tarbiat Modares University, Tehran, Islamic Republic of Iran

⁴ Pediatric Inherited Diseases Research Center, Research Institute for Primordial Prevention of Noncommunicable Disease, Isfahan University of Medical Sciences, Isfahan, Islamic Republic of Iran.

⁵ Department of Research and Development, Harmonic Medical Genetics Lab, Isfahan, Islamic Republic of Iran.

*Email: tabatabaiefar@med.mui. ac.ir, tabatabaiefar@gmail.com

Comparison between HLA-B Allele Groups among Peripheral Blood Stem Cell Donation Volunteers from Various Iranian Ethnicities

F. Yari^{1*}, F. Sabaghi^{1, 2}, N. Bagheri¹, A. Teimurpour¹, M. Zaman-Vaziri¹,

F. Mortezapour Barfi¹, M. Sobhani¹

¹ Blood Transfusion Research Center, High Institute for Research and Education in Transfusion, Tehran, Islamic Republic of Iran

*Email: yarii.fatemeh@gmail.com

مقایسه بین گروههای آللی HLA-B در بین داوطلبان اهدای سلولهای بنیادی خون محیطی از اقوام مختلف ایرانی

فاطمه ياري الله فاطمه صباغي الأم ناديا باقرى ا، امير تيمورپور ا، مريم زمان وزيري ا، فرزانه مرتضي پور ا، مريم سبحاني ا

ٔ مرکز تحقیقات انتقال خون، موسسه عالی تحقیقات و آموزش انتقال خون، تهران، جمهوری اسلامی ایران اگروه هماتولوژی، دانشکده بیرایزشکی، دانشگاه علوم بزشکی ایران، بزرگراه همت، تهران، جمهوری اسلامی ایران

چکیده

این مطالعه، شامل ۲۰۶۴ اهداکننده سلول های بنیادی خونساز از اقوام مختلف ایران بود. هدف اولیه تحقیق، ایجاد پایگاه داده HLA و ارزیابی تنوع ژنتیکی در قومیت های مختلف بود. DNA با استفاده از روش مغناطیسی استخراج، و HLA-typing با وضوح پایین با روش PCR-SSP انجام شد. نتایج به صورت دستی توسط کارشناسان مستقل و نیز نرم افزار مورد تجزیه و تحلیل قرار گرفت. داده های HLA از چهار گروه قومی، گیلک کارشناسان مستقل و نیز نرم افزار مورد تجزیه و تحلیل قرار گرفت. داده های HLA از چهار گروه قومی، گیلک (n=4)، لا n=4)، کرد (n=4)، و عرب (n=4)، جهت ارتباط بین آلل ها و قومیت، بررسی شد. فراوانی آللی با روشهای آماری برای شناسایی روابط معنی دار با سطح معنی داری n=4 از با مورد انتظار، محاسبه شد. جهت تعیین فرکانس آللی گروههای قومی و بر اساس فرضیات مستقل از مقادیر فراتر از مورد انتظار، محاسبه شد. n=4 با n=4 با n=4 با n=4 با مطالعه وجود نداشتند. تفاوت معنی دار در n=4 الل در بین گروه های استاندارد بیشتر از ۲، تفاوت معنی داری بین مقادیر قومی برای n=4 با n=4 با n=4 با n=4 با مشاهده شد. باقیمانده های استاندارد بیشتر از ۲، تفاوت معنی داری بین مقادیر قومی برای n=4 با n=4 با n=4 با n=4 با میام شیاهتها و تفاوتها در بین گروه های قومی و توسعه استراتژی های خدمات اهدا در مناطق مختلف ایران و ایجاد رجستری سلولهای بنیادی کمک کند. در آینده، این دادهها می تواند به کاربردهای بالینی در پیوند، توسعه و اکسن و تحقیقات بیماریهای عفونی کمک نماید.

واژههای کلیدی: HLA؛ سلولهای بنیادی خونساز؛ اهداکنندگان؛ قومیت؛ ایران

² Hematology Department, Faculty of Allied Medicine, Iran University of Medical Science, Hemmat Highway, Tehran, Islamic Republic of Iran

On Projection Invariant Rickart Modules

Y. Maleki¹, A. Moussavi^{1*}, Y. Kara²

¹Department of Pure Mathematics, Faculty of Mathematical Sciences, Tarbiat Modares University, Tehran, Islamic Republic of Iran

²Department of Mathematics, Bursa Uludağ University, Görükle, 16059 Bursa, Turkey

*Email: moussavi.a@modares.ac.ir and a.moussavi@gmail.com

مدولهای ریکارت تصویری پایا

یاسر مالکی '، احمد موسوی '، یلیز کارا^۲

ا گروه ریاضی محض، دانشکده علوم ریاضی، دانشگاه تربیت مدرس، تهران، جمهوری اسلامی ایران ۲ دانشکده علوم ریاضی، دانشگاه بورسا اولداغ، قویروک، بورسا ۱۲۰۵۹، ترکیه

در این مقاله، به کمک حلقه همریختیهای یک مدول، به معرفی و بررسی مدولهای π -ریکارت میپردازیم. نشیان میدهیم که مدولهای π -ریکارت به طور سیره بین مدولهای π -بئر و شبه-بئر اصلی قرار میگیرند. هم چنین حلقه همریختی این مدولها، حلقه ای π -ریکارت راست است. در ادامه، مدولهای π - e. AIP را معرفی میکنیم و به بررسی رابطه مدولهای π -ریکارت، π - e. AIP و π - e. AIP میپردازیم.

واژههای کلیدی: مدولهای بئر؛ حلقههای ریکارت؛ حلقههای خودریختی؛ پوچ سازها؛ مدولهای ریکارت

A New Bivariate Shock Model Covering All Degrees of Dependencies

H. A. Mohtashami-Borzadaran, H. Jabbari*, M. Amini

Department of Statistics, Faculty of Mathematical Sciences, Ferdowsi University of Mashhad, Mashhad, Islamic Republic of Iran
*Email: Jabbarinh@um.ac.ir

مدل شوک دو متغیره جدید در برگیرنده همه درجات وابستگی

حسینعلی محتشمی برزادران، هادی جباری ، محمد امینی

گروه آمار، دانشکده علوم ریاضی، دانشگاه فردوسی مشهد، مشهد، جمهوری اسلامی ایران

چکیده

این مقاله یک توزیع دو متغیره ارایه میکند که مدل شوک مارشال-الکین را بهبود میبخشد. روش جدید ساخت، ظرفیت مدل را برای گنجاندن یک شوک مشترک در بین اجزا افزایش میدهد و آن را به ویژه برای ارزیابی قابلیت اعتماد و خطر اعتباری مناسب میسازد. این مدل دارای یک جزء واحد است و از ساختارهای وابستگی منفی پشتیبانی میکند. ویژگیهای وابستگی کلیدی بررسی شده و یک تحلیل تنش-مقاومت انجام میشود. پس از ارزیابی عملکرد براوردگر پارامتر، یک سری دادههای مهندسی شیمی مورد تجزیه و تحلیل قرار میگیرند.

واژههای کلیدی: وابستگی؛ مدل مارشال-الکین؛ مدل شوک

Modeling Mortality in Heart Failure Patients: Considering Time-Varying Effects - A Bayesian Survival Analysis Utilizing Bayesian AFT Model with the INLA Method

S. Vijayan, S Kavitha*, V. Saranaya

Department of Statistics, Periyar University, Salem, Tamil Nadu, India

*Email: pustatkavitha@gmail.com

مدلسازی مرگ و میر در بیماران نارسایی قلبی: بررسی اثرات متغیر با زمان -یک تحلیل بقاء بیزی با استفاده از مدل AFT بیزی و روش INLA

اس ویژایان، اس کاویتا*، وی سارانایا

گروه آمار، دانشگاه بریار، سالیم، تامیل نادو، هند

چکیده

این مطالعه به بررسی الگوهای مرگ و میر در بیماران مبتلا به نارسایی قلبی میپردازد و بر اهمیت در نظر گرفتن اثرات متغیر با زمان بر پیشآگهی بیماران تأکید دارد. ما یک رویکرد تحلیل بقاء بیزی را با استفاده از مدل شتابیافته شکست (AFT) بیزی معرفی میکنیم که به طور خاص برای ادغام اثرات متغیر با زمان طراحی شده است. برای انجام استنتاج بیزی کارآمد، از روش نوآورانه استنتاج یکپارچه توابع گاوسی (INLA) بهره میبریم. این چارچوب به ما امکان میدهد تا نه تنها عوامل خطر سینتی، بلکه تغییرات پویا در تأثیر آنها را بر بقاء بیماران نارسایی قلبی در طول زمان، به دقت ارزیابی کنیم. نتایج حاصل از این رویکرد، درک عمیقتری از پویایی مرگ و میر ارائه میدهد و میتواند به تصمیمگیریهای بالینی و طراحی مداخلات درمانی هدفمندتر کمک کند.

واژههای کلندی: نارسایی قلبی؛ مرگ و میر؛ تحلیل بقاء بیزی؛ مدل AFT؛ اثرات متغیر با زمان؛ روش INLA

Preparation of Polymer Nanocomposites Containing Multiwall Carbon Nanotubes Functionalized by Chloroform Plasma

F. Pourfayaz*, A. Gholami

School of Energy and Sustainable Resources Engineering, College of Interdisciplinary Science and Technologies, University of Tehran, Tehran, Islamic Republic of Iran

* Email: pourfayaz@ut.ac.ir

ساخت نانوکامپوزیتهای پلیمری حاوی نانولولههای کربنی چندلایه عاملدار شده با پلاسمای کلروفرم

فتح اله يورفياض*، على غلامى

دانشکده مهندسی انرژی و منابع پایدار، دانشکدگان علوم و فناوریهای میانرشته ای، دانشگاه تهران، تهران، ایران

چکیده

نانو لولههای کربنی به دلیل خواص فیزیکی و شیمیایی منحصی بفرد خود در مقایسه با دیگر نانوپرکنها خواص پلیمرها را با بازدهی بهتری بهبود میدهند. اما توزیع مناسب نانولولههای کربنی در شیبکه پلیمر چالش برانگیز است، زیرا این نانولولهها به دلیل برهمکنش قوی واندروالس میان آنها تمایل به تشکیل رسوب دارند. این مشکل را میتوان با عاملدار کردن نانولولههای کربنی مرتفع نمود. در این مطالعه نانولولههای کربنی چندلایه با استفاده از پلاسمای هلیوم اشباع شده با کلروفرم عاملدار شدند. سیس، نانولوله های کربنی چندلایه عاملدار شده برای تولید نانوکامپوزیتهایی با خاصیت توزیع مناسب مورد استفاده قرار گرفتند. نتایج طیفسنجی تبدیل فوریه فروسرخ نشان داد که سطح نانولوله های کربنی چندلایه با قرارگرفتن درمعرض پلاسی با گروه عاملی کلرینه عاملدار شدهاند. همچنین تصاویر میکروسکوپ نوری و خواص رئولوژیک نانوکامپوزیتها نشیان داد که نانولولههای کربنی چندلایه عاملدار شده در قیاس با نانولولههای عاملدار نشده به طور یکنواختتری در شبکه پلیمر چندلایه قاملدار غرین ترتیب عاملدار کردن با پلاسیما موجب بهبود برهمکنش بین نانولولههای کربنی چندلایه و شندههای یلیمری میگردد.

واژههای کلیدی: نانوکامیوزیتهای پلیمری؛ نانولولههای کربنی؛ عاملدار کردن؛ پلاسما

Author Index

Volume 35, Numbers 1-4 (2024)

BIOLOGY

Author	Title	Number	Pages
Abdoli A.	Azithromycin Therapy Changed the Intestinal Microbiota, Caused Oxidative Stress, and Decreased Memory Function in Adult Wistar Rats	1	5-14
Ahmadianpour M. V.	Nanoparticle-Protein Corona Interactions in Biological Milieu: Differential Toxicity Profiles in Prostate Cancer and Normal Cell Lines	2	115-124
Aleyasin S. A.	Nanoparticle-Protein Corona Interactions in Biological Milieu: Differential Toxicity Profiles in Prostate Cancer and Normal Cell Lines	2	115-124
Bagheri N.	Comparison Between HLA-B Allele Groups Among Peripheral Blood Stem Cell Donation Volunteers from Various Iranian Ethnicities	4	311-319
Darbandi N.	Azithromycin Therapy Changed the Intestinal Microbiota, Caused Oxidative Stress, and Decreased Memory Function in Adult Wistar Rats	1	5-14
Dargahi Gh.	Identification of <i>TYR</i> Whole Gene Deletion in a Patient with Oculocutaneous Albinism by Next Generation Sequencing	4	305-310
Ghasemi-Varnamkhasti M.	An Impedimetric Genosensor for Ultrasensitive Detection of SARS-Cov-2 Genome Based on 3D Reduced Graphene Oxide and Gold Nanoparticle Composite	2	105-114
Hoseinzadeh M.	Identification of <i>TYR</i> Whole Gene Deletion in a Patient with Oculocutaneous Albinism by Next Generation Sequencing	4	305-310
Izadi Z.	An Impedimetric Genosensor for Ultrasensitive Detection of SARS-Cov-2 Genome Based on 3D Reduced Graphene Oxide and Gold Nanoparticle Composite	2	105-114
Jahangiri B.	Nanoparticle-Protein Corona Interactions in Biological Milieu: Differential Toxicity Profiles in Prostate Cancer and Normal Cell Lines	2	115-124
Karbalaee M.	Nanoparticle-Protein Corona Interactions in Biological Milieu: Differential Toxicity Profiles in Prostate Cancer and Normal Cell Lines	2	115-124
Komijani M.	Azithromycin Therapy Changed the Intestinal Microbiota, Caused Oxidative Stress, and Decreased Memory Function in Adult Wistar Rats	1	5-14
Mobini Gh.	An Impedimetric Genosensor for Ultrasensitive Detection of SARS-Cov-2 Genome Based on 3D Reduced Graphene Oxide and Gold Nanoparticle Composite	2	105-114
Mortezapour Barfi F.	Comparison Between HLA-B Allele Groups Among Peripheral Blood Stem Cell Donation Volunteers from Various Iranian Ethnicities	4	311-319
Pourreza M. R.	Identification of <i>TYR</i> Whole Gene Deletion in a Patient with Oculocutaneous Albinism by Next Generation Sequencing	4	305-310
Raheb J.	Nanoparticle-Protein Corona Interactions in Biological Milieu: Differential Toxicity Profiles in Prostate Cancer and Normal Cell Lines	2	115-124
Sabaghi F.	Comparison Between HLA-B Allele Groups Among Peripheral Blood Stem Cell Donation Volunteers from Various Iranian	4	311-319

Vol. 35 No. 4 Autumn 2024 J. Sci. I. R. Iran

	,		
	Ethnicities		
0 1 1 7	Nanoparticle-Protein Corona Interactions in Biological Milieu:		115 104
Sadeghi Z.	Differential Toxicity Profiles in Prostate Cancer and Normal	2	115-124
	Cell Lines		
	An Impedimetric Genosensor for Ultrasensitive Detection of		
Shakhsi-Niaei M.	SARS-Cov-2 Genome Based on 3D Reduced Graphene Oxide	2	105-114
	and Gold Nanoparticle Composite		
	Comparison Between HLA-B Allele Groups Among Peripheral		211 212
Sobhani M.	Blood Stem Cell Donation Volunteers from Various Iranian	4	311-319
	Ethnicities		
Tabatabaiefar M. A.	Identification of TYR Whole Gene Deletion in a Patient with	4	305-310
	Oculocutaneous Albinism by Next Generation Sequencing	•	
Tabibi N.	Identification of TYR Whole Gene Deletion in a Patient with	4	305-310
	Oculocutaneous Albinism by Next Generation Sequencing		
	Comparison Between HLA-B Allele Groups Among Peripheral		244 240
Teimurpour A.	Blood Stem Cell Donation Volunteers from Various Iranian	4	311-319
	Ethnicities		
	Nanoparticle-Protein Corona Interactions in Biological Milieu:		
Valipour R.	Differential Toxicity Profiles in Prostate Cancer and Normal	2	115-124
	Cell Lines		
_	Comparison Between HLA-B Allele Groups Among Peripheral		
Yari F.	Blood Stem Cell Donation Volunteers from Various Iranian	4	311-319
	Ethnicities		
	Comparison Between HLA-B Allele Groups Among Peripheral		
Zaman-Vaziri M.	Blood Stem Cell Donation Volunteers from Various Iranian	4	311-319
	Ethnicities		

Author Index

Volume 35, Numbers 1-4 (2024)

CHEMISTRY

Author	Title	Number	Pages
Abbasi A.	From The Rational Design of Cobalt-zinc Bimetallic MOF to Catalytic Behavior in Knoevenagel Condensation Reaction	1	15-23
Chanar A.	Gas Chromatography of Environmentally Active Aromatic Amines in Industrial Dyes Effluents and Human Blood Serum	2	125-134
Ghoto S.	Gas Chromatography of Environmentally Active Aromatic Amines in Industrial Dyes Effluents and Human Blood Serum	2	125-134
Hosseini M.S.	From The Rational Design of Cobalt-zinc Bimetallic MOF to Catalytic Behavior in Knoevenagel Condensation Reaction	1	15-23
Jahangir T. M.	Gas Chromatography of Environmentally Active Aromatic Amines in Industrial Dyes Effluents and Human Blood Serum	2	125-134
Khuhawar M.Y.	Gas Chromatography of Environmentally Active Aromatic Amines in Industrial Dyes Effluents and Human Blood Serum	2	125-134
Khuhawar M.Y.	Gas Chromatography of Environmentally Active Aromatic Amines in Industrial Dyes Effluents and Human Blood Serum	2	125-134
Lanjwani M.F.	Gas Chromatography of Environmentally Active Aromatic Amines in Industrial Dyes Effluents and Human Blood Serum	2	125-134
Masnabadi N.	Adsorption Investigation of Boron Nitride Nanoparticle as Biodegradable Drug Delivery Carriers for the Mercaptopurine Anti-cancer Drug by Density Functional Theory	1	25-39
Samadizadeh M.	Adsorption Investigation of Boron Nitride Nanoparticle as Biodegradable Drug Delivery Carriers for the Mercaptopurine Anti-cancer Drug by Density Functional Theory	1	25-39
Sardarzadeh L.	Adsorption Investigation of Boron Nitride Nanoparticle as Biodegradable Drug Delivery Carriers for the Mercaptopurine Anti-cancer Drug by Density Functional Theory	1	25-39
Tavakoli S.	From The Rational Design of Cobalt-zinc Bimetallic MOF to Catalytic Behavior in Knoevenagel Condensation Reaction	1	15-23

Vol. 35 No. 4 Autumn 2024 J. Sci. I. R. Iran

Author Index

Volume 35, Numbers 1-4 (2024)

GEOLOGY

Author	Title	Number	Pages
Modjarrad M.	Tectonic Setting of the Serow-Torshab Ophiolite		
	Related Mafic Rocks, NW-Iran: Implications from	1	41-54
	Minerals and Whole-Rock Geochemistry		
Uysal I.	Tectonic Setting of the Serow-Torshab Ophiolite		
	Related Mafic Rocks, NW-Iran: Implications from	1	41-54
	Minerals and Whole-Rock Geochemistry		

Author Index

Volume 35, Numbers 1-4 (2024)

MATHEMATICS, STATISTICS, AND COMPUTER SCIENCES

Author	Title	Number	Pages
Alavi S. M. R.	Modeling Some Repeated Randomized Responses	3	221-231
Amini M.	A New Bivariate Shock Model Covering All Degrees of Dependencies	4	329-339
Asadi S.	Bayesian Clustering of Spatially Varying Coefficients Zero-Inflated Survival Regression Models	3	205-219
Farzammehr M. A.	Classifying Divorce Cases in Iranian Judiciary Courts Using Machine Learning: A Predictive Perspective	2	147-157
Golalizadeh M.	Supervised Clustering of Persian Handwritten Images	1	55-62
Goldani M.	Evaluating Feature Selection Methods for Macro-Economic Forecasting, Applied for Iran's Macro-Economic Variables	3	243-256
Goodarzi F.	Bounds for the Varentropy of Basic Discrete Distributions and Characterization of Some Discrete Distributions	3	233-241
Herdiani E. T.	The Principal Component Linear Spline Quantile Regression Model in Statistical Downscaling for Rainfall Data	2	159-166
Islamiyati A.	The Principal Component Linear Spline Quantile Regression Model in Statistical Downscaling for Rainfall Data	2	159-166
Jabbari H.	A New Bivariate Shock Model Covering All Degrees of Dependencies	4	329-339
Kara Y.	On Projection Invariant Rickart Modules	4	321-328
Kavitha S.	Modeling Mortality in Heart Failure Patients: Considering Time- Varying Effects - A Bayesian Survival Analysis Utilizing Bayesian AFT Model with the INLA Method	4	341-349
Maleki Y.	On Projection Invariant Rickart Modules	4	321-328
Moghimbeygi M.	Prediction of Anoxic Tonic Seizures due to Asthma in Children: Using Machine Learning Methods	1	63-69
Mohammadzadeh M.	Bayesian Clustering of Spatially Varying Coefficients Zero-Inflated Survival Regression Models	3	205-219
Mohammadzadeh M.	Penalized Composite Likelihood Estimation for Spatial Generalized Linear Mixed Models	2	135-145
Mohtashami-	A New Bivariate Shock Model Covering All Degrees of	4	329-339
Borzadaran H. A.	Dependencies	4	329-339
Moradnia S.	Supervised Clustering of Persian Handwritten Images	1	55-62
Motarjem K.	Prediction of Anoxic Tonic Seizures due to Asthma in Children: Using Machine Learning Methods	1	63-69
Moussavi A.	On Projection Invariant Rickart Modules	4	321-328
Mutmainnah A.	Comparison of Adaptive Neural-Based Fuzzy Inference System and Support Vector Machine Methods for the Jakarta Composite Index Forecasting	3	257-265
Salehi L.	Penalized Composite Likelihood Estimation for Spatial Generalized Linear Mixed Models	2	135-145
Saranaya V.	Modeling Mortality in Heart Failure Patients: Considering Time- Varying Effects - A Bayesian Survival Analysis Utilizing Bayesian AFT Model with the INLA Method	4	341-349
Tabrizi E.	Classifying Divorce Cases in Iranian Judiciary Courts Using Machine Learning: A Predictive Perspective	2	147-157
Tarhani M.	Modeling Some Repeated Randomized Responses	3	221-231

Vol. 35 No. 4 Autumn 2024 J. Sci. I. R. Iran

Thamrin S. A.	Comparison of Adaptive Neural-Based Fuzzy Inference System and Support Vector Machine Methods for the Jakarta Composite Index Forecasting	3	257-265
	Comparison of Adaptive Neural-Based Fuzzy Inference System and		
Tinungki G. M.	Support Vector Machine Methods for the Jakarta Composite Index	3	257-265
	Forecasting		
Wilessen C	Modeling Mortality in Heart Failure Patients: Considering	4	341-349
Vijayan S.	Time-Varying Effects - A Bayesian Survival Analysis Utilizing Bayesian AFT Model with the INLA Method	4	341-349
Yulianti A. S.	The Principal Component Linear Spline Quantile Regression Model	2.	159-166
	in Statistical Downscaling for Rainfall Data	2	139-100
Zadkarami M. R.	Modeling Some Repeated Randomized Responses	3	221-231

Author Index

Volume 35, Numbers 1-4 (2024)

PHYSIQUE

Author	Title	Number	Pages
Gholami A.	Preparation of Polymer Nanocomposites Containing Multiwall Carbon Nanotubes Functionalized by Chloroform Plasma	4	351-357
Pourfayaz F.	Preparation of Polymer Nanocomposites Containing Multiwall Carbon Nanotubes Functionalized by Chloroform Plasma	4	351-357

Keywords Index Volume 35, Numbers 1-4

Volume 35, Numbers 1-4 (2024)

BIOLOGY

Keyword	Title	Number	Pages
Azithromycin	Azithromycin Therapy Changed the Intestinal Microbiota, Caused		
Antibiotic	Oxidative Stress, and Decreased Memory Function in Adult Wistar	1	5-14
Corona Protein	Rats Nanoparticle-Protein Corona Interactions in Biological Milieu: Differential Toxicity Profiles in Prostate Cancer and Normal Cell Lines	2	115-124
Donors	Comparison Between HLA-B Allele Groups Among Peripheral Blood Stem Cell Donation Volunteers from Various Iranian Ethnicities	4	311-319
Electrochemical genosensor	An Impedimetric Genosensor for Ultrasensitive Detection of SARS-Cov-2 Genome Based on 3D Reduced Graphene Oxide and Gold Nanoparticle Composite	2	105-114
Ethnicity	Comparison Between HLA-B Allele Groups Among Peripheral Blood Stem Cell Donation Volunteers from Various Iranian Ethnicities	4	311-319
Gold Nanoparticles	Nanoparticle-Protein Corona Interactions in Biological Milieu: Differential Toxicity Profiles in Prostate Cancer and Normal Cell Lines	2	115-124
Graphene Oxide	Nanoparticle-Protein Corona Interactions in Biological Milieu: Differential Toxicity Profiles in Prostate Cancer and Normal Cell Lines	2	115-124
Gut Microbiome	Azithromycin Therapy Changed the Intestinal Microbiota, Caused Oxidative Stress, and Decreased Memory Function in Adult Wistar Rats	1	5-14
Hematopoietic Stem Cell	Comparison Between HLA-B Allele Groups Among Peripheral Blood Stem Cell Donation Volunteers from Various Iranian Ethnicities	4	311-319
HLA	Comparison Between HLA-B Allele Groups Among Peripheral Blood Stem Cell Donation Volunteers from Various Iranian Ethnicities	4	311-319
Iran	Comparison Between HLA-B Allele Groups Among Peripheral Blood Stem Cell Donation Volunteers from Various Iranian Ethnicities	4	311-319
Memory	Azithromycin Therapy Changed the Intestinal Microbiota, Caused Oxidative Stress, and Decreased Memory Function in Adult Wistar Rats	1	5-14
Next-generation sequencing (NGS)	Identification of <i>TYR</i> Whole Gene Deletion in a Patient with Oculocutaneous Albinism by Next Generation Sequencing	4	305-310
Oculocutaneous albinism (OCA)	Identification of <i>TYR</i> Whole Gene Deletion in a Patient with Oculocutaneous Albinism by Next Generation Sequencing	4	305-310
Oxidative Stress	Azithromycin Therapy Changed the Intestinal Microbiota, Caused Oxidative Stress, and Decreased Memory Function in Adult Wistar Rats	1	5-14
Pencil graphite electrode	An Impedimetric Genosensor for Ultrasensitive Detection of SARS-Cov-2 Genome Based on 3D Reduced Graphene Oxide and Gold Nanoparticle Composite	2	105-114
Prostate Cancer	Nanoparticle-Protein Corona Interactions in Biological Milieu: Differential Toxicity Profiles in Prostate Cancer and Normal Cell Lines	2	115-124
Rat	Azithromycin Therapy Changed the Intestinal Microbiota, Caused Oxidative Stress, and Decreased Memory Function in Adult Wistar Rats	1	5-14
SARS-CoV-2 virus	An Impedimetric Genosensor for Ultrasensitive Detection of SARS-Cov-2 Genome Based on 3D Reduced Graphene Oxide and Gold Nanoparticle Composite	2	105-114

Vol. 35 No. 4 Autumn 2024 J. Sci. I. R. Iran

SPION	Nanoparticle-Protein Corona Interactions in Biological Milieu: Differential Toxicity Profiles in Prostate Cancer and Normal Cell Lines	2	115-124
TYR gene deletion	Identification of <i>TYR</i> Whole Gene Deletion in a Patient with Oculocutaneous Albinism by Next Generation Sequencing	4	305-310

Keywords Index Volume 35, Numbers 1-4

Volume 35, Numbers 1-4 (2024)

CHEMISTRY

Keyword	Title	Number	Pages
	Adsorption Investigation of Boron Nitride Nanoparticle as		
Adsorption energy	Biodegradable Drug Delivery Carriers for the Mercaptopurine	1	25-39
	Anti-cancer Drug by Density Functional Theory		
Aromatic amines	Gas Chromatography of Environmentally Active Aromatic	2	125-134
Aromatic animes	Amines in Industrial Dyes Effluents and Human Blood Serum	2	123-134
Bimetal-MOF	From The Rational Design of Cobalt-zinc Bimetallic MOF to	1	15-23
Billictal-IVIOI	Catalytic Behavior in Knoevenagel Condensation Reaction	1	13-23
	Adsorption Investigation of Boron Nitride Nanoparticle as		
Boron nitride nanotube	Biodegradable Drug Delivery Carriers for the Mercaptopurine	1	25-39
	Anti-cancer Drug by Density Functional Theory		
D	Adsorption Investigation of Boron Nitride Nanoparticle as		
Density functional theory	Biodegradable Drug Delivery Carriers for the Mercaptopurine	1	25-39
(DFT)	Anti-cancer Drug by Density Functional Theory		
Effluents	Gas Chromatography of Environmentally Active Aromatic	2	125-134
Efficients	Amines in Industrial Dyes Effluents and Human Blood Serum	2	123-134
Ethyl chloroformate	Gas Chromatography of Environmentally Active Aromatic	2	125-134
Linyi emororormate	Amines in Industrial Dyes Effluents and Human Blood Serum	2	123-13-
Factorial design	Gas Chromatography of Environmentally Active Aromatic	2	125-134
i detoriar design	Amines in Industrial Dyes Effluents and Human Blood Serum	2	123 13 1
GC	Gas Chromatography of Environmentally Active Aromatic	2	125-134
	Amines in Industrial Dyes Effluents and Human Blood Serum	_	125-15-
Heterogeneous catalyst	From The Rational Design of Cobalt-zinc Bimetallic MOF to	1	15-23
5	Catalytic Behavior in Knoevenagel Condensation Reaction		
ID .	Adsorption Investigation of Boron Nitride Nanoparticle as	1	25.20
IR spectra	Biodegradable Drug Delivery Carriers for the Mercaptopurine	1	25-39
	Anti-cancer Drug by Density Functional Theory From The Rational Design of Cobalt-zinc Bimetallic MOF to		
Knoevenagel	Catalytic Behavior in Knoevenagel Condensation Reaction	1	15-23
	Adsorption Investigation of Boron Nitride Nanoparticle as		
Mercaptopurine	Biodegradable Drug Delivery Carriers for the Mercaptopurine	1	25-39
Wereaptopurme	Anti-cancer Drug by Density Functional Theory	1	23-37
	From The Rational Design of Cobalt-zinc Bimetallic MOF to		
Metal-organic framework	Catalytic Behavior in Knoevenagel Condensation Reaction	1	15-23
_	Gas Chromatography of Environmentally Active Aromatic	_	
Serum	Amines in Industrial Dyes Effluents and Human Blood Serum	2	125-134

Vol. 35 No. 4 Autumn 2024 J. Sci. I. R. Iran

Keywords Index Volume 35, Numbers 1-4 (2024)

GEOLOGY

Keyword	Title	Number	Pages
Fore-Arc Setting	Tectonic Setting of the Serow-Torshab Ophiolite Related Mafic Rocks, NW-Iran: Implications from Minerals and Whole-Rock Geochemistry	1	41-54
Mineral Chemistry	Tectonic Setting of the Serow-Torshab Ophiolite Related Mafic Rocks,	1	41-54
•	NW-Iran: Implications from Minerals and Whole-Rock Geochemistry Tectonic Setting of the Serow-Torshab Ophiolite Related Mafic Rocks,	•	11 51
NW Iran Ophiolites	NW-Iran: Implications from Minerals and Whole-Rock Geochemistry	1	41-54
Ophiolite-Related Gabbro	Tectonic Setting of the Serow-Torshab Ophiolite Related Mafic Rocks, NW-Iran: Implications from Minerals and Whole-Rock Geochemistry	1	41-54
Serow-Torshab	Tectonic Setting of the Serow-Torshab Ophiolite Related Mafic Rocks, NW-Iran: Implications from Minerals and Whole-Rock Geochemistry	1	41-54

Keywords Index Volume 35, Numbers 1-4

Volume 35, Numbers 1-4 (2024)

MATHEMATICS, STATISTICS, AND COMPUTER SCIENCES

Keyword	Title	Number	Pages
Adaptive Neural-based Fuzzy Inference System	Comparison of Adaptive Neural-Based Fuzzy Inference System and Support Vector Machine Methods for the Jakarta Composite Index Forecasting	3	257-265
Annihilators	On Projection Invariant Rickart Modules	4	321-328
Asthma	Prediction of Anoxic Tonic Seizures due to Asthma in Children:	1	63-69
Baer modules	Using Machine Learning Methods On Projection Invariant Rickart Modules	4	321-328
Bayesian	Modeling Mortality in Heart Failure Patients: Considering Time-Varying Effects - A Bayesian Survival Analysis Utilizing Bayesian AFT Model with the INLA Method	4	341-349
Binomial transform	Bounds for the Varentropy of Basic Discrete Distributions and Characterization of Some Discrete Distributions	3	233-241
Cauchy-Schwarz inequality	Bounds for the Varentropy of Basic Discrete Distributions and Characterization of Some Discrete Distributions	3	233-241
Childhood	Prediction of Anoxic Tonic Seizures due to Asthma in Children: Using Machine Learning Methods	1	63-69
Composite likelihood	Penalized Composite Likelihood Estimation for Spatial Generalized Linear Mixed Models	2	135-145
Continuous Sensitive Variable	Modeling Some Repeated Randomized Responses	3	221-231
Data Mining	Classifying Divorce Cases in Iranian Judiciary Courts Using Machine Learning: A Predictive Perspective	2	147-157
Dependence	A New Bivariate Shock Model Covering All Degrees of Dependencies	4	329-339
Dimension Reduction	Supervised Clustering of Persian Handwritten Images	1	55-62
Divorce Cases	Classifying Divorce Cases in Iranian Judiciary Courts Using Machine Learning: A Predictive Perspective	2	147-157
Endomorphism rings	On Projection Invariant Rickart Modules	4	321-328
Feature Selection	Evaluating Feature Selection Methods for Macro-Economic Forecasting, Applied for Iran's Macro-Economic Variables	3	243-256
Forecasting	Comparison of Adaptive Neural-Based Fuzzy Inference System and Support Vector Machine Methods for the Jakarta Composite Index Forecasting	3	257-265
Heart Failure	Modeling Mortality in Heart Failure Patients: Considering Time-Varying Effects - A Bayesian Survival Analysis Utilizing Bayesian AFT Model with the INLA Method	4	341-349
High Dimensional Data	Supervised Clustering of Persian Handwritten Images	1	55-62
Hoda	Supervised Clustering of Persian Handwritten Images	1	55-62
INLA	Modeling Mortality in Heart Failure Patients: Considering Time-Varying Effects - A Bayesian Survival Analysis Utilizing Bayesian AFT Model with the INLA Method	4	341-349
Iran	Classifying Divorce Cases in Iranian Judiciary Courts Using Machine Learning: A Predictive Perspective	2	147-157
Jakarta Composite Index	Comparison of Adaptive Neural-Based Fuzzy Inference System and Support Vector Machine Methods for the Jakarta Composite Index Forecasting	3	257-265
Judiciary	Classifying Divorce Cases in Iranian Judiciary Courts Using	2	147-157

Vol. 35 No. 4 Autumn 2024 J. Sci. I. R. Iran

	Machine Learning: A Predictive Perspective		
Kaplan-Meier	Modeling Mortality in Heart Failure Patients: Considering Time-Varying Effects - A Bayesian Survival Analysis Utilizing	4	341-349
Linear Regression Model	Bayesian AFT Model with the INLA Method Modeling Some Repeated Randomized Responses	3	221-231
Machine Learning	Prediction of Anoxic Tonic Seizures due to Asthma in Children: Using Machine Learning Methods	1	63-69
Machine Learning Techniques	Classifying Divorce Cases in Iranian Judiciary Courts Using Machine Learning: A Predictive Perspective	2	147-157
Macroeconomic Analysis	Evaluating Feature Selection Methods for Macro-Economic Forecasting, Applied for Iran's Macro-Economic Variables	3	243-256
Marshall-Olkin model	A New Bivariate Shock Model Covering All Degrees of Dependencies	4	329-339
Penalized pairwise likelihood	Penalized Composite Likelihood Estimation for Spatial Generalized Linear Mixed Models	2	135-145
Persian Handwritten Images	Supervised Clustering of Persian Handwritten Images	1	55-62
Prediction Model	Prediction of Anoxic Tonic Seizures due to Asthma in Children: Using Machine Learning Methods	1	63-69
Predictive Accuracy	Evaluating Feature Selection Methods for Macro-Economic Forecasting, Applied for Iran's Macro-Economic Variables	3	243-256
Principal Component	The Principal Component Linear Spline Quantile Regression Model in Statistical Downscaling for Rainfall Data	2	159-166
Quantile Regression	The Principal Component Linear Spline Quantile Regression Model in Statistical Downscaling for Rainfall Data	2	159-166
Rainfall	The Principal Component Linear Spline Quantile Regression Model in Statistical Downscaling for Rainfall Data	2	159-166
Randomized Response	Modeling Some Repeated Randomized Responses	3	221-231
Repeated Individual Observations	Modeling Some Repeated Randomized Responses	3	221-231
Repeated Randomized Response	Modeling Some Repeated Randomized Responses	3	221-231
Reversed hazard rate	Bounds for the Varentropy of Basic Discrete Distributions and Characterization of Some Discrete Distributions	3	233-241
Rickart modules Rickart ring	On Projection Invariant Rickart Modules On Projection Invariant Rickart Modules	4 4	321-328 321-328
Shock model	A New Bivariate Shock Model Covering All Degrees of Dependencies	4	329-339
Similarity Methods	Evaluating Feature Selection Methods for Macro-Economic Forecasting, Applied for Iran's Macro-Economic Variables	3	243-256
Spatial Clustering	Bayesian Clustering of Spatially Varying Coefficients Zero- Inflated Survival Regression Models	3	205-219
Spatial generalized linear model	Penalized Composite Likelihood Estimation for Spatial Generalized Linear Mixed Models	2	135-145
Spline	The Principal Component Linear Spline Quantile Regression Model in Statistical Downscaling for Rainfall Data	2	159-166
Statistical Downscaling	The Principal Component Linear Spline Quantile Regression Model in Statistical Downscaling for Rainfall Data	2	159-166
Supervised Clustering	Supervised Clustering of Persian Handwritten Images	1	55-62
Support Vector Machine	Comparison of Adaptive Neural-Based Fuzzy Inference System and Support Vector Machine Methods for the Jakarta	3	257-265
Survival Analysis	Composite Index Forecasting Bayesian Clustering of Spatially Varying Coefficients Zero- Inflated Survival Regression Models	3	205-219
Survival time	Modeling Mortality in Heart Failure Patients: Considering	4	341-349

-			
	Time-Varying Effects - A Bayesian Survival Analysis Utilizing		
	Bayesian AFT Model with the INLA Method		
Manantuany	Bounds for the Varentropy of Basic Discrete Distributions and	3	233-241
Varentropy	Characterization of Some Discrete Distributions	3	
Various Coefficient	Bayesian Clustering of Spatially Varying Coefficients Zero-	3	205-219
Varying Coefficient	Inflated Survival Regression Models	3	
Weighted pairwise	Penalized Composite Likelihood Estimation for Spatial	2	105 145
likelihood	Generalized Linear Mixed Models	2	135-145
World Bank Indicators	Evaluating Feature Selection Methods for Macro-Economic	2	242.256
	Forecasting, Applied for Iran's Macro-Economic Variables	3	243-256

Vol. 35 No. 4 Autumn 2024 J. Sci. I. R. Iran

Keywords Index Volume 35, Numbers 1-4 (2024)

PHYSIQUE

Keyword	Title	Number	Pages
Carbon nanotubes	Preparation of Polymer Nanocomposites Containing Multiwall Carbon Nanotubes Functionalized by Chloroform Plasma	4	351-357
Functionalization	Preparation of Polymer Nanocomposites Containing Multiwall Carbon Nanotubes Functionalized by Chloroform Plasma	4	351-357
Plasma	Preparation of Polymer Nanocomposites Containing Multiwall Carbon Nanotubes Functionalized by Chloroform Plasma	4	351-357
Polymer nanocomposites	Preparation of Polymer Nanocomposites Containing Multiwall Carbon Nanotubes Functionalized by Chloroform Plasma	4	351-357

JOURNAL OF SCIENCES

ISLAMIC REPUBLIC OF IRAN

SUBSCRIPTION FORM

Please enter my annual subscrincluding 4 quarterly issues for			
			ublic of Iran
	Iran	Other	r Countries
□ Personal	R. 30,000		80.00
☐ Institutional	R. 40,000		100.00
☐ Student	R. 16,000		50.00
			20.00
☐ Check enclosed	⊔В	Bill me	
Name: Mailing Address:		City:	Country:
Check or money order must be made to order of: Journal of Sciences, Islamic Republic of Iran, University of Tehran Enghelab Ave., P.O. Box 13145-478, Tehran, Iran Payment can be made via our transfer account. Iran: Account No. 5225458914 Mellat Bank, Branch of University of Tehran, Central Income of Vice President of Research. Foreign: Account No. 162454986 tejarat Bank, Branch of University of Tehran, Islamic Republic of Iran. * Please allow 6-8 weeks for delivery.			
_			
J	ISLAMIC REPU		S ======
J		BLIC OF IRAN	S ======
Please enter my annual subscrincluding 4 quarterly issues for	SUBSCRIPT iption to the Journal of	BLIC OF IRAN FION FORM Sciences, Islamic Repr	
Please enter my annual subscr	SUBSCRIPT iption to the Journal of or the Year Vol.	Sciences, Islamic Repr	ublic of Iran
Please enter my annual subscrincluding 4 quarterly issues for	SUBSCRIPT iption to the Journal of or the Year Vol. Iran	Sciences, Islamic Repr	ublic of Iran
Please enter my annual subscrincluding 4 quarterly issues for Personal	SUBSCRIPT iption to the Journal of or the Year Vol. Iran R. 30,000	Sciences, Islamic Repr	ublic of Iran r Countries 80.00
Please enter my annual subscrincluding 4 quarterly issues for Personal	SUBSCRIPT iption to the Journal of or the Year Vol. Iran R. 30,000 R. 40,000	Sciences, Islamic Repr	r Countries 80.00 100.00
Please enter my annual subscrincluding 4 quarterly issues for Personal	subscription to the Journal of or the Year Vol. Iran R. 30,000 R. 40,000 R. 16,000	Sciences, Islamic Repr	ublic of Iran r Countries 80.00
Please enter my annual subscrincluding 4 quarterly issues for Personal Institutional Student Check enclosed	subscription to the Journal of or the Year Vol. Iran R. 30,000 R. 40,000 R. 16,000	Sciences, Islamic Repr	r Countries 80.00 100.00
Please enter my annual subscrincluding 4 quarterly issues for Personal Institutional Student	subscription to the Journal of or the Year Vol. Iran R. 30,000 R. 40,000 R. 16,000	Sciences, Islamic Repr	r Countries 80.00 100.00

To: Journal of Sciences Islamic Republic of Iran

University of Tehran Enghelab Ave., Tehran P.O. Box 13145-478 Islamic Republic of Iran Stamp

ک نده:

تمبر

تهران – مجله بین المللی علوم پایه جمهوری اسلامی ایران تهران، خیابان انقلاب، دانشگاه تهران، صندوق پستی ۴۷۸ – ۱۳۱۴۵

Cover Legend:

"Abu Reyhan al-Biruni (973-1048) was one of the greatest scholars and philosopher in the history of Islamic civilization. He was equally well versed in a number of fields including mathematics, astronomy, physical and natural sciences, geography, history, chronology, and linguistics. George Sarton has called the first half of the 11th century «the age of Biruni». He wrote over 150 works, including 18 volumes on astronomy, 15 volumes on geography, 13 on literature, 12 volumes on astrology, 6 on religious ideology, 6 on astrolabes, 5 on timing devices, 5 on comets and 4 on the physics of light and optics. His scientific contributions also include the accurate determination of the density of eighteen different metals and minerals. He calculated the sine and cosine of angles from zero to 90 degrees and recorded them in a table. He made a remarkably accurate determination of the radius of the earth, which is very close to the latest estimate. He wrote dissertations regarding comets and meteorites, sun rays, light, twilight and dawn, time and space, astrolabes, methods to determine Qibla, the values of numerals, the relativity between precious stones and metals, ways of determining the longitude and latitude of cities, and the distances between them, and devised a method of measuring the earth's circumference, and complex problems of trigonometry. In addition to his native language (Persian) he also mastered Arabic, Sanskrit, Hebrew, Greek, Syriac and Turkish."

"Ref.: Noori-Daloii, M.R., J. Sci. I.R. Iran, Vol. 1, No. 1, pp. 2-3,. Autumn 1988"

JOURNAL OF SCIENCES

ISLAMIC REPUBLIC OF IRAN

University of Tehran

Indexed by Thomson Reuters, Scopus, Islamic World Science Citation Center (ISC), Scientific Information Database (SID) and/Abstracted in

Biological Abstracts
Biosis Selective Coverage Unique
Biosis Previews
Zoological Records
Chemical Abstracts
Methods in Organic Synthesis
Mathematical Reviews
Current Mathematical Publications
MathSciNet